U. S. Department of Commerce
National Oceanic and Atmospheric Administration
National Weather Service
National Centers for Environmental Prediction
4700 Silver Hill Road, Mail Stop 9910
Washington, DC 20233-9910

Technical Note

Testing of WAVEWATCH III version 2.22 in NCEP's NWW3 ocean wave model suite.[†]

Hendrik L. Tolman [‡]
SAIC-GSO at
Environmental Modeling Center
Ocean Modeling Branch

July 2002

[†] OMB Contribution No. 214.

[‡] e-mail: Hendrik.Tolman@NOAA.gov

Abstract

This report presents the results of studies into the effect of upgrades of the generic WAVEWATCH III model on the performance of the operational wave models at NCEP. The impact is assessed with a year-long hindcast with all models, validated with ERS-2 altimeter and buoy data. These studies were performed to justify the upgrades of these operational model. Upgrades include a conversion to FORTRAN 90. This upgrade is shown to have no impact on model results, and is made mainly with regards to ease of code maintenance. The second improvement includes some small changes in the numerical integration techniques. These changes are made to result in somewhat smoother spectra as well as more responsive model behavior. As expected the impact of these changes proved to be minor. The third model change considers a new Garden Sprinkler Effect (GSE) alleviation method. This method is adopted mainly to improve model economy for high resolution models. For the NAH model, the run time can be reduced by as much as 33%. The impact of these changes on model results is shown to be minimal, except for very high latitudes. The later changes are due to the fact that the new method does not need artificial numerical filtering at such latitudes. The fourth model change considers the explicit representation of islands (and ice) not resolved by the model grid resolution. This change is shown to have a massive local impact on model performance. In terms of bulk statistics, however, its impact is small. Finally, the model is retuned. This improves statistics in the tropics moderately, again with small impact on bulk model statistic.

The combined model changes show a massive local improvement of model behavior, which will make the model a more useful forecast tool for higher resolution forecasts that critically depend on the proper representation of islands. The fact that the impact on bulk statistics and validation against buoy data is small, and sometimes even negative, is mostly a statement of the fact that the bulk statistics are not the proper tool to assess the impact of the present changes, and that due to their spatial distribution, buoy data do not properly represent an entire model in term of validation statistics.

Acknowledgments. The present study was made possibly by funding from the NOAA High Performance Computing and Communication (HPCC) office.

This report is available with either color or black and white graphics as a pdf file from

http://polar.ncep.noaa.gov/waves/references.html

Because there are separate color and black and white versions of this report, some references in the text and caption refer to either color or line style.

Contents

1 Introduction

1.1 Background

On March 9, 2000, WAVEWATCH III version 1.18 (Tolman, 1999) was officially implemented as the cornerstone of the new NOAA WAVEWATCH III (NWW3) ocean wave forecast model suite at the National Centers for Environmental Prediction (NCEP). This model suite at that time consisted of a global model (carrying the generic NWW3 name, Chen et al., 1999), an Alaskan Waters model (AKW, Chao et al., 1999a), and a Western North Atlantic model (WNA, Chao et al., 1999b). In 2001, this model suite was augmented with a seasonal North Atlantic Hurricane wave model (NAH, Chao et al., 2001). Additional Eastern North Pacific regular and hurricane models are under development to complete the wave model suite as originally envisioned.

With the implementation of WAVEWATCH III at NCEP, its source code was made available to the public. Since then, more than 500 copies of the code have been distributed through the WAVEWATCH III web page[1]. The model is run successfully in many countries, and at several institutes has become the operational model of choice.

Since the implementation of version 1.18 of the model, much development has been done (see Tolman, 2002c). The entire code has been converted from FORTRAN 77 to FORTRAN 90. Subtle but important changes have been made to the source term integration scheme. New Garden Sprinkler Effect (GSE) alleviation methods have been developed. These changes were made predominantly for model economy, and ease of model maintenance. Furthermore, a sub-grid treatment of islands and ice concentrations has been developed, aimed at reducing local errors in the models. The present model version (2.22), including all these changes, is presently being prepared for operational implementation (replacing version 1.18), and subsequent public distribution. This report presents extensive test results to document the effect of all changes, and to justify the upgrades at NCEP.

1.2 Test cases

The effects of changes in the wave model have been assessed with a one year hindcast with the global NWW3 and regional AKW and WNA models.

[1] http://polar.ncep.noaa.gov/waves/wavewatch

Table 1.1: Model identification

ID.	Model description.
0	Model version 1.18.
A	Conversion to FORTRAN 90
B	Changes in time integration of physics.
C	GSE alleviation modified.
D	Sub-grid islands and ice concentrations
E	Retuning of model

The required driving wind, temperature and ice fields are routinely archived at NCEP. The wind and temperature fields consist of analyses from the Global Data Assimilation System (GDAS, Kanamitsu, 1989; Derber et al., 1991; Kanamitsu et al., 1991; Caplan et al., 1997), which are available at 3h intervals (alternate analyses and 3h forecasts). Originally, these wind speeds were bias corrected (Tolman, 1998b). Due to subsequent improvements to the GDAS, this bias correction is no longer needed. It is well known that the quality of wave model systems crucially depends on the quality of the wind fields. The quality of the above wind fields will therefore be assessed briefly in section 1.4.

Ice concentrations are obtained from NCEP's automated passive microwave sea ice concentration analysis (Grumbine, 1996), and are updated daily.

The one year runs cover the period of March 2000 through February 2001. In this period, the resolution of the wind fields was T170. The actual calculations all started February 1, 2000, to assure proper model spin up at the start of the model comparison period.

Individual additions or changes to the model typically include several, sometimes non-contiguous model versions. It is therefore more convenient to use a model identifier independent of the actual model version number. A list of such identifiers as used here is given in Table 1.1.

In the first part of the model testing, incremental changes are addressed. Hence, model A is compared to model 0, model B is compared to model A, etc. Because the model version 1.18 is by definition tuned for its physical and numerical approaches, some deterioration of model behavior in terms of gross statistics might occur in some incremental changes. It is therefore useful to consider retuning as the final part of the testing. The model versions D and

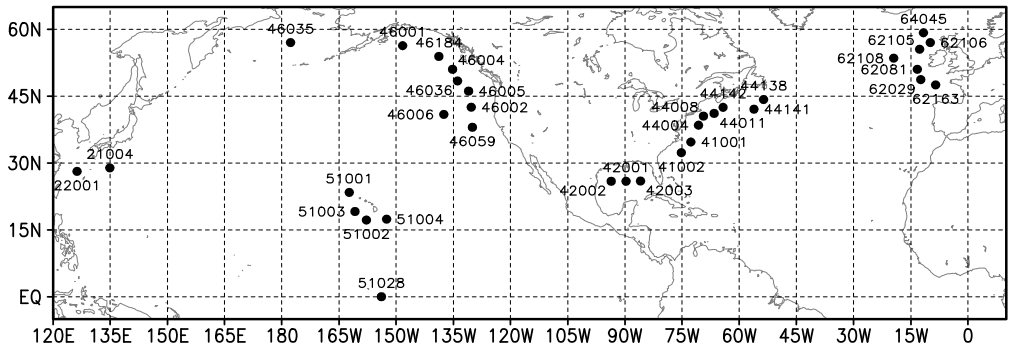

Fig. 1.1 : Buoys used for validation of global NWW3 wave model. Buoys with IDs starting with 2 are denoted as Japanese buoys, with 5 as Hawaii buoys, with 46 as NE Pacific buoys, with 42 as Gulf of Mexico buoy, with 41 and 44 as NW Atlantic buoys, and with 6 as NE Atlantic buoys.

E are identical in terms of the source code, but differ in terms of parameter settings. Finally, the retuned model is compared directly to data and to the presently operational model 0.

All runs were performed on a four processor 700 MHz Intel Zeon machine running Red Hat Linux 6.2 and using a Portland Group compiler version 3.2. The OpenMP version of WAVEWATCH III was run on all processors for the full test period in four day increments. Note that the operational model is running on different hardware; an IBM RS6000-SP using an xlf compiler and MPI. As a pre-test it was verified that the model version 0 on both machines indeed give for all practical purposes identical results.

1.3 Data and data processing

The model validation is carried out with conventional buoy data and with ERS-2 altimeter wave data. Details on data capturing, quality control and archiving can be found in Tolman et al. (2002).

Figure 1.1 shows the buoys used for the validation of the global NWW3 model. Also identified are the different groupings of buoys as will be used in the following sections. Figures 1.2 and 1.3 show the corresponding buoys used in the regional models. In these figures, $\circ$ identify buoys that are also used in the global model, where $\bullet$ identify additional 'coastal' buoys that could not be resolved in the global model.

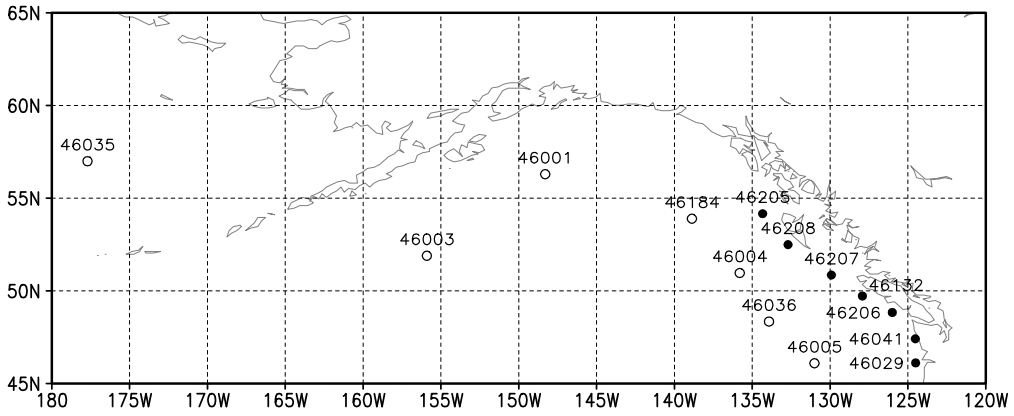

Fig. 1.2 : Buoys used for validation of regional AKW wave model. ○: Deep ocean buoys. ●: Coastal buoys.

Buoy data are captured on the fly from NCEP's operational data steam. Some buoy data are captured after the fact from the National Data Buoy Center (NDBC) quality controlled on-line archive. All buoy data are automatically and visually quality controlled. Most buoys report at 1 hour intervals. In case of a higher sampling rate, only hourly data are used. Hourly data are also extracted from all models, interpolated to the actual buoy location.

The ERS-2 altimeter data are also captured from NCEP's operational data stream. These data are error-corrected as described in Tolman et al. (2002). For the global NWW3 model, the altimeter data are averaged over 10 s intervals to obtain data at scales comparable to the resolution of this model. For the regional models, the altimeter data are used at their native resolution. These data are automatically quality controlled. Apart from gross error checks, signal variability is used for quality control. For the averaged data, the quality control mostly uses internal variability within the averaging period. For the regional models, running average outlier detection is used. The ERS-2 data are collocated with model results using tri-linear interpolation is space and time from hourly model results at the native spatial resolution of the model considered.

Particularly buoy data are first assessed using time series. Due to the sheer volume of data, such time series can generally only be used for spot checking and to give selected examples. More concise ways to look at buoy data is by means joint probability density functions (pdf), and by means of

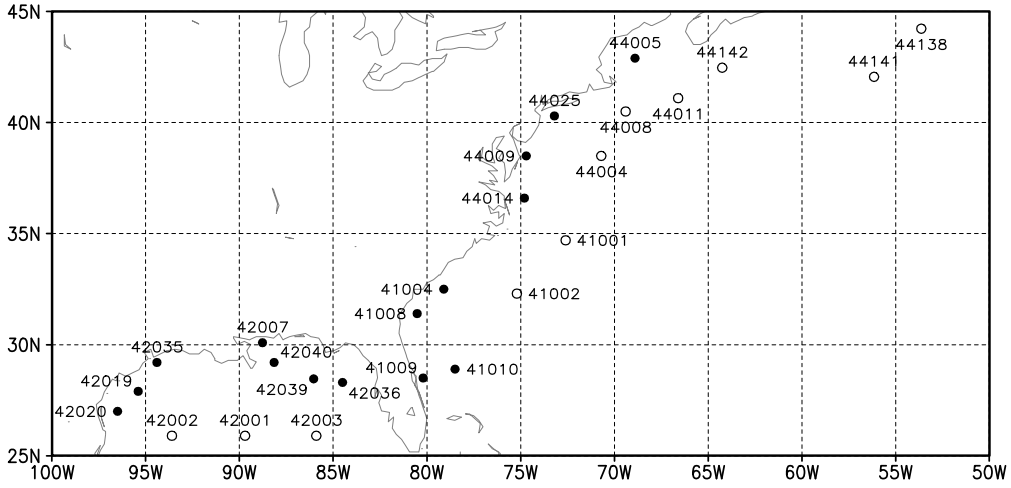

Fig. 1.3 : Buoys used for validation of regional WNA wave model. ○: Deep ocean buoys. ●: Coastal buoys.

bulk statistics. The bulk statistics considered here are the bias, standard deviation (std) root mean square error (rms), correlation coefficients (c.c.) and regression lines. Definitions and considerations regarding these parameters are found in the Appendix of Tolman et al. (2002). Particularly the slope of the regression line is sensitive to the estimated observation error. For the buoy wind speeds U_{10} and wave height H_s, the observation errors are estimated as

$$\max\left[\ 1.5\ \mathrm{ms}^{-1}\ ,\ 0.10\,U_{10}\ \right]\quad , \tag{1.1}$$

$$\max\left[\ 0.05\ \mathrm{m}\ ,\ 0.05\,H_s\ \right]\quad . \tag{1.2}$$

For the ERS-2 wave heights, the errors are estimated as

$$\max\left[\ 0.05\ \mathrm{m}\ ,\ 0.03\,H_s\ \right]\quad , \tag{1.3}$$

for the (averaged) global data, and as

$$\max\left[\ 0.05\ \mathrm{m}\ ,\ 0.04 H_s\ \right]\quad , \tag{1.4}$$

for the (raw) regional data. Note that these error estimates are smaller than those used in Tolman et al. (2002). The latter values proved to give unrealistically steep regression lines for small data ranges. The present values

have been 'reverse engineered' to get reasonable regression lines for cases with small data ranges (in particular, Hawaii buoys, and tropical altimeter data). Note furthermore that by definition, such error estimated are subjective. The resulting regression slopes therefore have an uncertainty of typically 5%, or even more if narrow data ranges are considered. This should always be considered, when addressing absolute values of regression slopes (e.g., Tolman, 1998a).

Along track records of altimeter data are not displayed here. These data are used either to generate pdf's and bulk statistics as for the buoys, or to generate maps of spatial distributions of model errors etc. Techniques used for generating these maps can be found in Tolman (1998b) or Tolman et al. (2002). For the global NWW3 model, such maps are generated at the resolution of the wave model. For the regional models, the maps are generated at a resolution of 0.5°. Higher resolution is not useful for the regional models, because at higher resolution, many grid boxes will see no altimeter data at all. To remove noise, in particular track signatures, spatial averaging is used in the maps using 2 grid points in N and S direction, and 3 in E and W directions.

1.4 Quality of wind fields

As mentioned in section 1.2, the quality of the wind fields is of paramount importance for a wave forecast system. Unfortunately, it is difficult to assess the quality of the analyzed wind fields used here, because most data that could be used to test the quality of the wind fields is included in the analysis. Thus, such data is no longer independent, and cannot be used to assess the quality of the analysis.

Only buoy observations can be considered more or less independent, because only a fraction of these data are used in the analysis, and because buoy data represent only a small fraction of all data used. Figure 1.4 shows the joint pdf of the NWW3 and buoy wind speeds and accompanying statistics. This figure indicates that the wind speeds are well correlated, with a small negative bias and a slightly low slope of the regression line. This behavior appears mostly related to the underestimation of wind speeds in a limited number of storm events that are not properly resolved in space or time in the GDAS. This is manifested as occasional data points in the lower right part of the figure. Because this behavior appears mostly related to isolated events (as will be illustrated in the following sections), systematic bias corrections

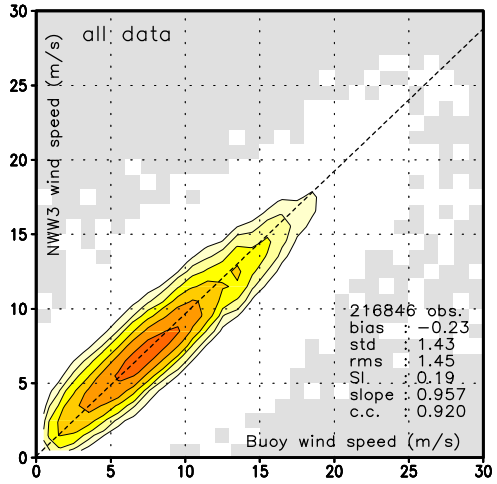

Fig. 1.4 : Probability density function (pdf) of NWW3 model wind speeds U_{10} against buoy data and mean statistics. pdf resolution $\Delta U_{10} = 1$ ms^{-1}. Lowest contour at 0.001 m^{-2}s^{2}. Contours increase by factor 2. Shaded area identifies no data.

as used before (Tolman, 1998b) are no longer an option.

Note that altimeter wind data are not useful as independent validation data, due to their systematic contamination with wave information (Tolman, 1998b).

1.5 Layout of report

The general layout of this report follows the incremental test cases as identified in section 1.2 and in Table 1.1. In sections 2 through 5, the conversion to FORTRAN 90, the modifications to the source term integration scheme, the change in GSE alleviation, and the inclusion of a sub-grid treatment of islands and ice are discussed, respectively. Up to the latter section, incremental impacts are discussed, i.e., the new model is always compared to the previous model version. In section 6, the need for retuning, and the retuning strategy are discussed. In section 7, the behavior of the new model is analyzed, including seasonal behavior. A summary and conclusions are presented in section 8.

2 Conversion to FORTRAN 90

2.1 Description of changes

WAVEWATCH III version 1.18 is written in ANSI standard FORTRAN 77. This choice was made to assure portability of the code. For practical purposes, the main drawback of this choice is that this language version does not support dynamically allocated arrays. In practice this means that for any given application, the dimensions of the model have to be set properly before compilation of the codes. Dynamic allocation is a part of the now established FORTRAN 90 standard. Since reliable FORTRAN 90 compilers are now available for virtually every platform, there is no longer a need to conform strictly to FORTRAN 77.

When converting to FORTRAN 90 to include dynamic allocation of arrays, it was decided to completely convert the code. In doing so, additional benefits of FORTRAN 90 can be utilized. An important additional benefit is the possibility of bundling of subroutines and their parameters in modules. The advantages of this are easier maintenance of the code, removal of all COMMON structures, and automated internal checking of consistency of data types in parameter lists. This greatly simplifies maintenance of the code, and upgrades of numerical or physical approaches.

In principle, this conversion should have no impact on the model results. However, to optimally use FORTRAN 90 features, some parts of the codes have been reorganized. Furthermore, precalculation of mean parameters for entire grids, introduced for efficiently on vector machines, now has been dropped to promote model transparency and clarity of the code. Due to the different order in which some calculations are now performed, some minor model differences are expected.

2.2 Test results

As expected, the results of models 0 and A are essentially identical. The rms significant wave height differences between models at the buoy locations or along altimeter tracks are always much less than 0.01 m, which is acceptable considering the above discussed model changes. The similarity of model results is illustrated here only with the pdf's of the global NWW3 models against buoy and altimeter data, respectively, in Figs. 2.1 and 2.2, and with some arbitrary time series in Fig. 2.3.

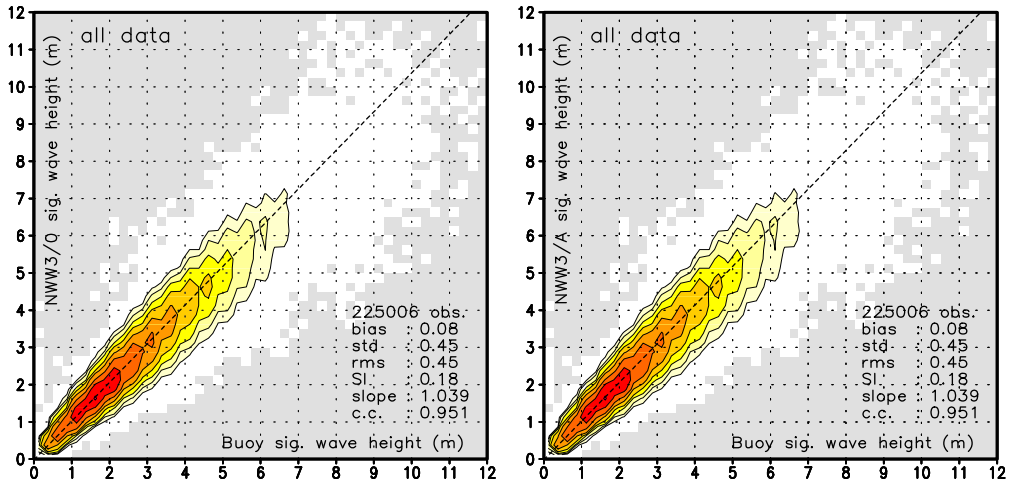

Fig. 2.1 : Probability density function (pdf) of model significant wave height H_s against buoy data and mean statistics. pdf resolution $\Delta H_s = 0.25$ m. Lowest contour at 0.005 m^{-2}. Contours increase by factor 2. Shaded area identifies no data. Left panel model NWW3/0, right panel model NWW3/A.

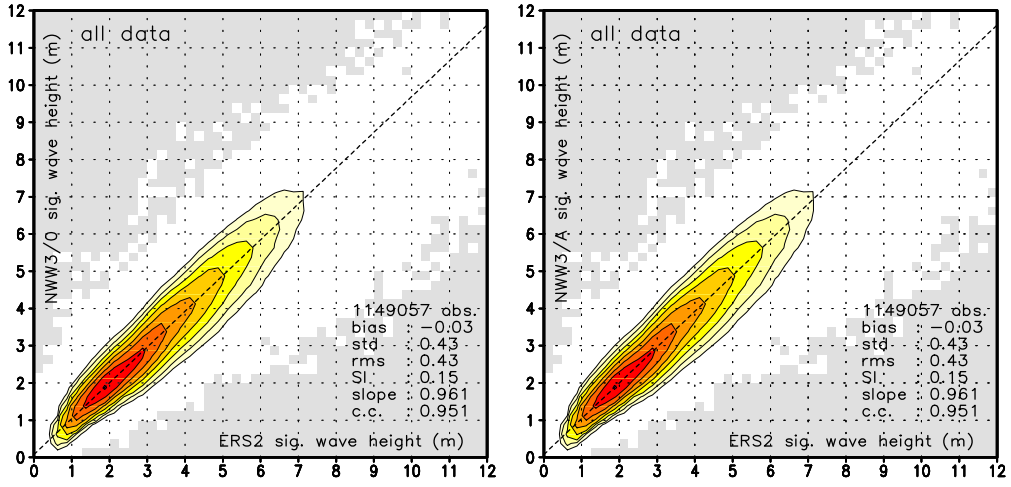

Fig. 2.2 : Like Fig. 2.1 for models against ERS-2 altimeter data.

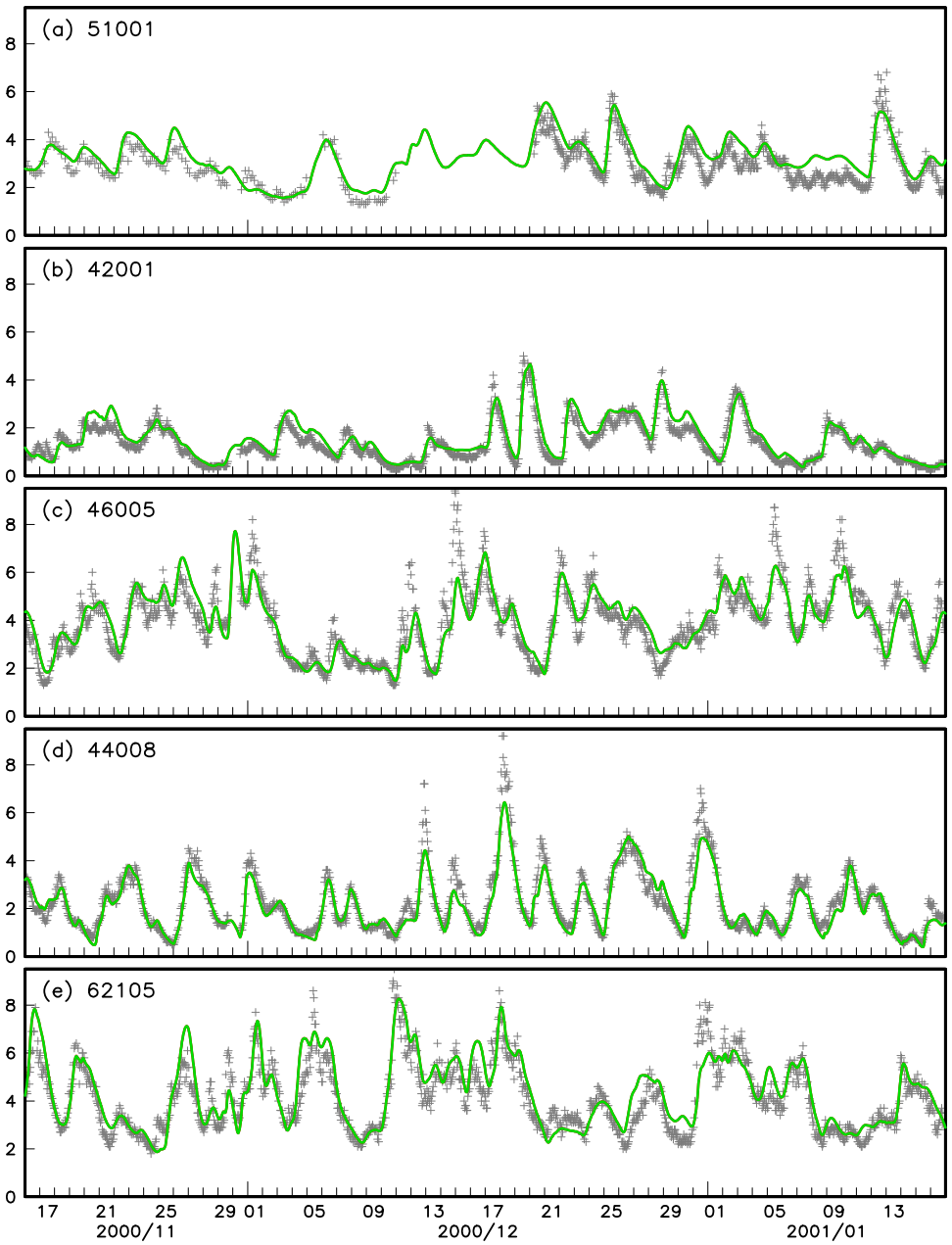

Fig. 2.3 : Selected time series of wave heights (H_s) observed at buoys (+), from model 0 (dashed or red lines) or model A (solid or green lines) for Nov. 17, 2000 through Jan. 16, 2001 for the global NWW3 model. Buoys as identified in panels. Note that model results in essence are identical.

3 Basic integration techniques

3.1 Description of changes

The WAVEWATCH III model solves the governing equation in fractional steps. In the source term integration step, the following equation is solved

$$\frac{\partial N(k,\theta)}{\partial t} = S(k,\theta) \quad , \tag{3.1}$$

where N is the spectrum, S represents the net source terms, and k and θ are the wavenumber and direction spanning spectral space. As in WAM, a semi-implicit integration scheme is used. In this scheme the discrete change of action density ΔN becomes (WAMDIG, 1988)

$$\Delta N(k,\theta) = \frac{S(k,\theta)}{1 - \epsilon D(k,\theta)\Delta t} \, , \tag{3.2}$$

where D represents the diagonal terms of the derivative of S with respect to N (WAMDIG, 1988, Eqs. 4.1 through 4.10). The parameter ϵ defines the offset of the scheme. Originally, $\epsilon = 0.5$ was implemented to obtain a second order accurate scheme.

The semi-implicit scheme is applied in the framework of a dynamic time-stepping scheme (Tolman, 1992). In this scheme, integration over the global time step can be performed in several dynamic time steps, depending on the net source term S, a maximum change of action density ΔN_m and the remaining time in the interval. Details of this scheme are not important here, and can be found in Tolman (1999) page 37.

The integration scheme (3.1) was introduced to allow for source term integration with large time steps. In its central form, with $\epsilon = 0.5$, however, it is notoriously noisy. As is shown by Hargreaves and Annan (1998, 2001), it is more appropriate to use $\epsilon = 1$ for extremely large time steps, because (3.1) then in essence becomes a Newton-Raphson root finder for the equilibrium. In WAVEWATCH III version 2.22, $\epsilon = 1$ has therefore been adopted. This change is not expected to result in large changes in model results. It will, however, result in smoother spectra, and therefore in a more economical dynamical integration method.

The dynamical integration scheme has three tunable parameters; X_p, X_r and X_f, see Tolman (1999, pages 37-38). In WAVEWATCH III version 1.18, no defaults where given. In model version 2.22, default values are set and are

given as $X_p = 0.15$, $X_r = 0.10$ and $X_f = 0.05$. These values differ slightly from settings used in the operational models at NCEP, but are not expected to result in significant model differences.

3.2 Test results

The impact of the above changes can be addressed by comparing the results of model versions B and A. Differences in general again proved to be small, but larger than in the previous section. A qualitative indication of the minor impact can be obtained from some selected time series as presented in Fig. 3.1. Maps from ERS-2 collocations, however, prove to give more insight.

Figures 3.2 through 3.4 show the model wave height biases ΔH_s against ERS-2 data for the entire year for the three models. Close inspection of these figures shows that the modified (B) model version (panels a) have systematically more positive biases throughout the domain in all three models. This might be expected because (i) the change in ϵ in Eq. (3.2) results in slightly higher growth rates in idealized conditions, and (ii) the new parameter settings in the dynamic time stepping algorithm have the same net effect.

Figures 3.5 through 3.7 show the model wave height scatter indices SI against ERS-2 data for the entire year for the three models. The (a) panels show the SI of the B model versions, the (b) panels show the changes from the A model versions to the B model versions. For all three models (NWW3, AKW, and WNA), the changes in scatter index between model versions (b panels of all figures) show alternating positive (ΔSI < 0) and negative impacts (ΔSI > 0). Considering that positive impact areas correspond to negative bias areas, the change of SI seems to be strongly related to the bias changes. Only for the AKW model in the north slope ice zones, the impact is systematically negative. Note that this corresponds to a very small part of the data, because this zone is only partially ice free for several months per year.

Figures 3.8 through 3.13 show the wave height joints pdf's and mean statistics of the models and altimeter or buoy data for the entire year for the three models. The left panels show he results for the old (A) model versions, the right panels for the new (B) model versions. For all models and data sources, the change to model version B results in a more positive bias and larger regression slope. Because regression slope already are too large in most cases in the A model versions, this generally leads to an increased rms and SI, and decreased c.c. All differences, however, are small.

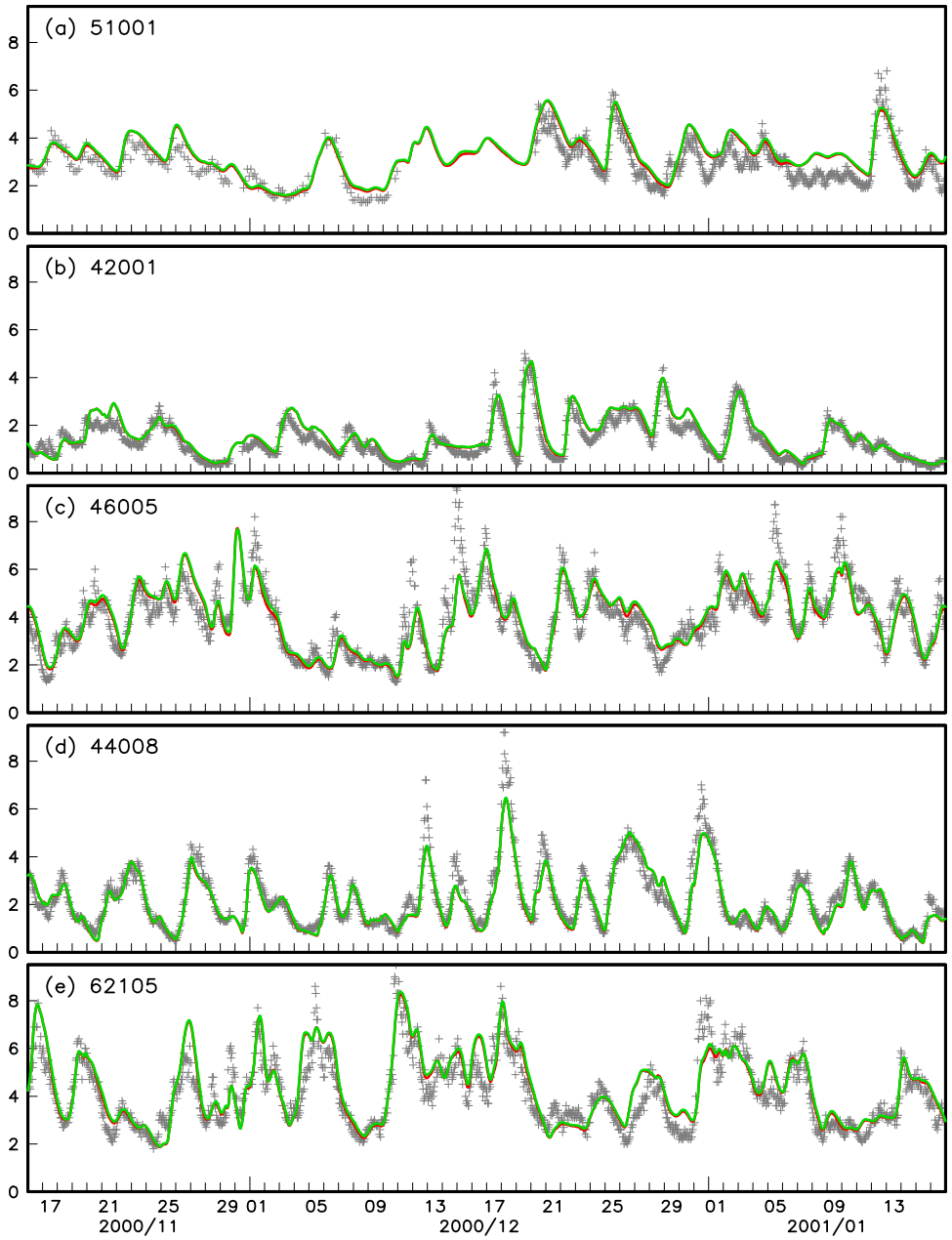

Fig. 3.1 : Selected time series of wave heights (H_s) observed at buoys (+), from model A (dashed or red lines) or model B (solid or green lines) for Nov. 16, 2000 through Jan. 16, 2001 for the global NWW3 model. Buoys as identified in panels.

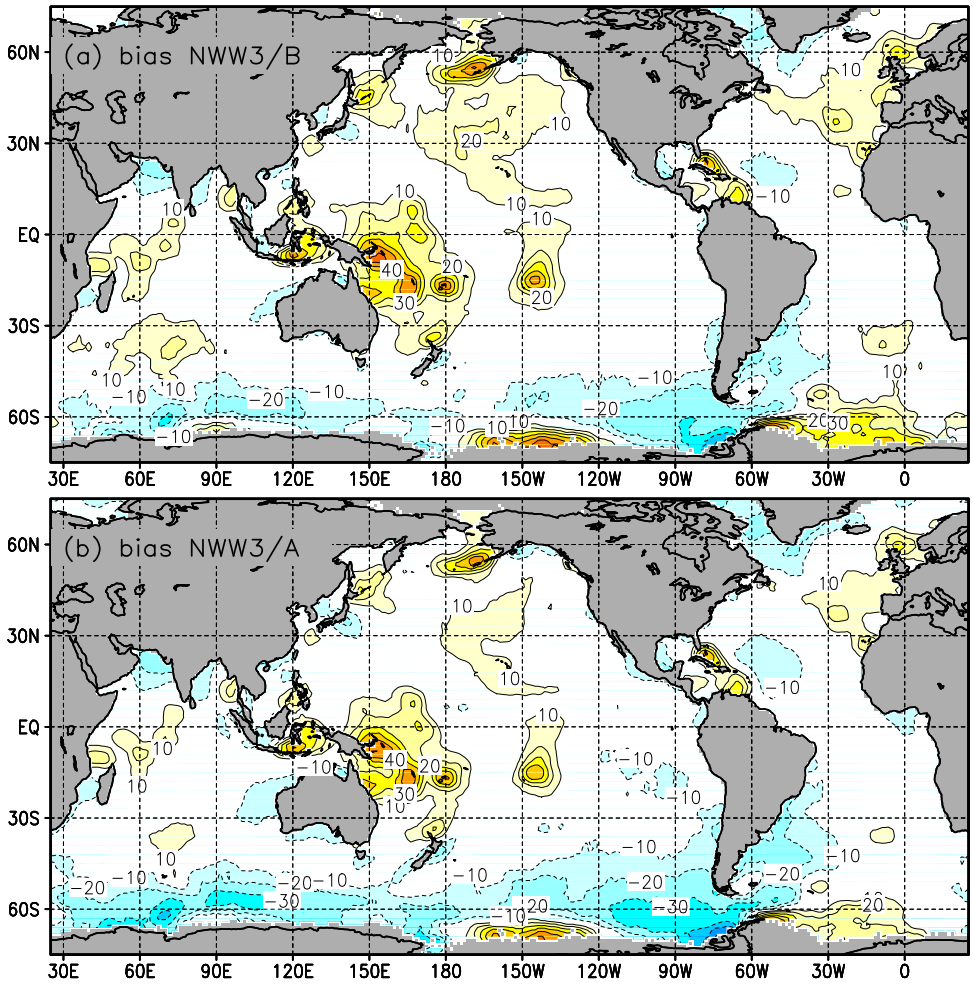

Fig. 3.2 : Bias ΔH_s in cm of models against ERS-2 wave height data. Dark gray identifies lack of data. Contours at 10 cm intervals. Dotted contours correspond to negative values, $\Delta H_s = 0$ contour not shown. Negative ΔH_s shaded light gray in black and white version. (a) NWW3/B, (b) NWW3/A.

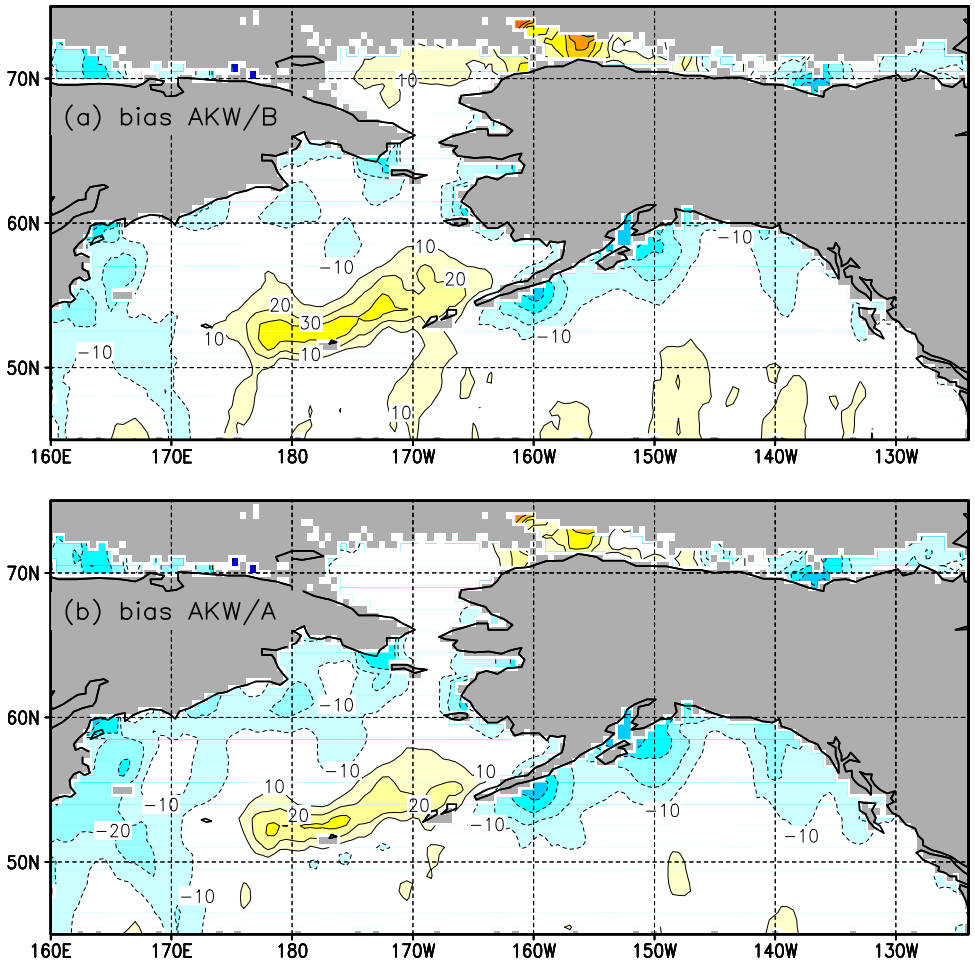

Fig. 3.3 : Biases like in Fig. 3.2 for regional AKW model.

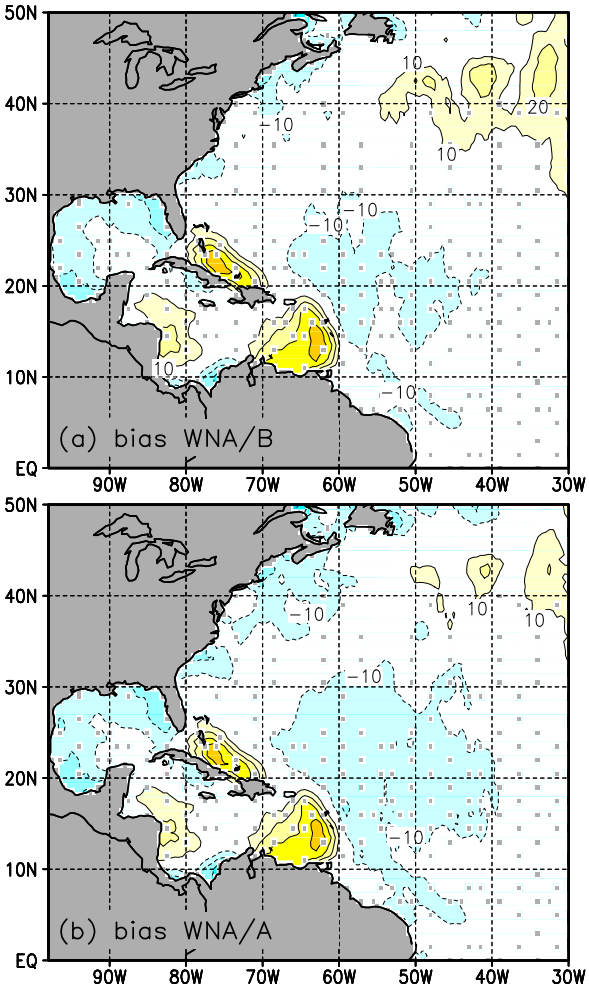

Fig. 3.4 : Biases like in Fig. 3.2 for regional WNA model.

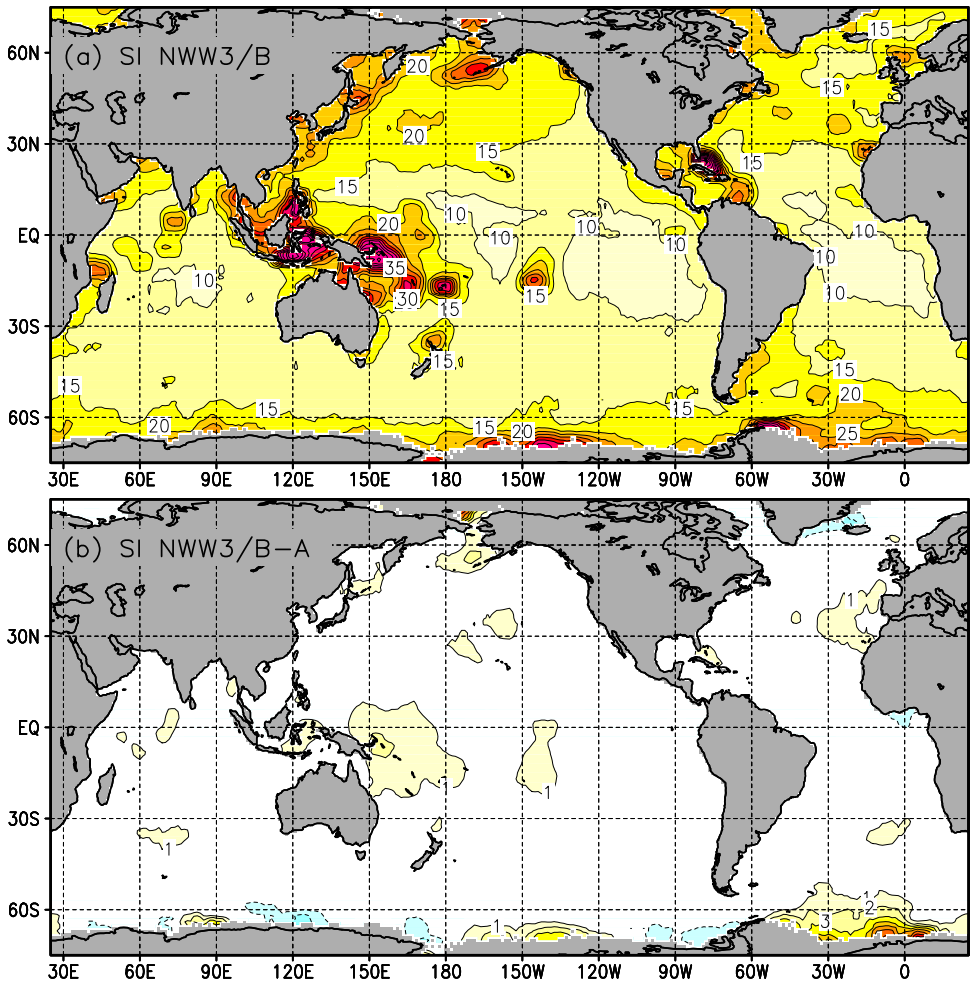

Fig. 3.5 : Scatter index (SI) in % of models against ERS-2 wave height data. Dark gray identifies lack of data. (a) NWW3/B model, contours at 5% intervals. (b) ΔSI = NWW3/B - NWW3/A, contours at 1% intervals. Dotted contours correspond to negative values, ΔSI = 0 contour not shown. Negative ΔSI shaded light gray in black and white version.

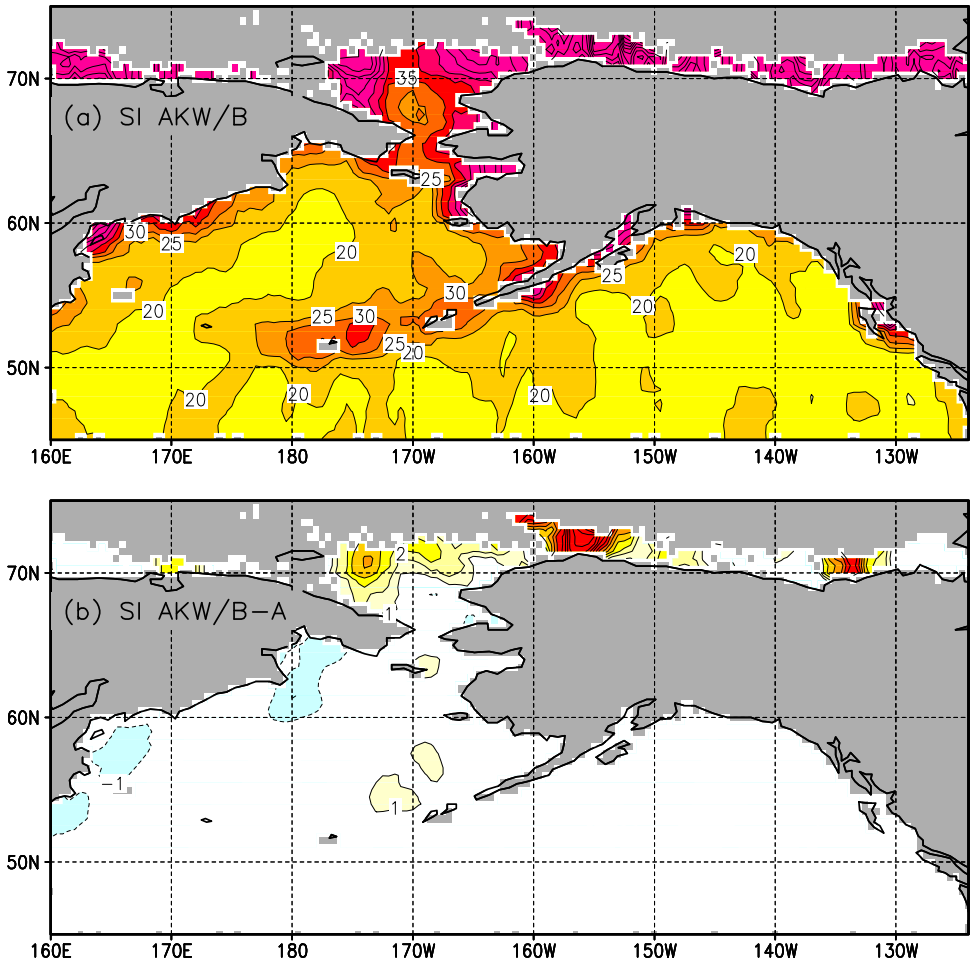

Fig. 3.6 : SI like in Fig. 3.5 for regional AKW model.

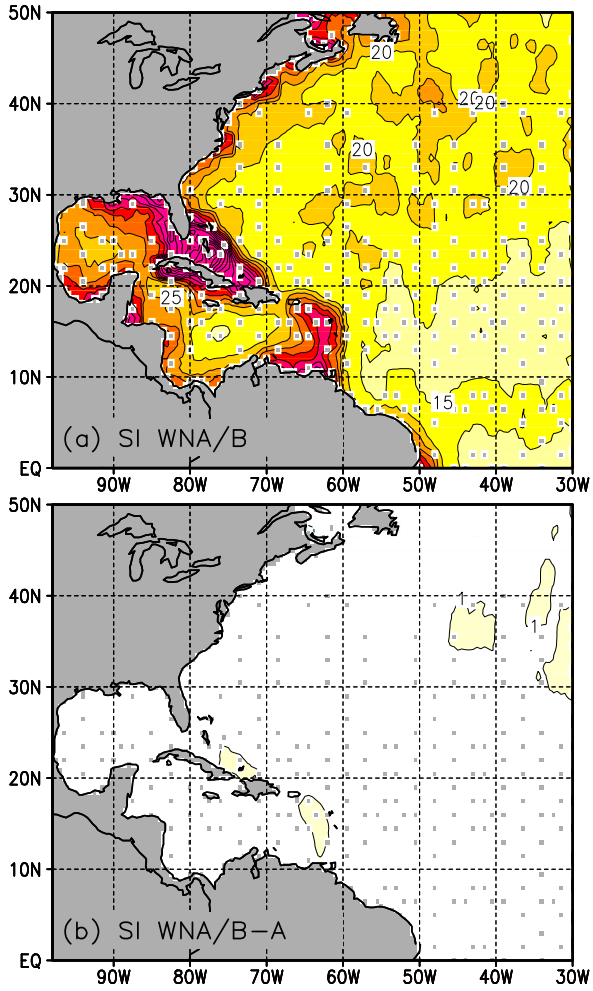

Fig. 3.7 : SI like in Fig. 3.5 for regional WNA model.

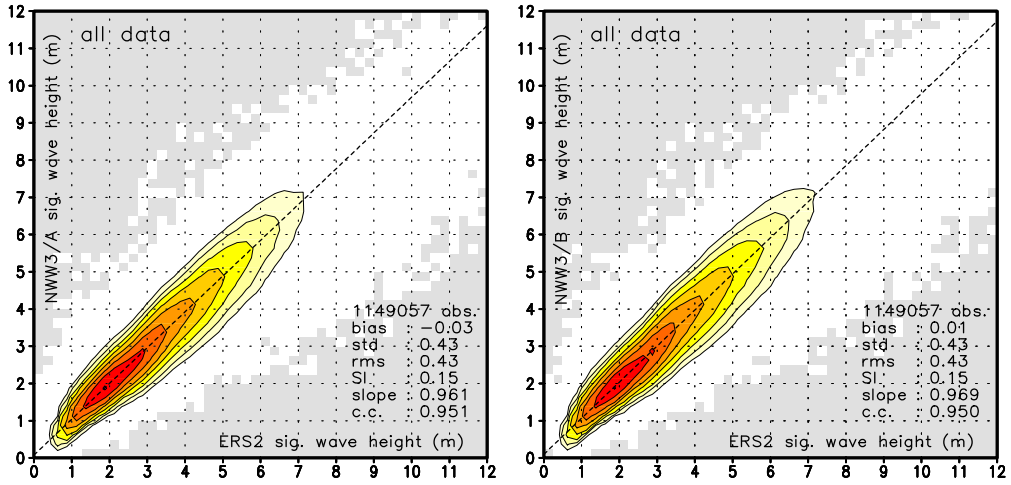

Fig. 3.8 : Probability density function (pdf) of model significant wave height H_s against ERS-2 altimeter data and mean statistics. pdf resolution $\Delta H_s = 0.25$ m. Lowest contour at 0.005 m^{-2}. Contours increase by factor 2. Shaded area identifies no data. Left panel model NWW3/A, right panel model NWW3/B

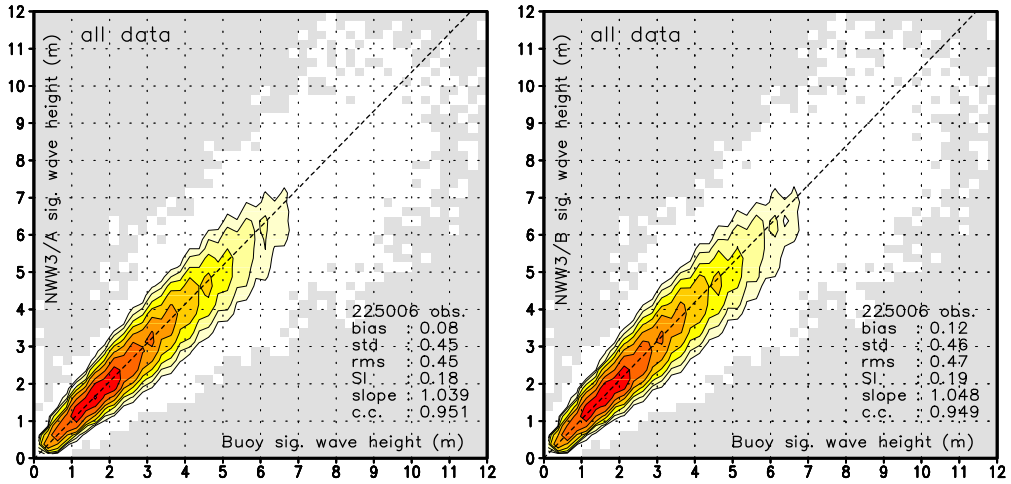

Fig. 3.9 : Probability density function (pdf) of model significant wave height H_s against buoy data and mean statistics, as in Fig. 3.8.

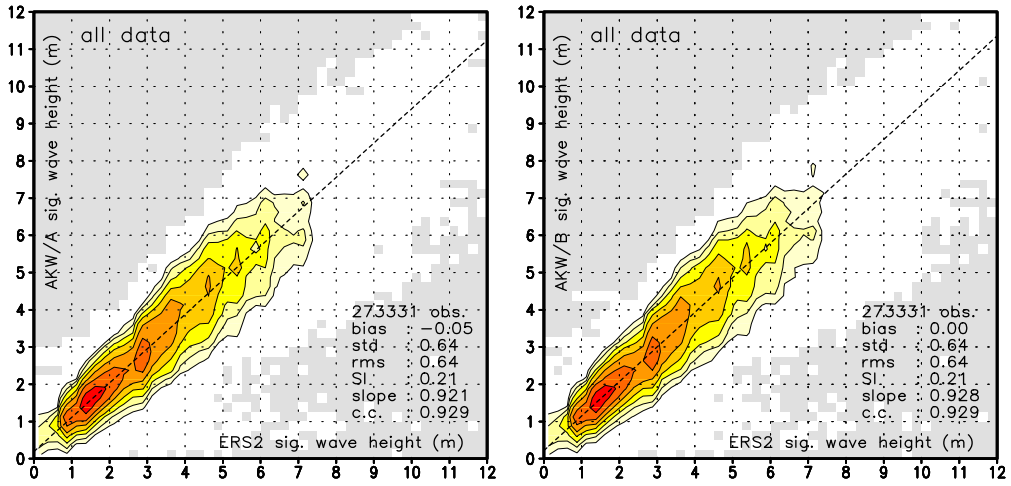

Fig. 3.10 : Like Fig. 3.8 for regional AKW model

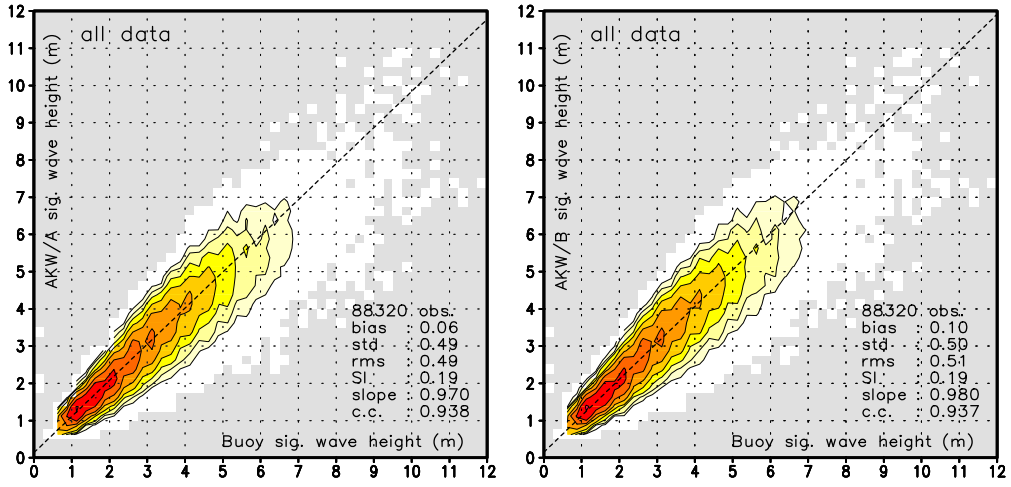

Fig. 3.11 : Like Fig. 3.9 for regional AKW model

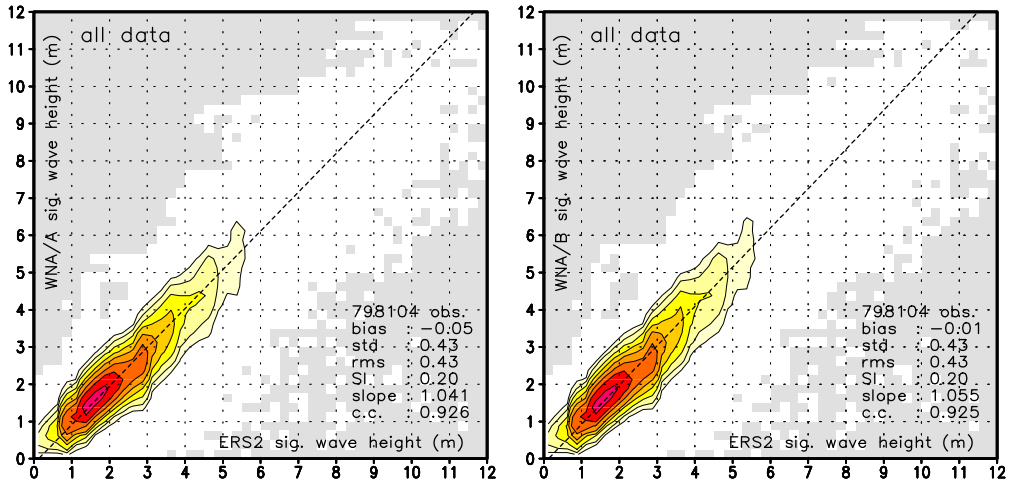

Fig. 3.12 : Like Fig. 3.8 for regional WNA model

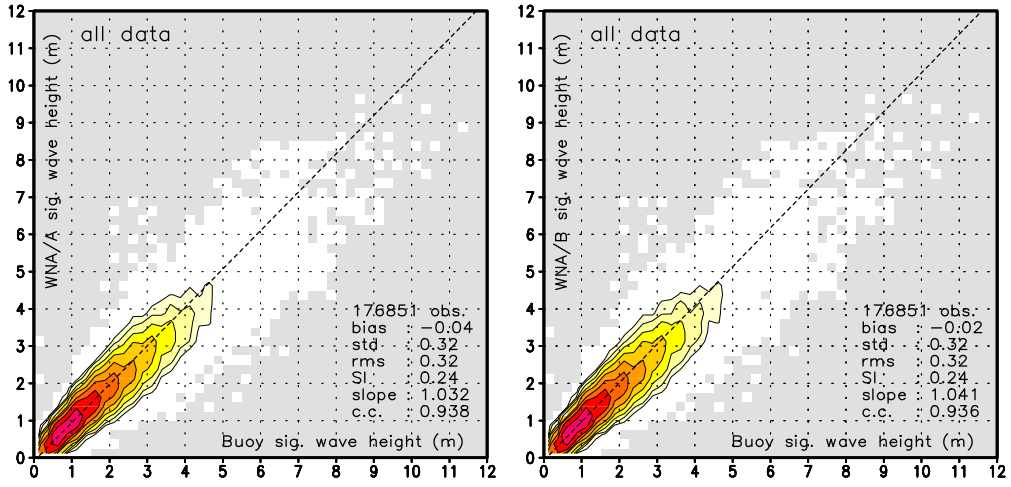

Fig. 3.13 : Like Fig. 3.9 for regional WNA model

4 GSE alleviation

4.1 Description of changes

In WAVEWATCH III, propagation in physical space is accounted for by solving the equation

$$\frac{\partial N}{\partial t} + \frac{\partial c_x N}{\partial x} + \frac{\partial c_y N}{\partial y} = 0 \quad , \tag{4.1}$$

where c_x and c_y are the advection velocities in physical space. This equation is solved for each discrete combination (k_i, θ_j) separately, where i and j are discrete grid counters. Each such individual spatial wave field travels in the mean direction and with the mean speed corresponding to the spectral bin (k_i, θ_j). When the spectral discretization $(\Delta k, \Delta\theta)$ is fairly coarse, as is common in operational models, this leads to he disintegration of continuous swell fields into discrete swell fields. This process is known as the Garden Sprinkler Effect (GSE). A more detail description of the GSE can be found in Booij and Holthuijsen (1987), or Tolman (1995, 2002a).

In WAVEWATCH III version 1.18, the GSE is removed using the method suggested by Booij and Holthuijsen (1987). Equation (4.1) is replaced by

$$\frac{\partial N}{\partial t} + \frac{\partial}{\partial x}\left[c_x N - D_{xx}\frac{\partial N}{\partial x}\right] + \frac{\partial}{\partial y}\left[c_y N - D_{yy}\frac{\partial N}{\partial y}\right] - 2D_{xy}\frac{\partial^2 N}{\partial x \partial y} = 0 \,, \tag{4.2}$$

where D_{xx}, D_{yy} and D_{xy} are the components of the diffusion tensor with main axis θ. The strength of the diffusion depends on the spectral resolution $(\Delta k, \Delta\theta)$, and on a user defined 'swell age' T_s. For details see Booij and Holthuijsen (1987) and Tolman (1999).

This GSE alleviation method has been used successfully in NCEP's operational implementation of WAVEWATCH III version 1.18. It has, however, a major disadvantage for high resolution models. In such models, choosing a sufficiently large T_s to remove the GSE negatively impacts numerical time steps of the model, and hence dramatically increases model run times (Tolman, 2001, 2002a).

A more economical way of dealing with the GSE for high-resolution models is to combine Eq. (4.1) with a spatial averaging technique. The area around discrete spatial grid points over which the averaging is performed is defined as

$$\pm\alpha_s \, \Delta c_g \, \Delta t \, \mathbf{e}_s \quad , \pm\alpha_n \, c_g \Delta\theta \, \Delta t \, \mathbf{e}_n \quad , \tag{4.3}$$

where $\mathbf{e}_s$ and $\mathbf{e}_n$ are unit vectors in the θ and normal direction, respectively, Δc_g is a range of group velocities corresponding to Δk, and α_s and α_n are tunable parameters. For details of this technique see Tolman (2002a). Due to the size and orientation of this averaging area, the resulting method is fairly similar to Eq. (4.2), but has no impact on numerical time steps. This method is marginally cheaper that the Booij and Holthuijsen method for large scale models, but dramatically cheaper for high resolution models.

The new averaging technique is the new default model setting for WAVEWATCH III version 2.22. In NCEP's operational models as used here it will be implemented with $\alpha_s = \alpha_n = 1.5$. The change from models versions B to C as identified in Table 1.1 reflects this change.

4.2 Test results

The impact of the above changes can be addressed by comparing the results of model versions C and B. Differences in general again proved to be small as expected, and generally smaller than in the previous section. The small differences make it less interesting to inspect individual time series at buoy locations. pdf's will also not be presented. Note that pdf's for all models B and C are presented in the figures of the previous and following sections.

The only notable differences occurred above 70° N and S. This can be explained because the diffusion in Eq. (4.2) is suppressed above these latitudes for increased numerical stability. Since such an adaptation is not needed in the averaging method, differences in models might be expected at such high latitudes. Indeed, Figs. 4.1 and 4.2, show negligible impact of these model changes, except for at high latitudes above 70° N and S.

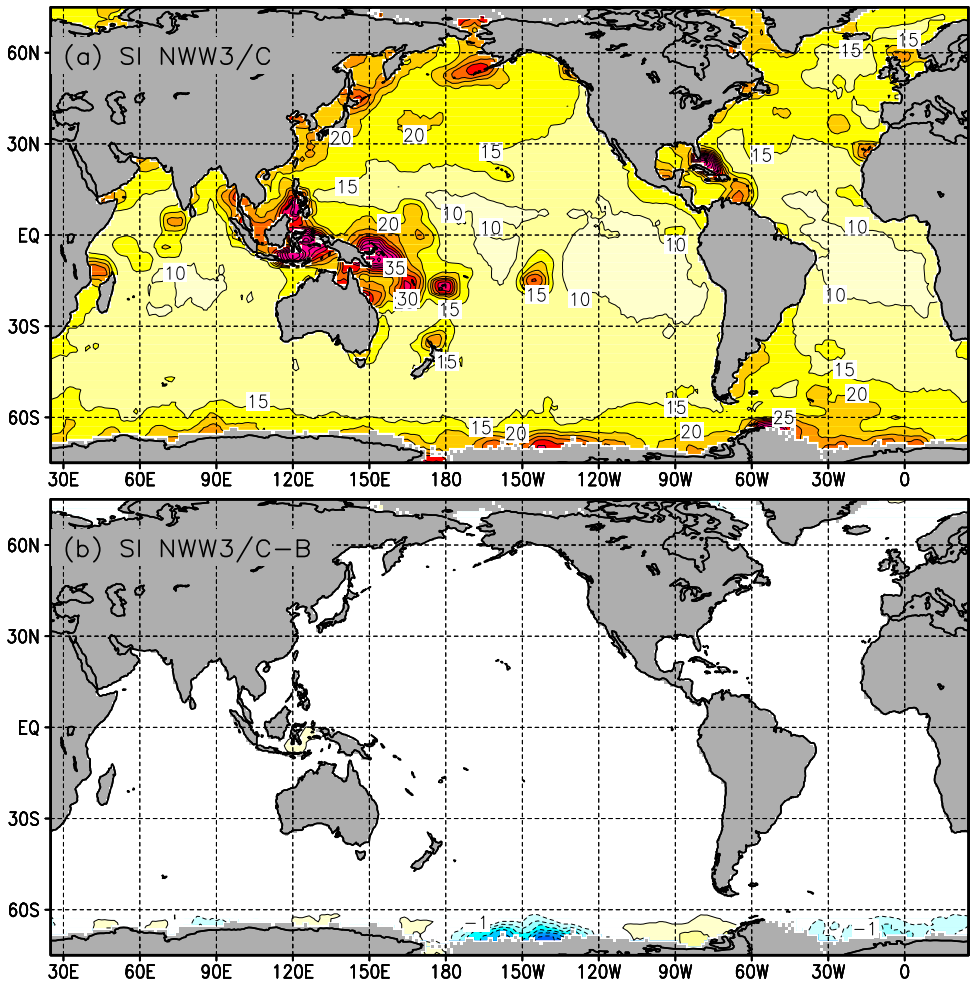

Fig. 4.1 : Scatter index (SI) in % of models against ERS-2 wave height data. Dark gray identifies lack of data. (a) NWW3/C model, contours at 5% intervals. (b) ΔSI = NWW3/C - NWW3/B, contours at 1% intervals. Dotted contours correspond to negative values, ΔSI = 0 contour not shown. Negative ΔSI shaded light gray in black and white version.

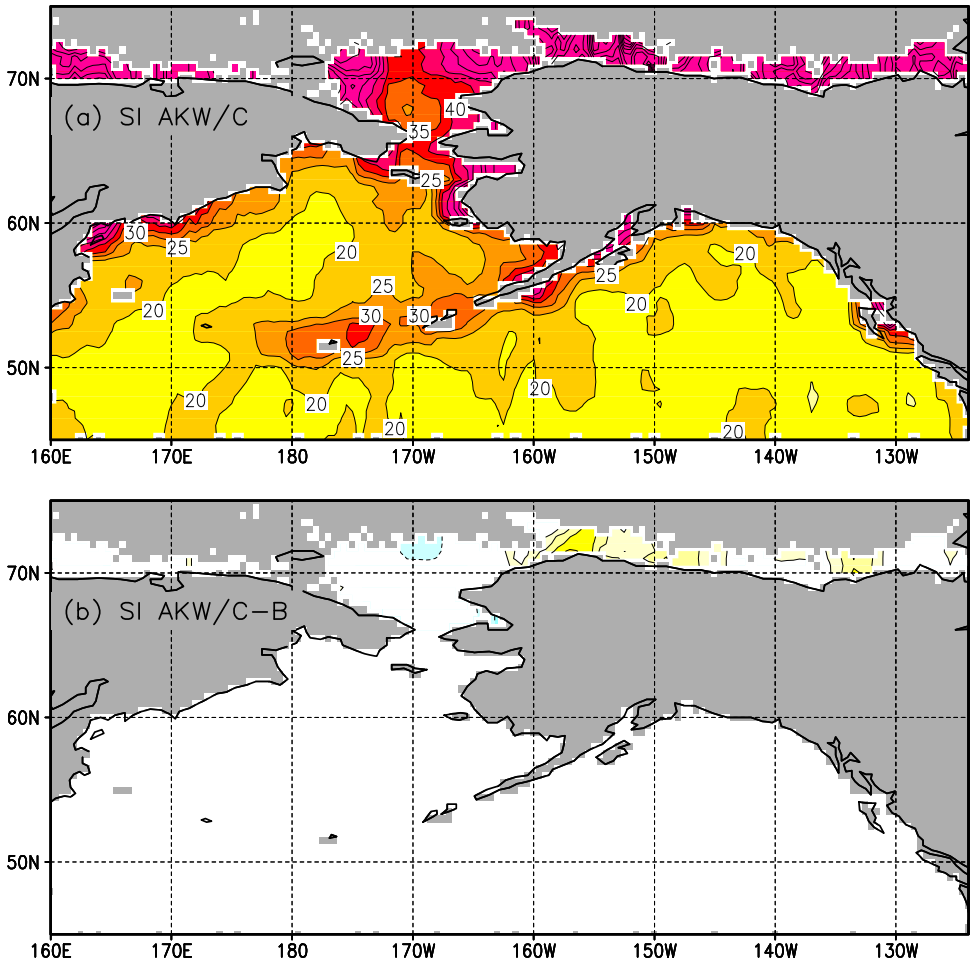

Fig. 4.2 : SI like in Fig. 4.1 for regional AKW model.

5 Sub-grid islands and ice treatment

5.1 Description of changes

In the biases and scatter indices of all three models against altimeter data as presented in the previous sections (see, e.g., Figs. 3.2 through 3.7), error distributions are for a large part dominated by 'bull's eye' type structures near unresolved islands and islands groups. This is in some more detail illustrated in Fig. 3 of Tolman (2001). On the coastlines of such islands swell energy is systematically dissipated. Yet in the model, such swell travels unhindered. Such islands can be modeled as sub-grid obstacles, similar to the approach introduced in the SWAN model (Holthuijsen et al., 2001).

The spatial propagation equation (4.1), for simplicity reduced to one dimension by removing the c_y term, is solved numerically in WAVEWATCH III by means of discrete cell boundary fluxes

$$N_i^{n+1} = N_i^n + \frac{\Delta t}{\Delta x} \left[\mathcal{N}_{i,-} - \mathcal{N}_{i,+} \right] \quad , \tag{5.1}$$

where i and n are discrete space and time counters, respectively, and where $\mathcal{N}_{i,-}$ is the discrete flux at the cell boundary between the grid points with counters i and $i-1$,

$$\mathcal{N}_{i,-} = 0.5 \left(c_{x,i-1} + c_{x,i} \right) F_b^n \quad , \tag{5.2}$$

where F_b is the spectral density at the cell boundary, as calculated according to the ULTIMATE QUICKEST scheme of Leonard (1979, 1991). $N_{i,+}$ is the flux at the cell boundary between grid points i and $i+1$, defined similarly, with $\mathcal{N}_{i,+} \equiv \mathcal{N}_{i+1,-}$. Sub-grid obstacles at cell boundaries can be included in Eq. (5.1) by changing this equation to

$$N_i^{n+1} = N_i^n + \frac{\Delta t}{\Delta x} \left[\alpha_{i,-} \mathcal{N}_{i,-} - \alpha_{i,+} \mathcal{N}_{i,+} \right] \quad , \tag{5.3}$$

where $\alpha_{i,-}$ and $\alpha_{i,+}$ are 'transparencies' of the corresponding cell boundaries, ranging from 0 (closed boundary) to 1 (no obstructions).

Generating the obstruction grids is a labor intensive task, that cannot be performed purely objectively. Fortunately, it only has to be performed once. A description of the techniques used to generate the NCEP wave model obstruction grids can be found in Tolman (2002b). Figures 5.1 through 5.4 show the resulting grids, whereas Table 5.1 shows some corresponding

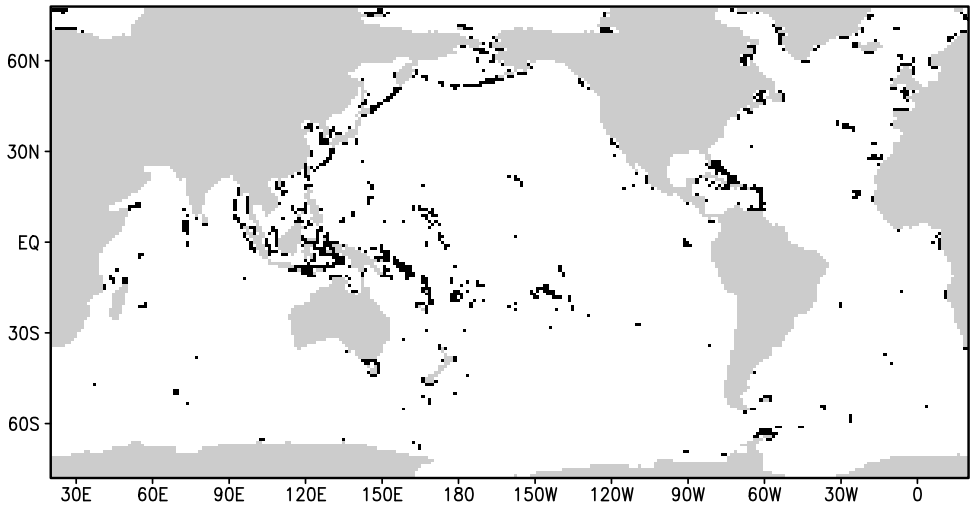

Fig. 5.1 : Grid layout of the global NWW3 wave model. Grey identifies land points, black identifies grid points with some obstruction in longitudinal or latitudinal direction ($\alpha \neq 1$). Note that this obstruction can be as small as 5%.

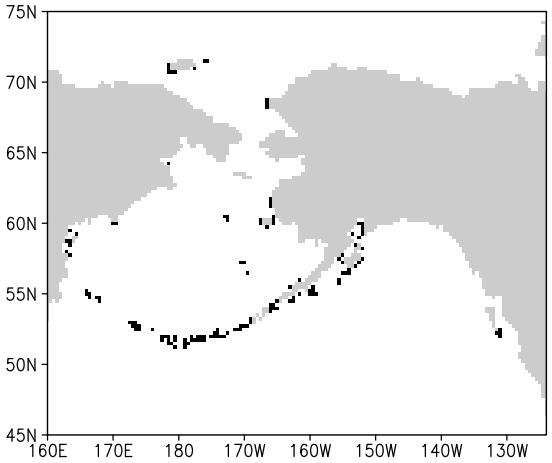

Fig. 5.2 : Like Fig. 5.1 for regional AKW model.

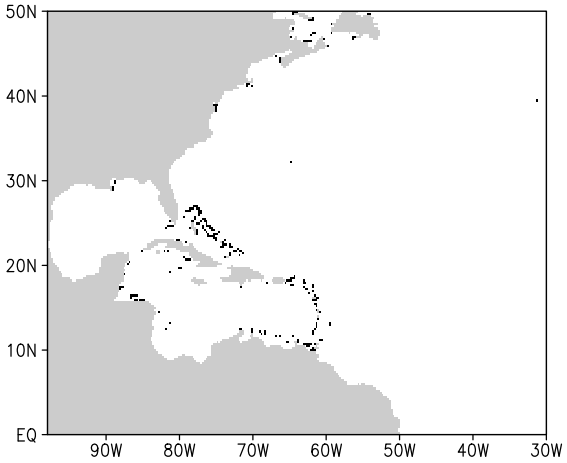

Fig. 5.3 : Like Fig. 5.1 for regional WNA model.

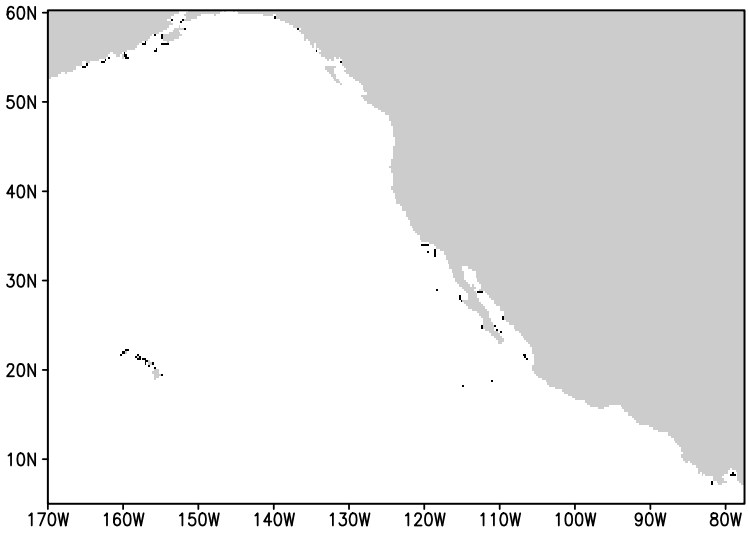

Fig. 5.4 : Like Fig. 5.1 for regional Eastern North Pacific (ENP) model.

Table 5.1: Grids of NCEP's wave models. Obstructed grid points identify all grid points where $\alpha \neq 1$ in longitudinal or latitudinal direction.

model	grid range	res.	# of grid points		
			total	sea	obstr.
NWW3	78°S - 78°N	1.00°	45,216	29,790	964 (3.2%)
	global	1.25°			
AKW	44.75°N - 75.25°N	0.25°	19,065	12,405	136 (1.1%)
	159.5°E - 123.5°W	0.50°			
WNA	0.25°S - 50.25°N	0.25°	55,825	36,379	231 (0.6%)
	98.25°W - 29.75°W	0.25°			
ENP	4.75°N - 60.50°N	0.25°	83,552	49,182	87 (0.2%)
	170.25°W - 77.25°W	0.25°			

grid statistics. For completeness of documentation, the grid for the newly introduced Eastern North Pacific (ENP) model is included.

Figures 5.1 through 5.4 shows that partially obstructed grid points are distinctly present (black in figures), and clearly identify major island groups. Nevertheless, they represent only about 3% of all sea points in the global model, and 1% or less in the regional models. Note furthermore, that even in the regional models, in spite of the higher model resolution, the partially obstructed grid points still represent major island groups.

The introduction of sub-grid obstacles to model unresolved islands also opens the way to model ice continuously. Defining the critical ice concentrations ϵ_0 and ϵ_n as the concentrations at which the obstruction of wave propagation by ice begins, and is complete, two local ice decay length scales l_0 and l_n are defined as

$$l_0 = \epsilon_{c,0} \min(\Delta x, \Delta y) \quad . \tag{5.4}$$

$$l_n = \epsilon_{c,n} \min(\Delta x, \Delta y) \quad . \tag{5.5}$$

The corresponding cell transparencies are then calculated as

$$\alpha_x = \frac{l_n - \epsilon \Delta x}{l_n - l_0} \quad , \tag{5.6}$$

$$\alpha_y = \frac{l_n - \epsilon \Delta y}{l_n - l_0} \quad , \tag{5.7}$$

Details of this method to continuously model ice can also be found in Tolman (2002b). The island and ice transparencies for a given grid cell are combined by multiplication of the individual transparencies. In the regional models critical ice concentrations $\epsilon_{c.0} = 0.25$ and $\epsilon_{c,n} = 0.75$ are used. After some more testing since Tolman (2002b), critical ice concentrations $\epsilon_{c.0} = 0.33$ and $\epsilon_{c,n} = 0.67$ are used in the global model.

5.2 Test results

The impact of the above changes can be addressed by comparing the results of model versions D and C. Results of the previous sections indicate that the effects of unresolved islands are geographically limited to an area fairly close to such islands. Similarly, the effects of continuous ice treatment are expected to be largely confined to the marginal ice zones. Because buoys are generally located outside such areas, buoy data is not very useful to assess the systematic impact of the sub-grid approaches introduced here. It is therefore more prudent to consider altimeter data first.

Figures 5.5 through 5.7 show the model wave height biases ΔH_s against ERS-2 data for the entire year for the three models. The global model (Fig. 5.5) shows dramatic differences between the two model biases. The model without sub-grid representation of islands (Fig. 5.5b) shows large positive biases at many unresolved islands and islands groups (compare Fig. 5.1). In the model with sub-grid representation of islands (Fig. 5.5a), the bull's eye patterns of positive biases have been removed almost completely. In the lower latitudes, the remaining biases are systematically negative but moderate. The impact of the continuous treatment of ice is limited to higher latitudes, and does not appear to be obvious in the global model.

In the AKW model (Fig. 5.6), similar observations can be made. Without sub-grid island representation (Fig. 5.6b), the Aleutian islands are associated with a distinct positive bias. In the model with sub-grid island representation (Fig. 5.6a), the positive bias is replaced by a slightly increased negative bias, compared to a systematic negative bias in the Bering Sea. Bias patterns in the ice covered areas (North of say 65°N), do not appear to be distinctly influenced.

In the WNA model (Fig. 5.7), severe positive biases related to the lesser Antilles and the Bahamas in the model without sub-grid representation of

islands (Fig. 5.7a), also have been virtually eliminated in the model with sub-grid representation (Fig. 5.7a). This model has virtually no seasonal ice coverage.

Figures 5.8 through 5.10 show the model wave height scatter indices SI against ERS-2 data for the entire year for the three models. The (a) panels show the SI of the D model versions, the (b) panels show the changes from the C model versions to the D model versions. The differences in SI patterns (b panels) closely correspond to the eliminated positive bias patterns in the previous figures. The impacts are clearly local and dramatic.

In the NWW3 model (Fig. 5.8), many islands locations are associated with reduction of SI by well over 0.1. For the Tuamotu Archipelago (in the NWW3 model 140°W, 15°S), the SI is reduced from over 0.35 to below 0.15! Near the Equator, several distinct areas with a moderately increased errors are found. This appears to be also related to bias patterns; here the near zero biases have become systematic negative biases (Fig. 5.5). In the ice covered regions, impact of the continuous ice treatment is alternately positive and negative.

In the AKW model (Fig. 5.9), the model improvement for the central Aleutians for the SI also surpasses 0.1. Contrary to in the global model, the effects of continuous ice treatment are here systematically positive (all impact north of 65°N can be attributed to continuous ice treatment alone).

In the WNA model (Fig. 5.10) similar improvements are found around the lesser Antilles and the Bahamas. Note that the remaining SI in the Bahamas and in the eastern Gulf of Mexico remain large. This is at least in part due to the fact that average wave height in this area are notoriously low. The normalization in the SI therefore generally results in large relative errors, even if absolute errors are still moderate. As mentioned above, ice is not an issue in this model.

Figures 5.5 through 5.10 show dramatic but localized impacts of the addition of sub-grid treatment of islands and ice to the model. It is therefore expected that the impact on overall statistics is limited. This in illustrated in Figs. 5.11 through 5.13 for all three models against the ERS-2 data. All models show a minimal impact of the changes on bulk model statistics. Most notable are systematic lower shift of biases, and the systematic increase of the correlation coefficient. The later, however, is negligible except for the statistics for the tropics in the global NWW3 model (third set of panels in Fig. 5.11).

The bulk statistics against buoy data (Figs. 5.14 through 5.16) show even

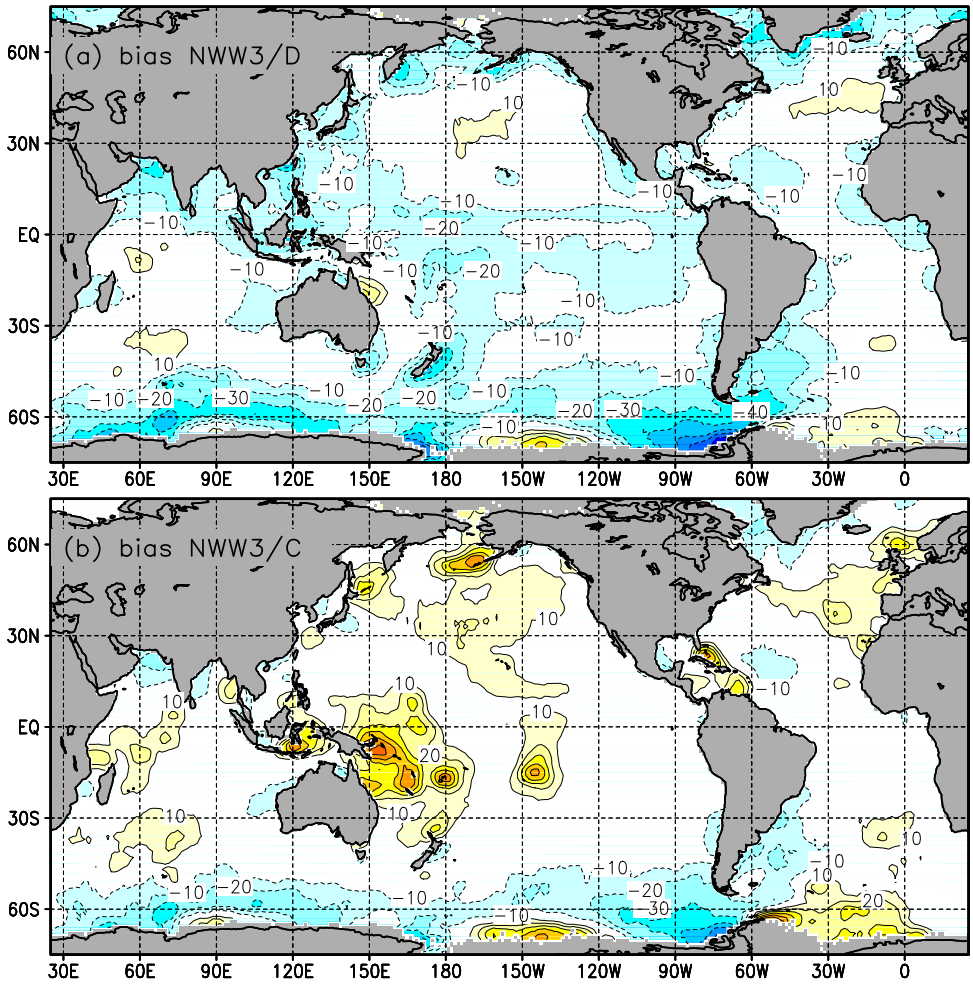

Fig. 5.5 : Bias ΔH_s in cm of models against ERS-2 wave height data. Dark gray identifies lack of data. Contours at 10 cm intervals. Dotted contours correspond to negative values, $\Delta H_s = 0$ contour not shown. Negative ΔH_s shaded light gray in black and white version. (a) NWW3/D, (b) NWW3/C.

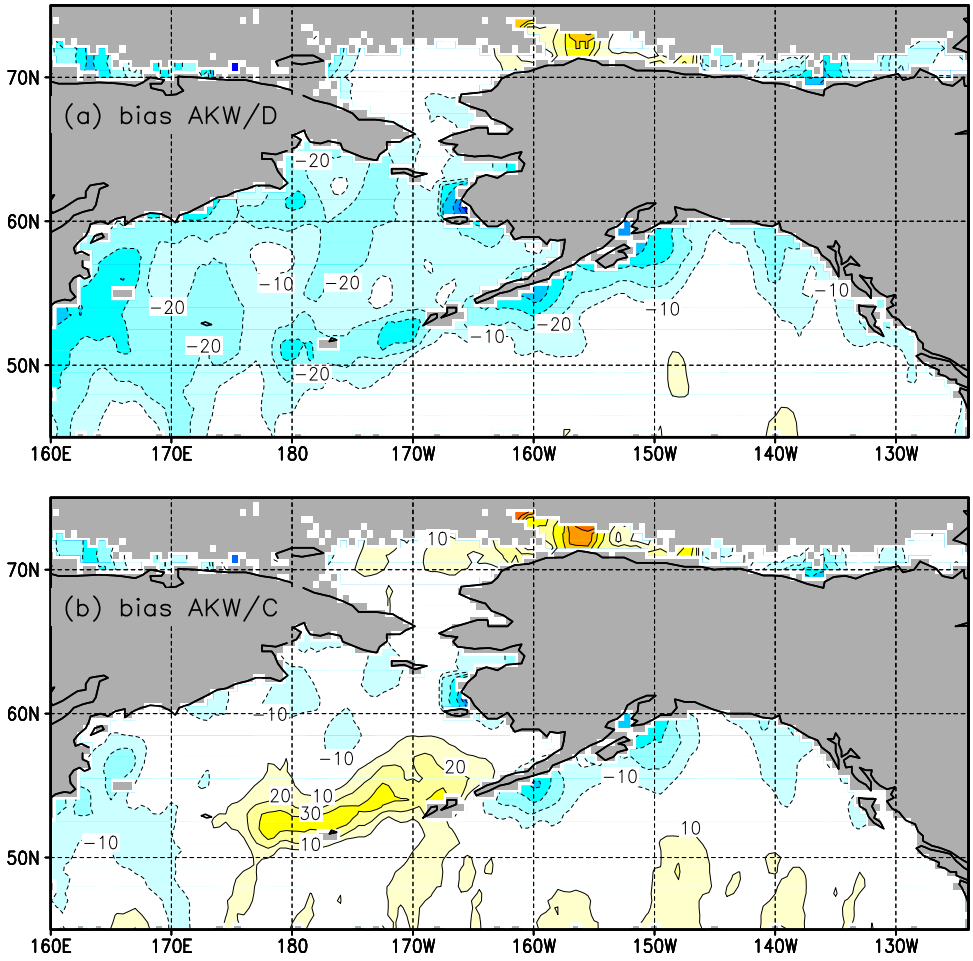

Fig. 5.6 : Biases like in Fig. 5.5 for regional AKW model.

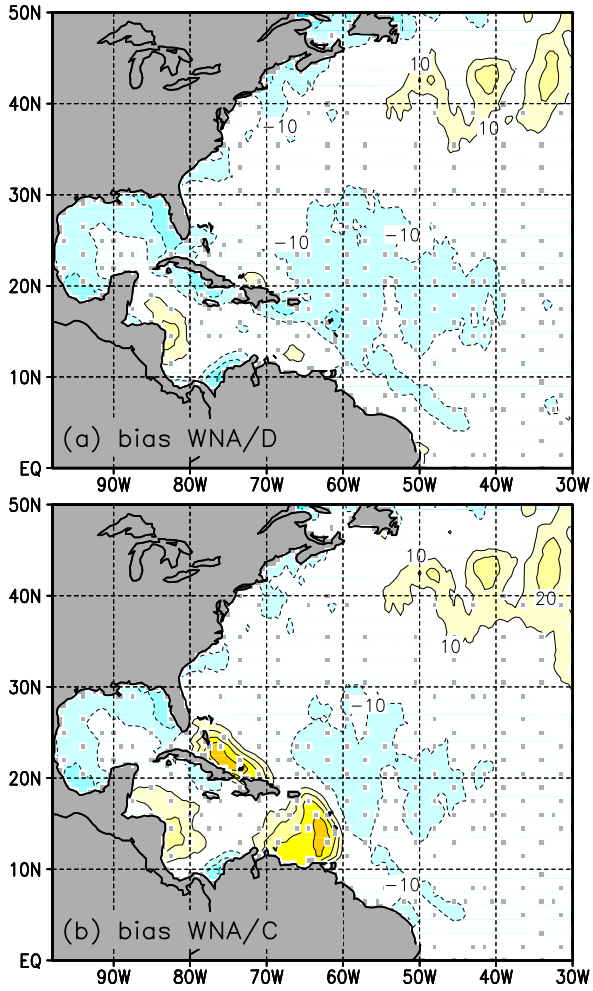

Fig. 5.7 : Biases like in Fig. 5.5 for regional WNA model.

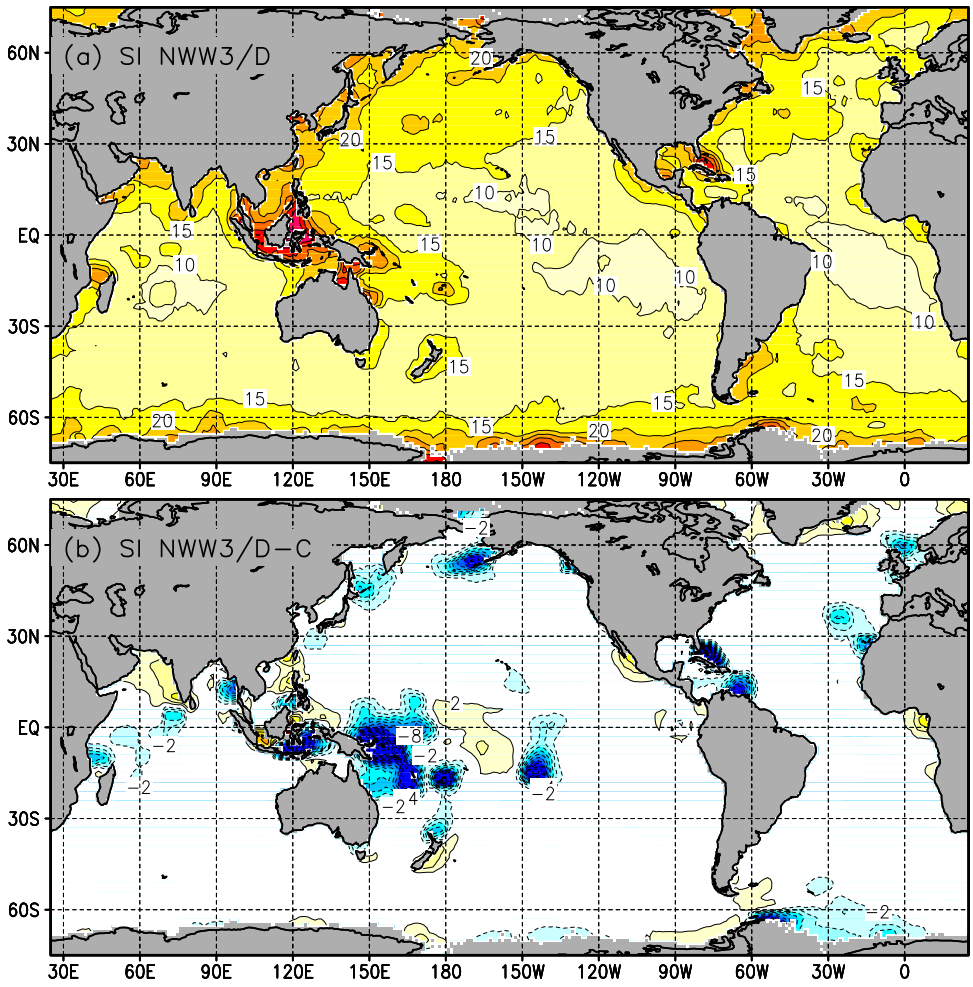

Fig. 5.8 : Scatter index (SI) in % of models against ERS-2 wave height data. Dark gray identifies lack of data. (a) NWW3/D model, contours at 5% intervals. (b) ΔSI = NWW3/D - NWW3/C, contours at 2% intervals. Dotted contours correspond to negative values, ΔSI = 0 contour not shown. Negative ΔSI shaded light gray in black and white version.

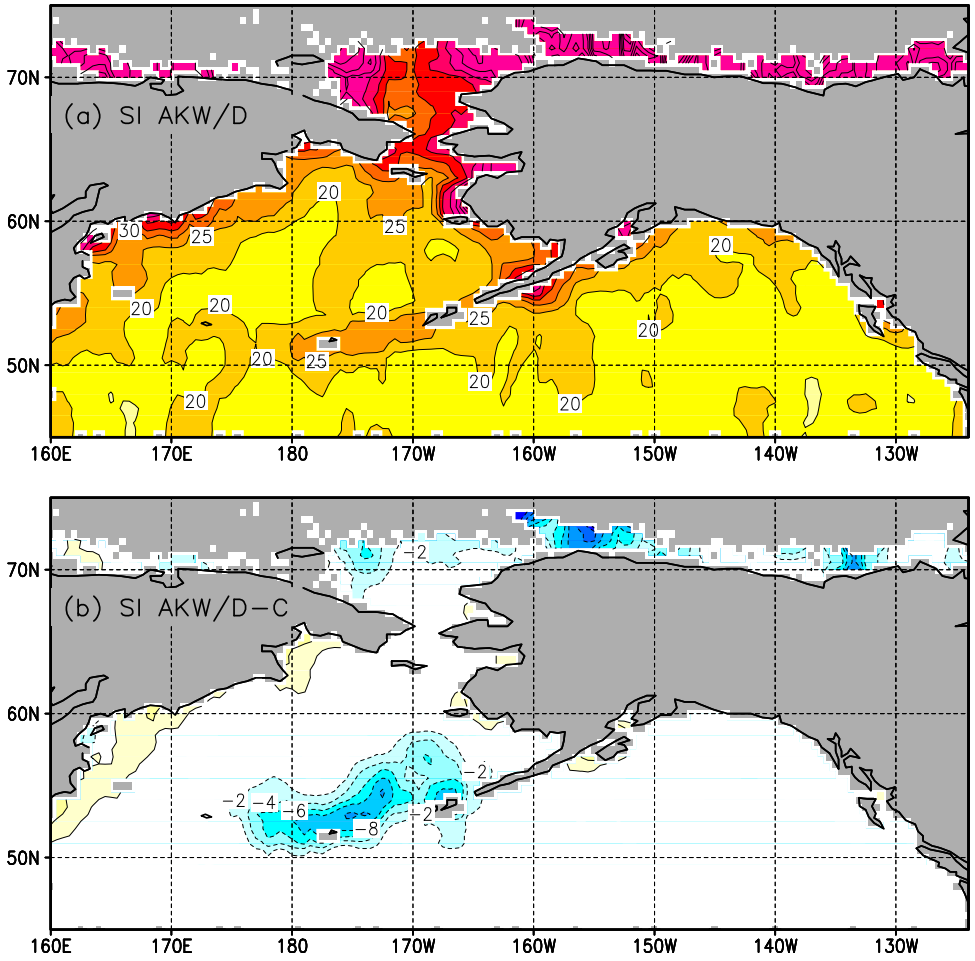

Fig. 5.9 : SI like in Fig. 5.8 for regional AKW model.

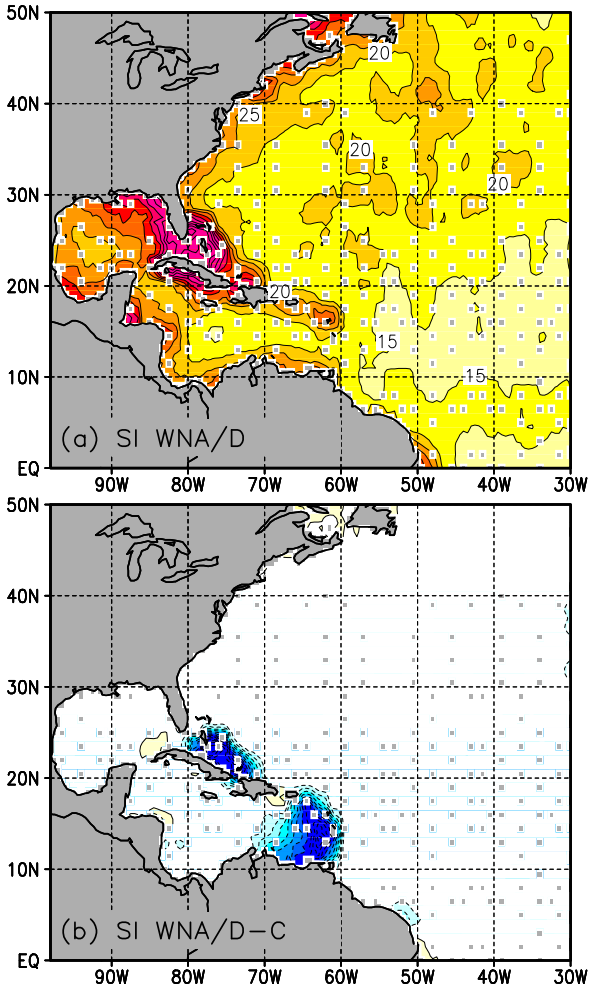

Fig. 5.10 : SI like in Fig. 5.8 for regional WNA model.

less differences, except for the systematic shift in biases. This could be expected, because in general the buoy locations are highly unrepresentative for showing the effects of the present sub-grid processes due to their location. The only exception occurs for the Hawaiian group of buoys (lower panels in Fig. 5.14), where all errors are reduced.

Finally, some time series of model results and buoy data will be presented for buoys at which the sub-grid island (and ice) treatment does have a notable effect.

In the global model, the Japanese buoys 21004 and 22001 straddle the Ryukyu Islands, with buoy 22001 being most sheltered inside the East China Sea (see Fig. 1.1). Figure 5.17 shows time series of wave heights H_s for both buoys for July and August 2000. For buoy 21004, which is located in the deep ocean, the impact of the sub-grid island treatment is small. For the more sheltered buoy 22001, the impact is much more substantial, and generally shows significantly improved model behavior for low wave conditions. This might be expected as low wave conditions are likely to be dominated by swell, and are therefore potentially sensitive to the model changes. Note the poor model behavior for 22001 around August 9. This is due to a tropical cyclone, which was not properly addressed in the GDAS, as is illustrated with wind speeds U_{10} in Fig. 5.18.

In the global model, the NE Pacific buoys are generally not influenced by the sub-grid islands or ice treatment (see Figs. 1.1 and 5.1). The only exception on both accounts can be expected for the Bering Sea buoy 46035. Indeed, for this location a systematic impact of sub grid island modeling is found, in particular for the swell dominated months. This is illustrated in Fig. 5.19 for the months April through June 2000. Obviously, the model changes result in improved model behavior for in particular low wave height conditions.

All buoys around Hawaii in the global model are potentially influenced by the sub grid modeling of Hawaii (see Fig. 1.1). For these buoys a distinctly different behavior can be expected for summer or winter conditions.

Figure 5.20 shows wave height time series for all for buoys for the summer months. In these months, wave fields are dominated by trade wind related wind seas from the east, and swells from the southern hemisphere. In such conditions, buoy 51004 is least sheltered, and indeed shows the least impact of model changes. Generally the explicit inclusion of Hawaii and other islands results in a systematic negative bias, consistent with the altimeter results (Fig. 5.5).

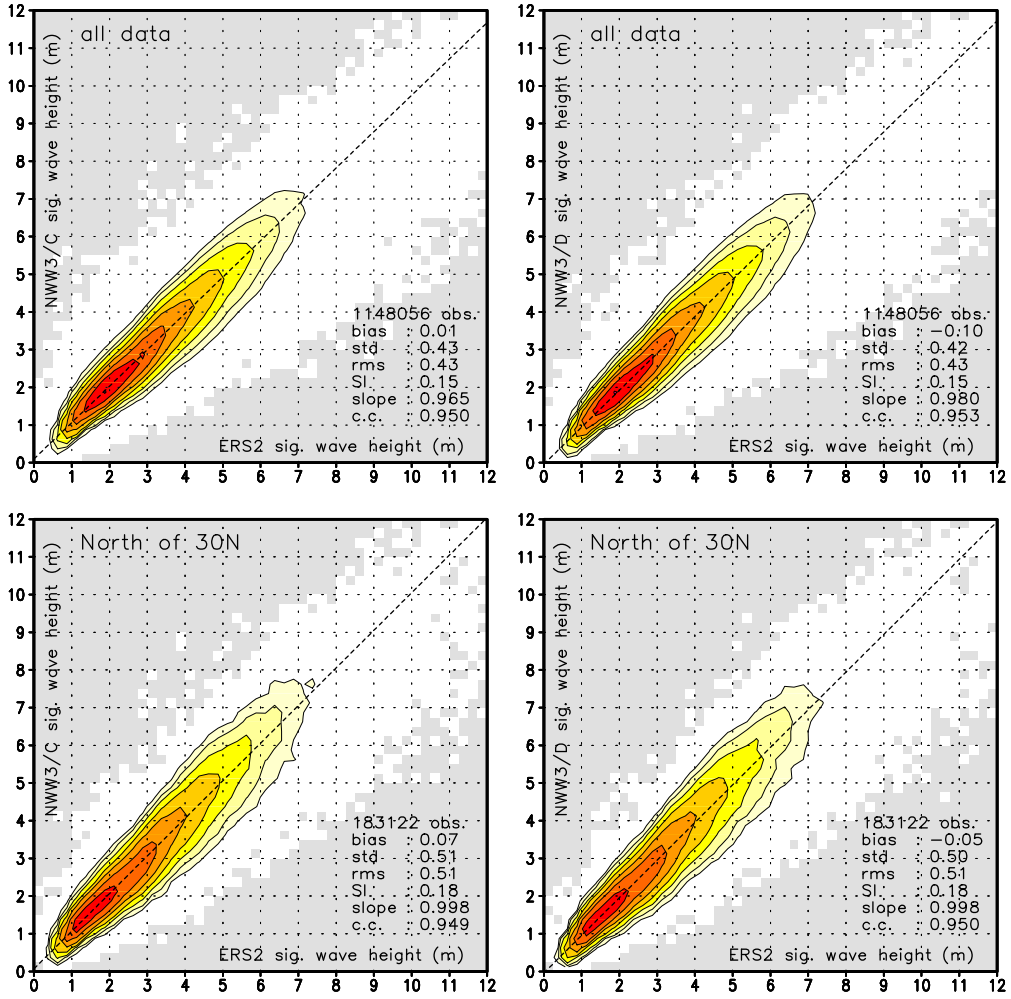

Fig. 5.11 : Probability density function (pdf) of model significant wave height H_s against ERS-2 altimeter data and mean statistics. pdf resolution $\Delta H_s = 0.25$ m. Lowest contour at 0.005 m^{-2}. Contours increase by factor 2. Shaded area identifies no data. Left panels model NWW3/C, right panels model NWW3/D. Data as identified in panels.

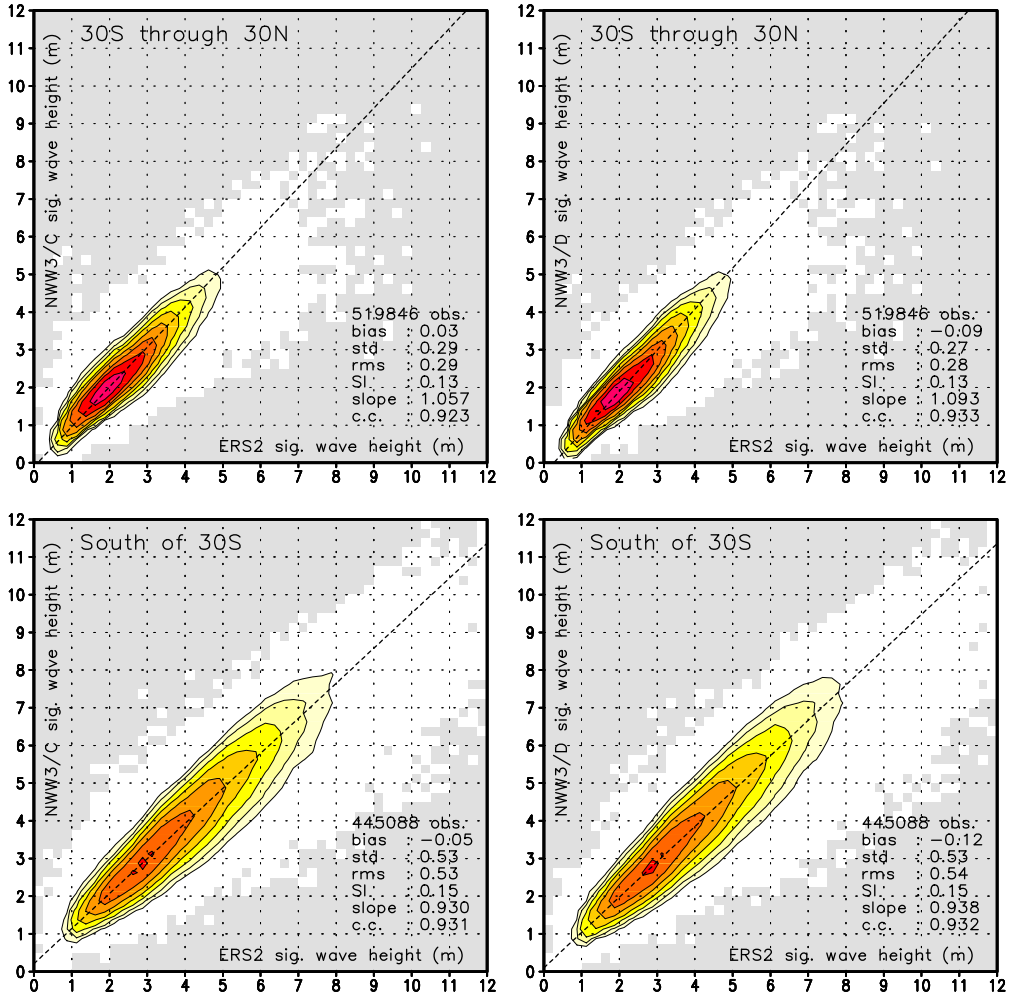

Fig. 5.11 continued.

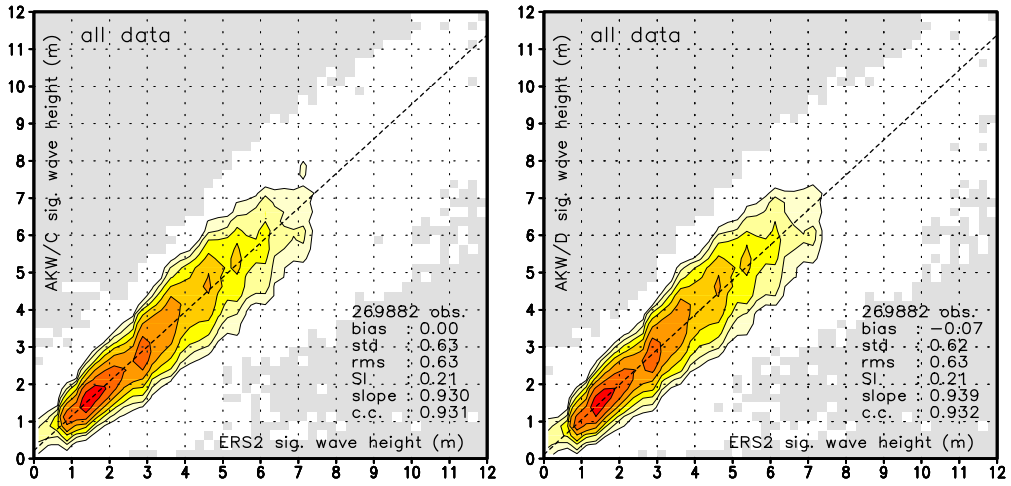

Fig. 5.12 : Like Fig. 5.11 for regional AKW model.

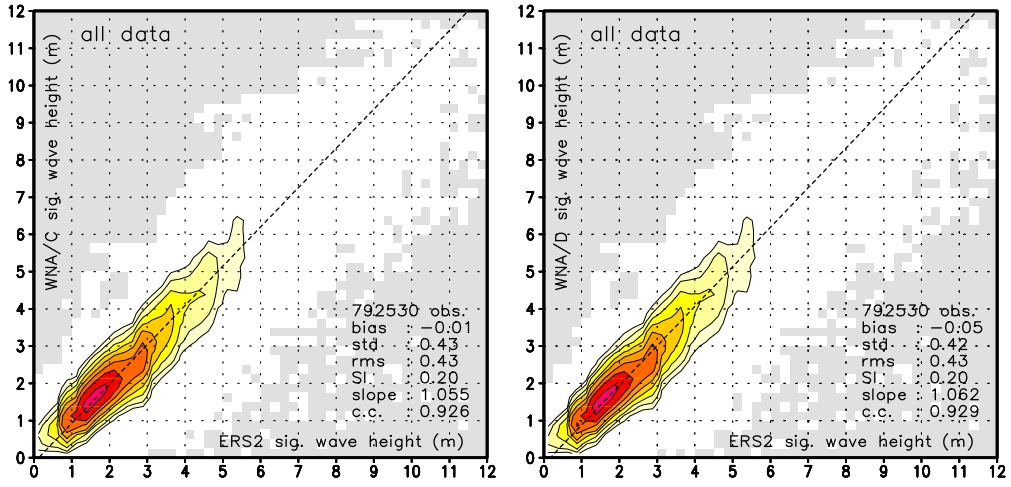

Fig. 5.13 : Like Fig. 5.13 for regional wna model.

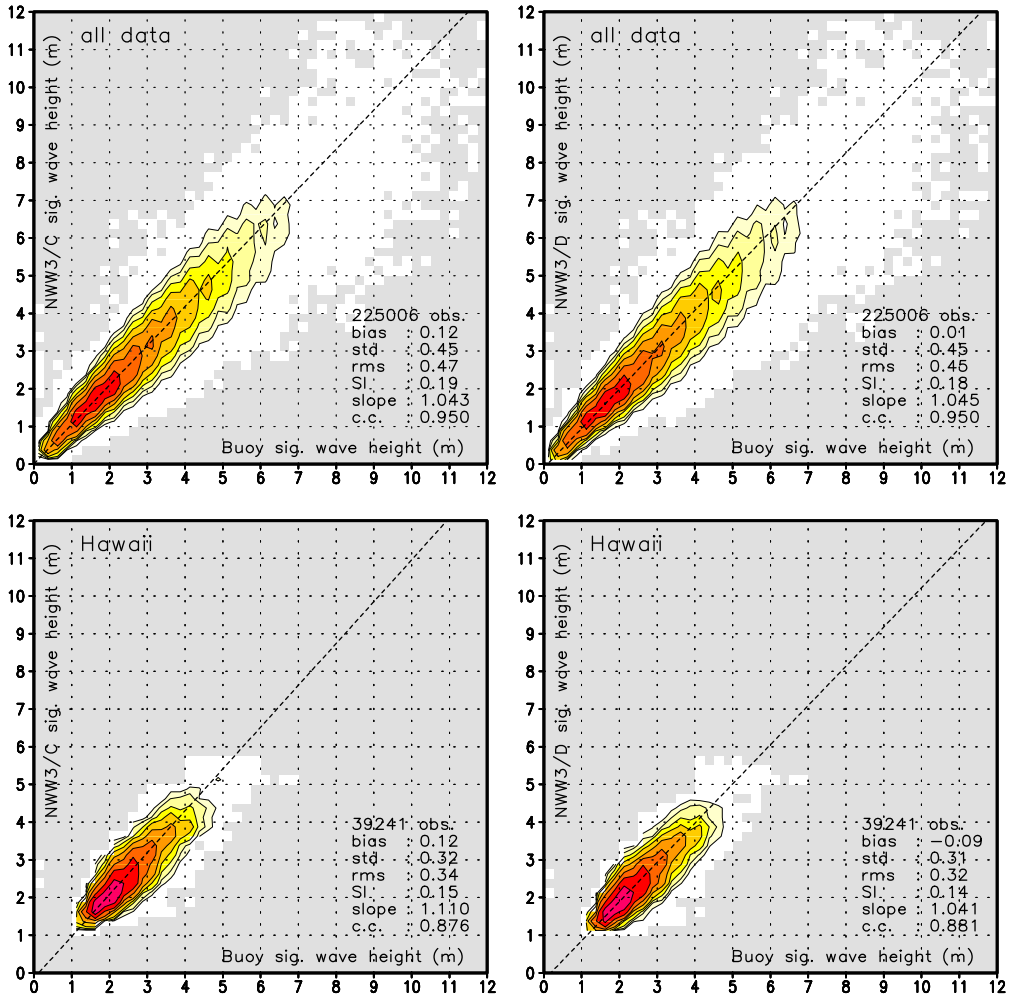

Fig. 5.14 : Like Fig. 5.11 for buoy data in global NWW3 model.

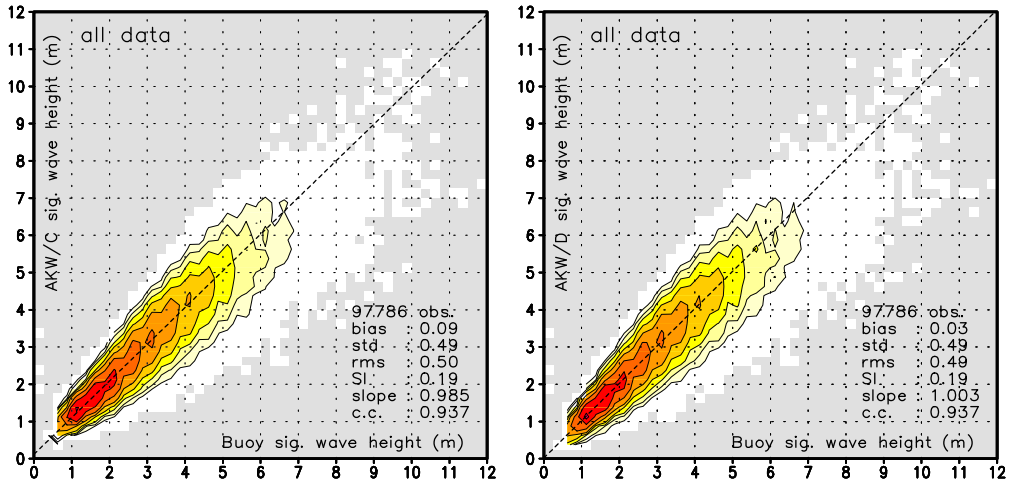

Fig. 5.15 : Like Fig. 5.14 for regional AKW model.

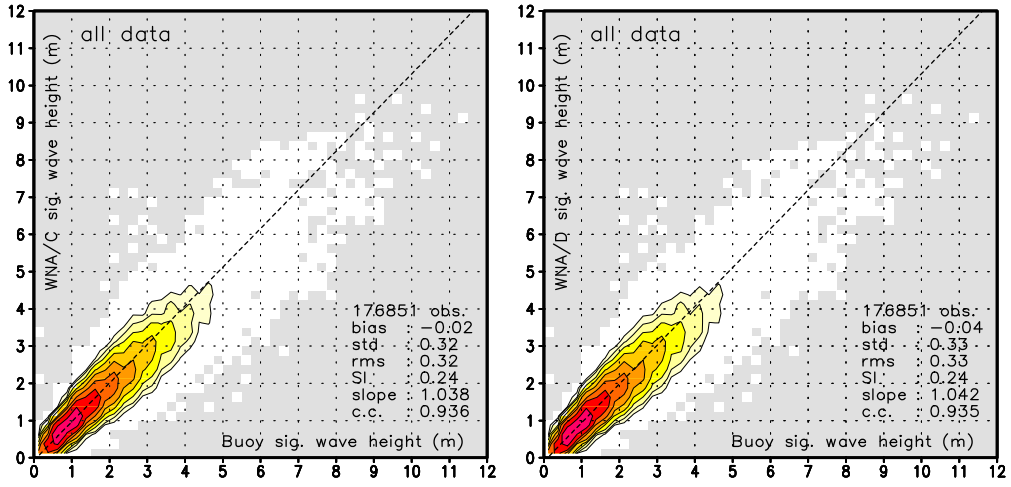

Fig. 5.16 : Like Fig. 5.14 for regional WNA model.

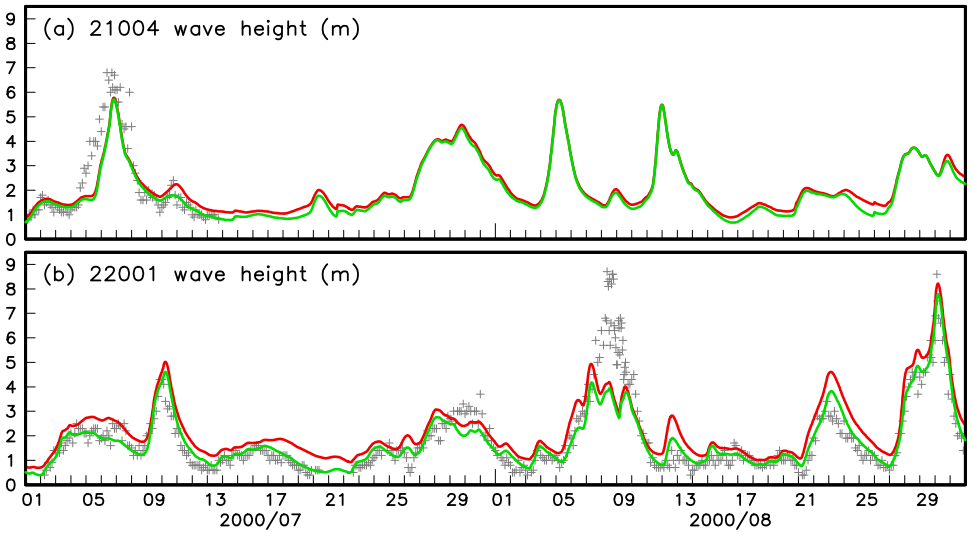

Fig. 5.17 : Time series of wave heights (H_s) observed at buoys (+), from model C (dashed or red lines) or model D (solid or green lines) for July and August 2000 from the global NWW3 model for the Japanese buoys, as identified in the panels.

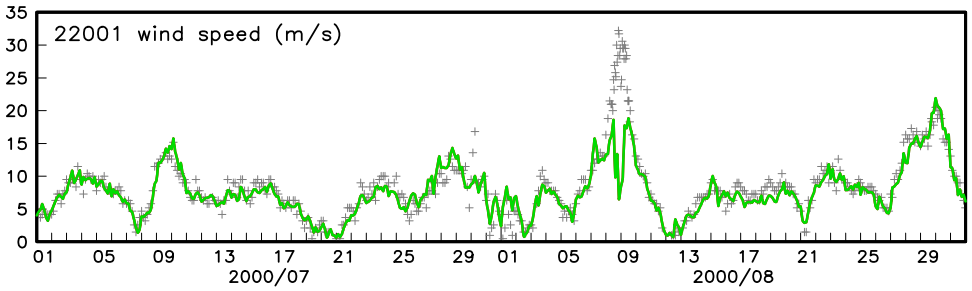

Fig. 5.18 : Time series of wind speeds (U_{10}) for buoy 22001 correpsonding to Fig. 5.17. Legend as in latter figure, wind speed identical in both models.

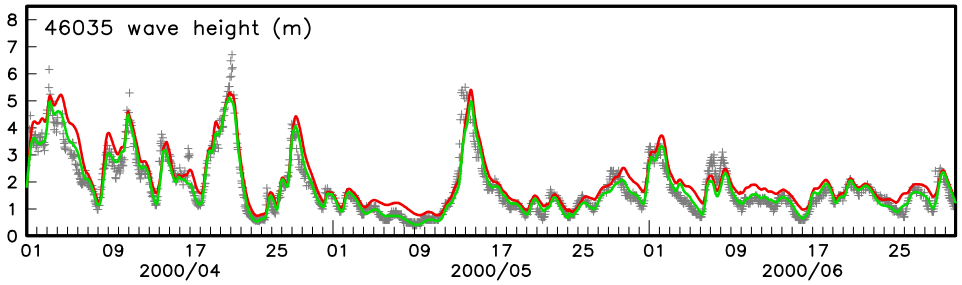

Fig. 5.19 : Time series of wave heights (H_s) observed at buoys (+), from model C (dashed or red lines) or model D (solid or green lines) for April through June 2000 from the global NWW3 model for the Bering Sea buoy 46035.

Figure 5.21 shows the corresponding wave heights for the winter months. In these month, wave heights are higher and dominated by swells from storm systems north of Hawaii. In such conditions, buoy 51001 is least sheltered, and indeed shows virtually no impact of the sub grid modeling of Hawaii. Now 51004 is most sheltered, and indeed shows a significant impact of the explicit modeling of Hawaii. Distinct positive biases in the C model (dashed or red lines), have been mostly eliminated in the D model (solid or green lines).

The buoys in the Gulf of Mexico in the global model are not clearly sheltered. Perhaps somewhat surprisingly, a distinct impact of the sub-grid islands was nevertheless found for low wave conditions in the summer. This is illustrated in Fig. 5.22. The occasionally reduced wave heights can be attributed to the sub grid modeling of the Bahamas. In the C model, the Bahamas are absent, allowing for spurious swell penetration into the Gulf of Mexico through the Straits of Florida. In the D model, this spurious swell source for the Gulf of Mexico has effectively been removed.

For the NW Atlantic buoys in the global wave model the impact of sub grid islands is generally negligible. For the NE Atlantic buoys in the global model only minor impacts were found for the buoys nearest to the Shetland Islands (62106 and 65045, see Fig. 1.1). Even there the impact is mostly negligible, because dominant wave information comes from the west (figures not presented).

For the deep ocean buoys in the regional AKW model ($\circ$ in Fig. 1.2), the impact of the sub-grid islands is expected to be smaller than for the

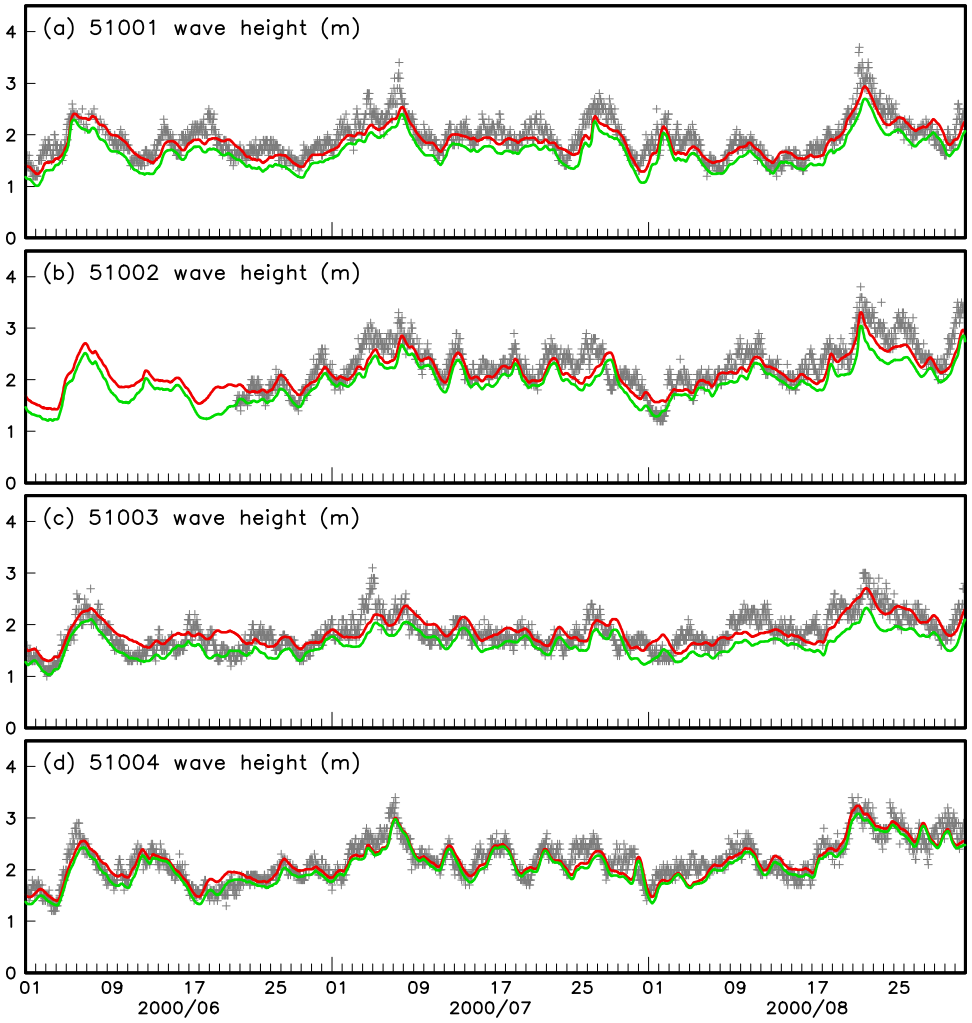

Fig. 5.20 : Like Fig. 5.17 for buoys near Hawaii in the global model in the summer.

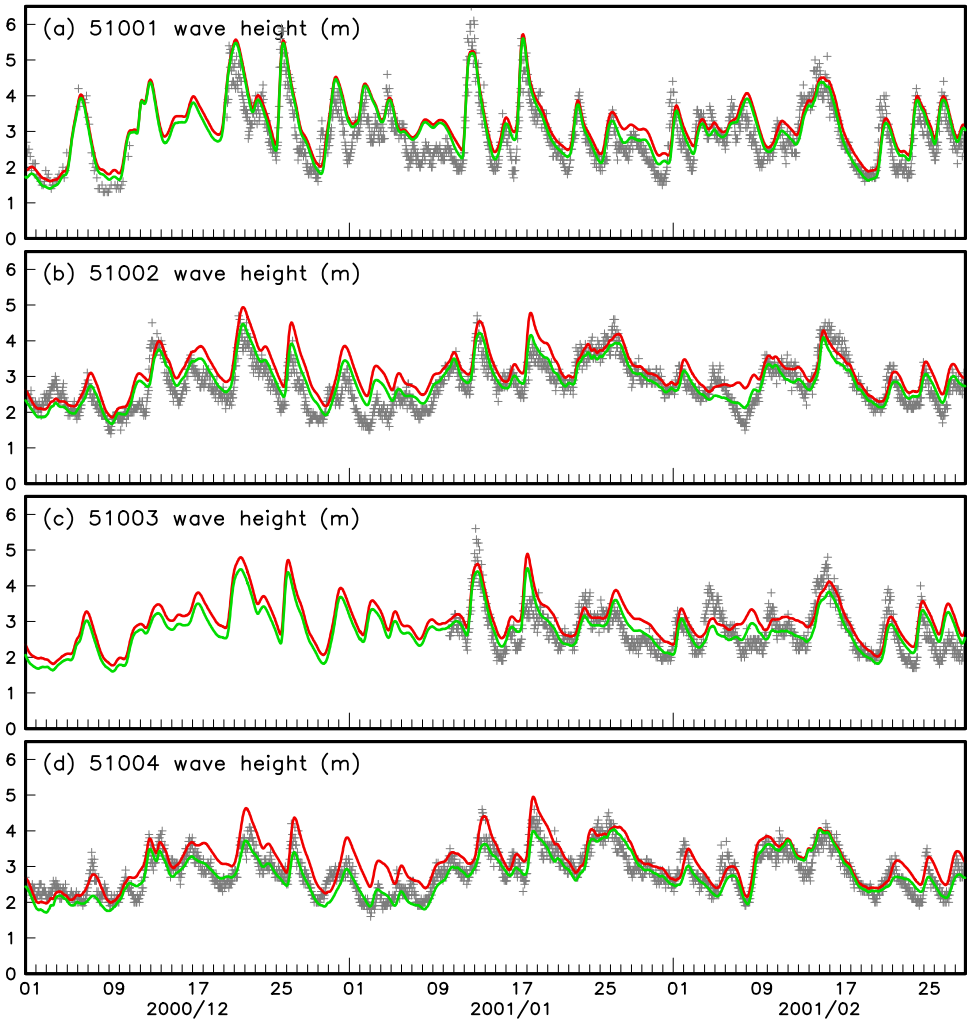

Fig. 5.21 : Like Fig. 5.20 in the winter.

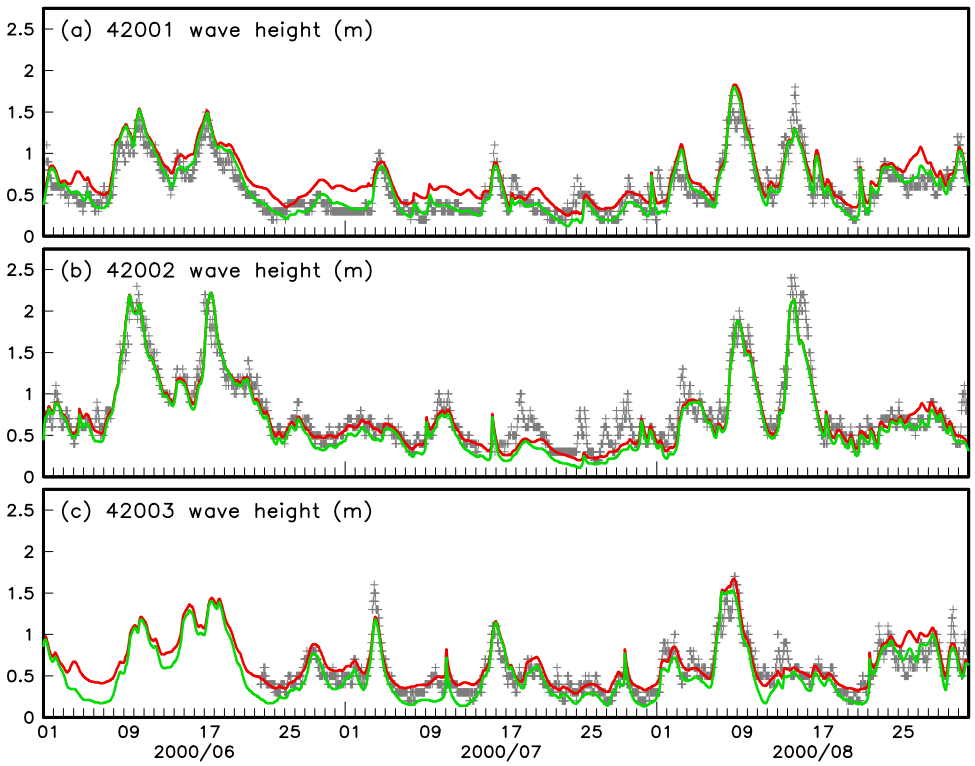

Fig. 5.22 : Like Fig. 5.17 for buoys in the Gulf of Mexico in the global model in summer.

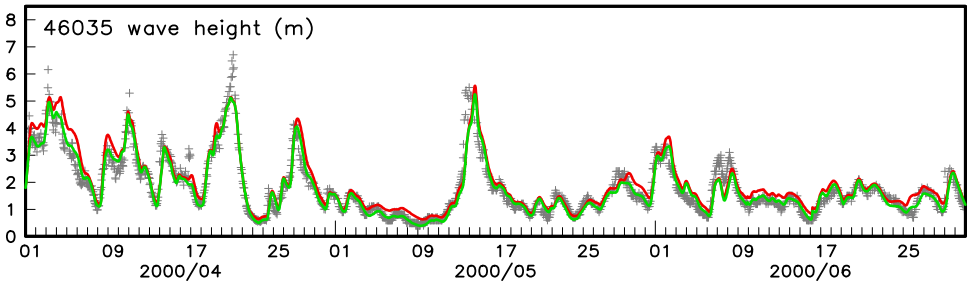

Fig. 5.23 : Like Fig. 5.19 for regional AKW model.

global model, because the regional model resolves the Aleutian Islands better, albeit not completely. Only for buoy 46035, some impact of sub grid island representation again is found (see Fig. 5.23), but less so than for the global model (compare Fig. 5.19).

For the buoys in the regional AKW model that are not properly resolved by the global model (• in Fig. 1.2), a minor impact of the sub grid representations can be found. This impact is generally negligible for practical purposes (figures not presented).

For the deep ocean buoys in the regional WNA model (◦ in Fig. 1.3), the impact of the introduction of sub-grid islands is essentially negligible. Like in the global model, some impact can be found in the Gulf of Mexico as is shown in Fig. 5.24. The reason for the model differences again is the improper description of the Bahamas, as in the global model. The model differences are smaller than in the global model (compare Fig. 5.22), because the C version of the WNA model partially resolves the Bahamas, unlike he NWW3 model.

For the buoys in the regional WNA model that are not properly resolved by the global model (• in Fig. 1.3), model differences are mostly negligible. The exceptions are buoys 42035 and to a lesser extend 42007, where systematic differences occur. These are most likely due to different depths in the model grids, and will be discussed in more detail in the following section.

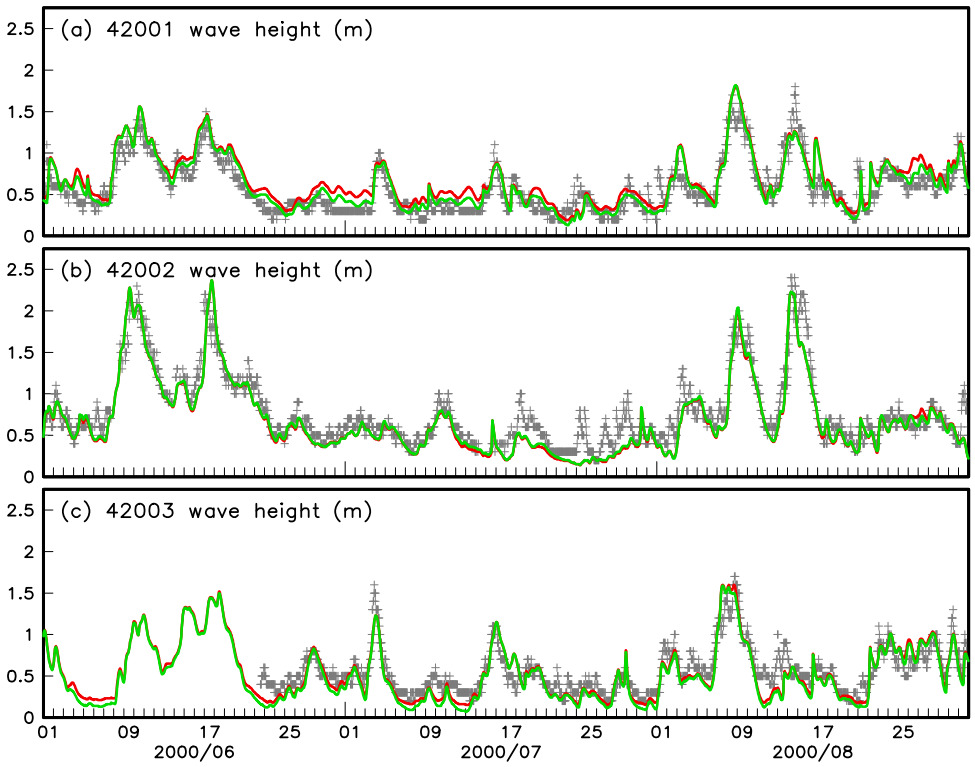

Fig. 5.24 : Like Fig. 5.22 for regional WNA model.

6 Retuning

6.1 Methodology

As mentioned in the introduction, model changes have a tendency to 'detune' a model, even if the changes are based on proper physical or numerical considerations. This becomes particularly obvious if the original tuning of WAVEWATCH III is considered (Tolman, 2002d). This tuning was mostly performed by minimizing global wave model biases against altimeter data, using figures similar to Figs. 3.2 and 5.5. For the original model, bull's eye bias patterns due to unresolved islands as in Fig. 5.5b imply that such a tuning at best can be subjective. The model with sub-grid islands (Fig. 5.5a) points to apparent shortcomings in the original tuning, as it shows clear systematic bias patterns.

The negative bias patterns in the tropics suggest that swell is attenuated too much by the winds. The same suggestion is given by systematically low biases near Hawaii in the summer (Fig. 5.20) with dominant long distance swells, whereas this bias is not obvious in the winter (Fig. 5.21), with dominant wave systems originating closer to Hawaii. The apparently too aggressive attenuation of swell was also found independently by Wingeart et al. (2001).

Originally, the attenuation of swell by winds was tuned by filtering the input source term

$$S_{i,m} = \begin{cases} S_i & \text{for } \beta \geq 0 \quad \text{or} \quad f > 0.8 f_p \\ X_s S_i & \text{for } \beta < 0 \quad \text{and} \quad f < 0.6 f_p \\ \mathcal{X}_s S_i & \text{for } \beta < 0 \quad \text{and} \quad 06 f_p < f < 0.8 f_p \end{cases} , \qquad (6.1)$$

where S_i is the original input source term, $S_{i,m}$ is the filtered source term, $\beta = S_i/(\sigma N)$ is the wind-wave interaction coefficient, f_p is the wind sea peak frequency (see Tolman, 1999, for details), X_s is a filter factor, and $\mathcal{X}_s$ represents a linear reduction of X_s with f providing a smooth transition between the original and reduced input. The original tuning of the model resulted in $X_s = 0.125$. The value of this filter factor will be reassessed here.

The second parameter considered in the original tuning of WAVEWATCH III was the effective wind speed U_e, which is used in the source terms instead of the actual wind speed U_{10},

$$\frac{U_e}{U_{10}} = \left(\frac{c_o}{1 + C_1 + C_2} \right)^{1/2} , \tag{6.2}$$

$$C_1 = c_1 \tanh \left[\max(0, f_1 \{ \mathcal{ST} - \mathcal{ST}_o \}) \right] , \tag{6.3}$$

$$C_2 = c_2 \tanh \left[\max(0, f_2 \{ \mathcal{ST} - \mathcal{ST}_o \}) \right] , \tag{6.4}$$

$$\mathcal{ST} = \frac{hg}{U_h^2} \frac{T_a - T_s}{T_0} , \tag{6.5}$$

where $\mathcal{ST}$ is a bulk stability parameter, h is the reference height for the air temperature and wind speed, and T_a, T_s and T_0 are the air, sea and reference temperature, respectively. Furthermore, $f_1 \leq 0$, c_1 and c_2 have opposite signs and $f_2 = f_1 c_1 / c_2$. In WAVEWATCH III version 1.18 $c_0 = 1.4$, $c_1 = -0.1$, $c_2 = 0.1$, $f_1 = -150$ and $\mathcal{ST}_o = -0.01$. In this correction c_0 addresses general retuning, and will need to be reassessed if X_s is modified. The other parameters provide a parametric treatment of boundary layer stability, and will be left unchanged here.

Considering the above, only c_0 and X_s will be considered in the retuning of the model. However, several other model aspects could also be considered as part of the retuning.

The second retuning related issue is the proper representation of buoy locations, particularly near the coast and/or in shallow water. Bottom friction and shallow water kinematics make a proper depth at the output point important. Proper proximity to the coast is important with respect to fetch in off-shore wind conditions.

For the global model, only two of the validation buoys as shown in Fig. 1.1 are in shallow water (see Table 6.1). For both the local water depth is poorly represented. Buoy 44004 is located on the shelf break, buoy 44011 is located on Georges Bank. For both cases, the local bathymetry is not sufficiently resolved by the global model to improve the local depth representation significantly by moving the output point for the buoy over a small distance. Therefore, the buoy locations have not been modified. Two more output points of the global model are in shallow water, but were not included in the present study due to lack of data. These are 63111 in the northern North Sea, with an adequate depth representation, and the Agulhas FA platform near South Africa, for which the depth again is too large due to unresolved bottom features. All other buoys are in water depths well over 1000 m, and hence are always in deep water. No apparent coastline resolution problems appear to exist.

Table 6.1: Shallow and intermediate depth buoy locations in global NWW3 model. Original model location as implemented operationally. Corrected model location based on better depth representation.

Buoy ID	Location	Model depth (m)	Actual depth (m)	New depth (m)	New location
44008	40.5°N 59.4°W	527.4	62.5	—	—
44011	41.1°N 56.6°W	1036.9	88.4	—	—

Table 6.2: Like Table 6.1 for regional AKW model.

Buoy ID	Location	Model depth (m)	Actual depth (m)	New depth (m)	New location
46029	46.12°N 145.51°W	255.9	128.0	—	—
46041	47.42°N 124.52°W	55.1	132.0	215.7[1,2]	47.34°N 124.67°W
46206	48.84°N 126.00°W	116.1	76.0	—	—

[1]) Moved to updated reported location.
[2]) Moved for better depth representation.

For the AKW model, three output points are in intermediate or shallow water depths (see Table 6.2). All three points are located on a shelf, that is still poorly resolved at the grid resolution of the AKW model, and the local depths are therefore not well represented. Buoy 46041 was redeployed after its initial inclusion of in the wave model. Its new location would severely overestimate the local depth, for which reason the location was slightly modified. Buoy 46206 is located on a ridge, that is not properly resolved by the AKW model.

For the WNA model, many output points are in intermediate or shallow water depths (see Table 6.3). For several of the buoy locations (41008, 42020, 42036), the water depth representation can be improved by moving the buoy to updated locations, dealing with either updated location data, or previous location round off errors. For buoy 44014, the output location has been up-

Table 6.3: Like Table 6.1 for regional WNA model.

Buoy ID	Location	Model depth (m)	Actual depth (m)	New depth (m)	New location
41004	32.50°N 79.10°W	38.5	36.6	—	—
41008	31.40°N 80.52°W	27.4	18.0	17.0[1]	31.40°N 80.87°W
41009	28.50°N 80.20°W	54.0	42.0	41.8[2]	28.50°N 80.23°W
42007	30.09°N 88.77°W	9.4	13.4	14.8[2,3]	30.00°N 88.70°W
42019	27.90°N 95.40°W	148.1	82.3	88.8[2]	27.97°N 95.40°W
42020	27.00°N 96.50°W	148.9	76.8	84.3[1]	26.95°N 96.70°W
42035	29.20°N 94.40°W	6.0	15.9	14.9[2]	28.92°N 94.40°W
42036	28.30°N 84.50°W	62.4	53.0	52.5[1]	28.51°N 84.51°W
44005	42.90°N 68.90°W	166.6	21.9	—	—
44008	40.50°N 69.40°W	62.1	62.5	—	—
44009	38.50°N 74.70°W	27.7	28.0	—	—
44011	41.10°N 56.60°W	162.5	88.4	—	—
44014	36.60°N 74.20°W	206.9	47.5	184.7[1]	36.58°N 74.16°W
44025	40.30°N 73.20°W	37.9	40.0	—	—

[1]) Moved to updated reported location.
[2]) Moved for better depth representation.
[3]) Moved for better coastline representation.

dated to little avail. This buoy and buoy 44011 are located near a shelf break with realistic depths in grid points around the output point, but no viable options to move the output point to get a better local depth representation. This problem is similar to the problem with points 44008 and 44011 in the global model (Table 6.1). In the regional model, the depth at 44008 now is excellently represented, and the depth at 44011 is better represented but not properly yet. For buoy 44005, the local depth shows major variability on scales that cannot be resolved by the grid. Buoys 41009, 42007, 42019 and 42035 are moved from their nominal location to get a better representation of the local depth in the grid. For buoy 42007, the proximity to the coast and sub-grid islands was also an issue in the move.

Considering the above, the modification of output locations in particular in the WNA model may be expected to have a notable impact in some of the

grid points affected.

A third tuning issue is the bottom friction coefficient. This is the only part of the operational models that has been retuned after the initial implementation of the models[2]. The need for additional retuning will not be addressed here, but is planned as part of the next round of updates of the WAVEWATCH III models at NCEP.

Of the above retuning issues, first he general retuning of the model will be considered. Because this retuning prominently touches upon long-distance swell propagation, it will be performed with the global model only. To also assess issues of seasonal cycles in model errors, a full year model run has been considered. After the general retuning of the global model, the effects of the change of output locations is addressed. Because this is in essence a post-processing issue, only a single month for all three models has been run.

6.2 Test results

The retuning of the global model considers the effective wind factor c_0 and the swell attenuation filter factor X_s. Both have been varied in a subjective manner to assess possible model improvements. A record of tested combinations is shown in Table 6.4. Run number 0 in this table identifies the present operational settings. In run 1 the swell attenuation was made weaker by lowering X_s in order to counter the systematic negative biases in the tropics. This had the desired effect, but also added positive biases in storm tracks. In run 2 c_0 was reduced to counter these positive biases. By suppressing somewhat the growth in the storm tracks., Not surprisingly, this also reintroduces negative biases in the tropics. Thus, not surprisingly, changes in c_0 and X_s are interlinked, as are storm track biases and tropical biases. Subsequent changes in the tuning parameters are documented in Table 6.4. For conciseness, only selected results will be shown here. Note that results of the final model settings will be discussed in detail in the following section.

Of the tuning runs, run 2 was unsuccessful as its changes compared to run 0 are systematically negative with respect to the SI. Similarly, run 3 was not satisfactory, as the small improvements in bias had no impact on the rms errors, or on the SI. Of the remaining runs, settings 1 and 4 show similar results, as do settings 5 and 6. In terms of biases, no clearly favorable runs

[2]see http://polar.wwb.noaa.gov/mod/bot1/

Table 6.4: Tested model versions with respect to tunable parameters c_0 and X_s. Number in table identifies consecutive runs. Run '0' identifies present operational settings.

$c_0 =$ / $X_s =$	1.35	1.38	1.40	1.42
0.087	3	–	–	–
0.100	2	6	1	–
0.110	–	–	5	4
0.125	–	–	0	–

can be identified. All runs essentially trade negative biases in the tropics for positive biases in the storm tracks. Runs 5 and 6 show a systematic positive impact on the SI in the tropics. Runs 1 and 4 show a stronger positive impact in the tropics, accompanied by a notable negative impact at higher latitudes. Because this negative impact is much smaller in runs 5 and 6, the latter two settings for the tunable parameter are preferable. A selection between setting 5 and 6 is rather subjective. Settings 6 have been selected, because of a slightly more favorable behavior against buoy data.

The resulting bias patterns for the retuned model will be presented extensively in the following section, and will therefore not be reproduced here. The impact of the retuning on the SI is illustrated in Fig. 6.1. Here model E corresponds to setting 6 in Table 6.4. The impact of the retuning is clearly positive in the tropics throughout the basins. The lower contour levels in Fig. 6.1b are chosen to illustrate that the negative impacts away from the tropics indeed are much smaller that the positive impact in the tropics. From this figure it is also clear that bulk statistics in the tropics improve, whereas at high latitudes the impact is near neutral. The impact of the retuning on statistics against buoy data is also in essence neutral. Such statistics for the final model version will be presented in the following section.

The impact of relocating buoys in the model has been assessed here using only a month of model results. Somewhat arbitrarily, March 2000 was chosen for this test. Considering the limited number of output locations for which the relocation is relevant, all changes can be assessed efficiently with time series of wave heights at the buoys.

For the global NWW3 model, no buoy locations have been changed (Ta-

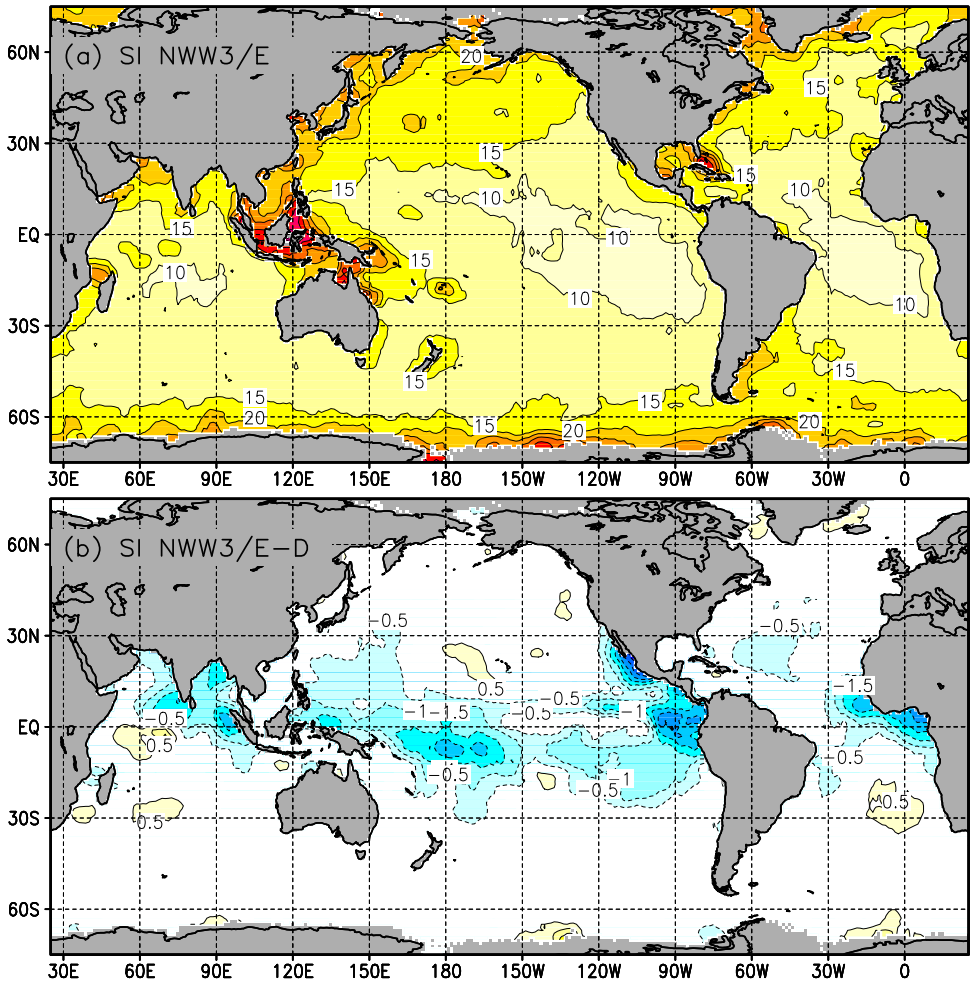

Fig. 6.1 : Scatter index (SI) in % of models against ERS-2 wave height data. Dark gray identifies lack of data. (a) NWW3/E model, contours at 5% intervals. (b) ΔSI = NWW3/E - NWW3/D, contours at 0.5% intervals (note that contour levels are different from previous figures). Dotted contours correspond to negative values, ΔSI = 0 contour not shown. Negative ΔSI shaded light gray in black and white version.

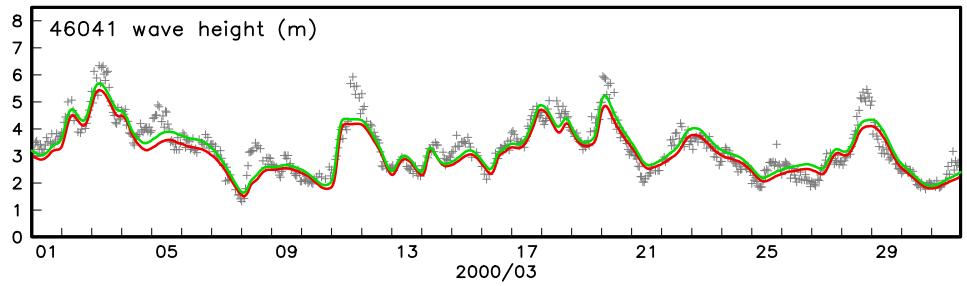

Fig. 6.2 : Time series of wave heights (H_s) observed at buoys (+), for original buoy location in model (dashed or red lines) or updated location (solid or green lines) for March 2000 from version E of the regional AKW model for buoy 46041.

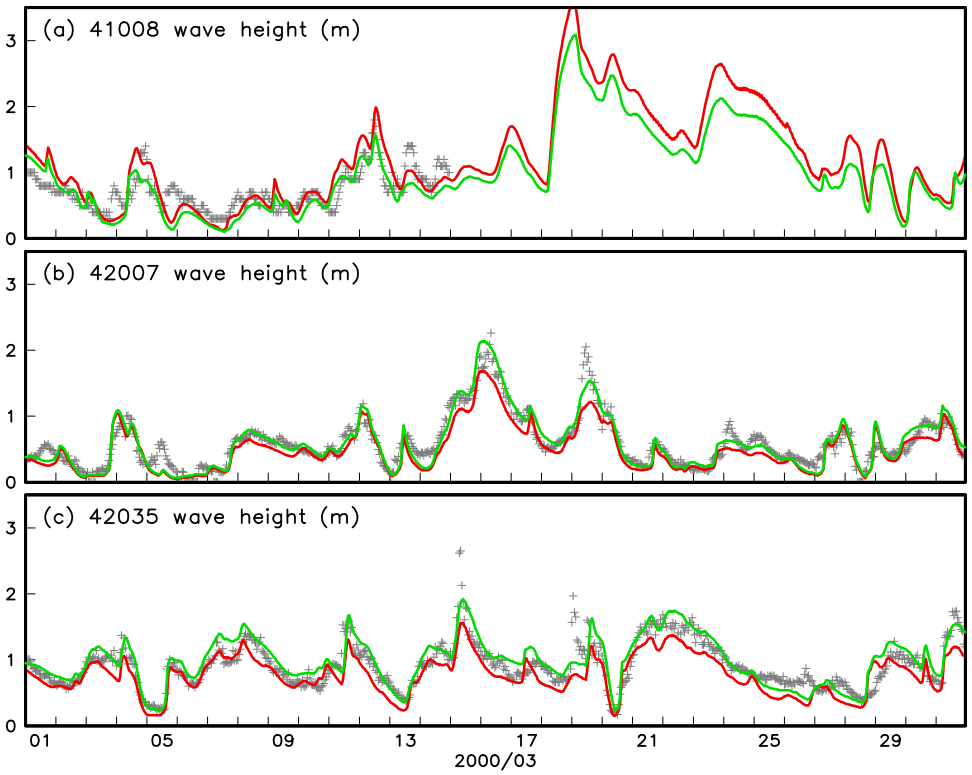

Fig. 6.3 : Like Fig. 6.2 for several buoys in the regional WNA model.

ble 6.1). For the regional AKW model, only the output location for buoy 46041 has been changed (Table 6.2). As is shown in Fig. 6.2, the relocation has a small impact on model results for this buoy, generally removing a small part of moderate negative biases.

For the regional WNA model, 8 buoys locations have been modified. For 7 of these buoys, this has resulted in excellent local depth representations. Only three of these buoys are in truly shallow water (less than 20). These are buoys 41008, 42007 and 42035. Only for these buoys the relocation of the model output points has a notable impact on the predicted wave conditions. The resulting wave heights are shown in Fig. 6.3. For the other buoys the impacts were smaller than for buoy 46041 in the AKW model (Fig. 6.2).

For buoy 41008, the relocation of the output point in the model resulted in a reduction of the modeled water depth, and hence in a reduction of the wave height (Fig. 6.3a). Visual inspection of this figure suggests a moderately positive impact of moving the output location. For buoys 42007 and 42035, the relocation of the output point results in a significantly larger water depth, and higher waves (Fig. 6.3b,c). At both locations, the relocation improves systematic negative model biases.

7 Behavior of the new models

In this section, the behavior of the new model will be compared to that of the old model, to assess the overall impact of the model changes. Furthermore, resulting model errors will be assessed with respect to seasonal trends. The analysis will be performed model by model, starting with the global NWW3 model. Furthermore, model behavior against altimeter data will be addressed first, based on the experience of the previous sections. The model versions considered here are model version '0' and 'E'. For simplicity they will simply be called the old and new model, respectively. From the previous sections it is clear that the effects of the model changes are dominated by the addition of the unresolved islands, and to a lesser extend by the retuning. The exception are the North Slope waters of Alaska in the AKW model, where the change in integration scheme also has a significant impact.

Figure 7.1 shows global wave height biases of the new and old model for the global NWW3 model against altimeter wave heights for the entire validation period. The large positive biases related to island groups in the tropics (Fig. 7.1b) have all but disappeared, and have been replaced by moderate negative biases. At higher latitudes, bias patterns are largely unchanged, with some notable negative biases introduced near the coast at higher northern latitudes (Fig. 7.1a).

Figure 7.2 shows the corresponding SI of the new model (panel a) and the difference in SI between the old and the new model (panel b). The new model (Fig. 7.2a), no longer displays a SI pattern dominated by 'bull's eye' patterns near unresolved islands. The latter behavior can still be observed in, for instance, Fig. 3.5a. The SI difference patterns in Fig. 7.2b are dominated by large local positive impacts near islands groups, combined with localized, but much more moderate negative impacts.

Figure 7.3 shows pdf's and bulk statistics of both models against altimeter data, both for the entire data set, and for selected latitude ranges. For the entire data set (top panels in Fig. 7.3), the impact of the model changes appears negligible. For selected latitude ranges, impacts can be found. In particular in the tropics, the new model gives clearly better results. Only at the highest southern latitudes, some negative impact can be observed.

Figure 7.4 shows pdf's and bulk statistics of both models against buoy data, both for the entire data set, and for selected geographical areas. For the composite data set (upper panels), the impact of the model changes appears negligible, as with the composite altimeter data set. For isolated regions,

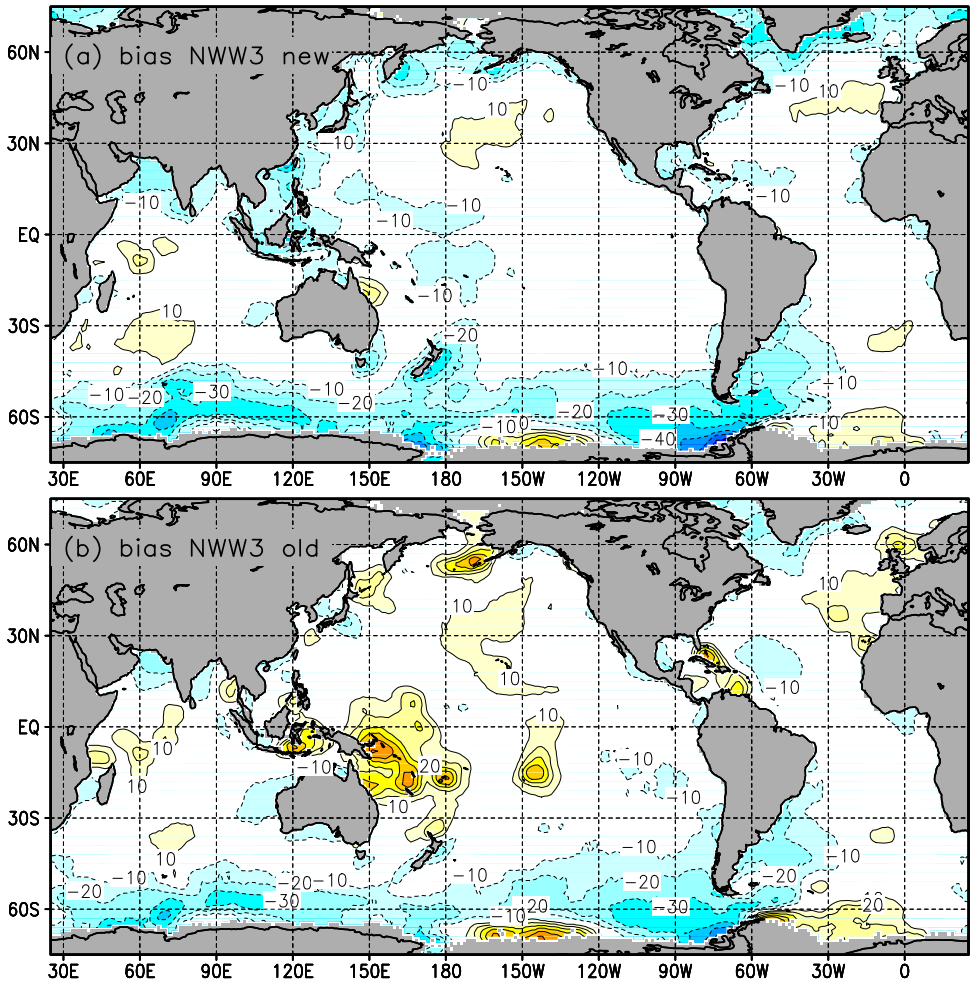

Fig. 7.1 : Bias ΔH_s in cm of models against ERS-2 wave height data. Dark gray identifies lack of data. Contours at 10 cm intervals. Dotted contours correspond to negative values, $\Delta H_s = 0$ contour not shown. Negative ΔH_s shaded light gray in black and white version. (a) New NWW3 (E), (b) Old NWW3 (0).

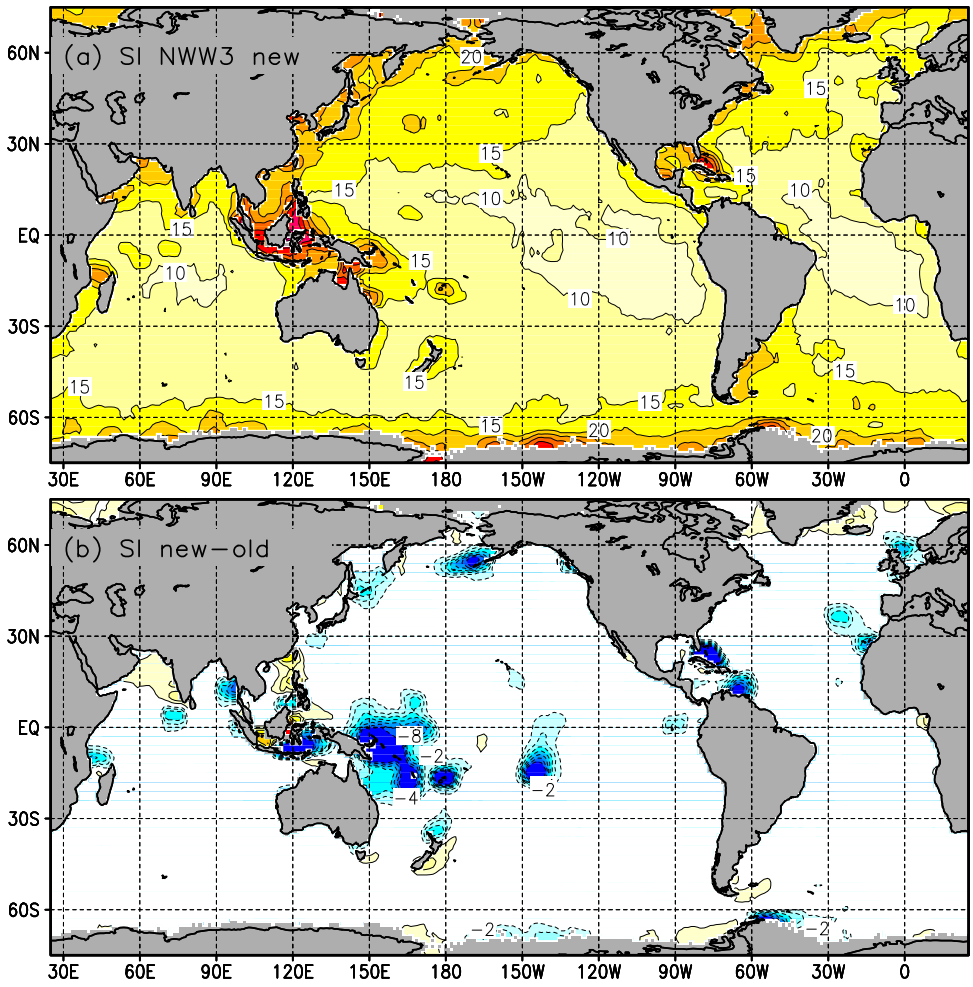

Fig. 7.2 : Scatter index (SI) in % of models against ERS-2 wave height data. Dark gray identifies lack of data. (a) New NWW3 model, contours at 5% intervals. (b) ΔSI = NWW3 new - old, contours at 2% intervals. Dotted contours correspond to negative values, ΔSI = 0 contour not shown. Negative ΔSI shaded light gray in black and white version.

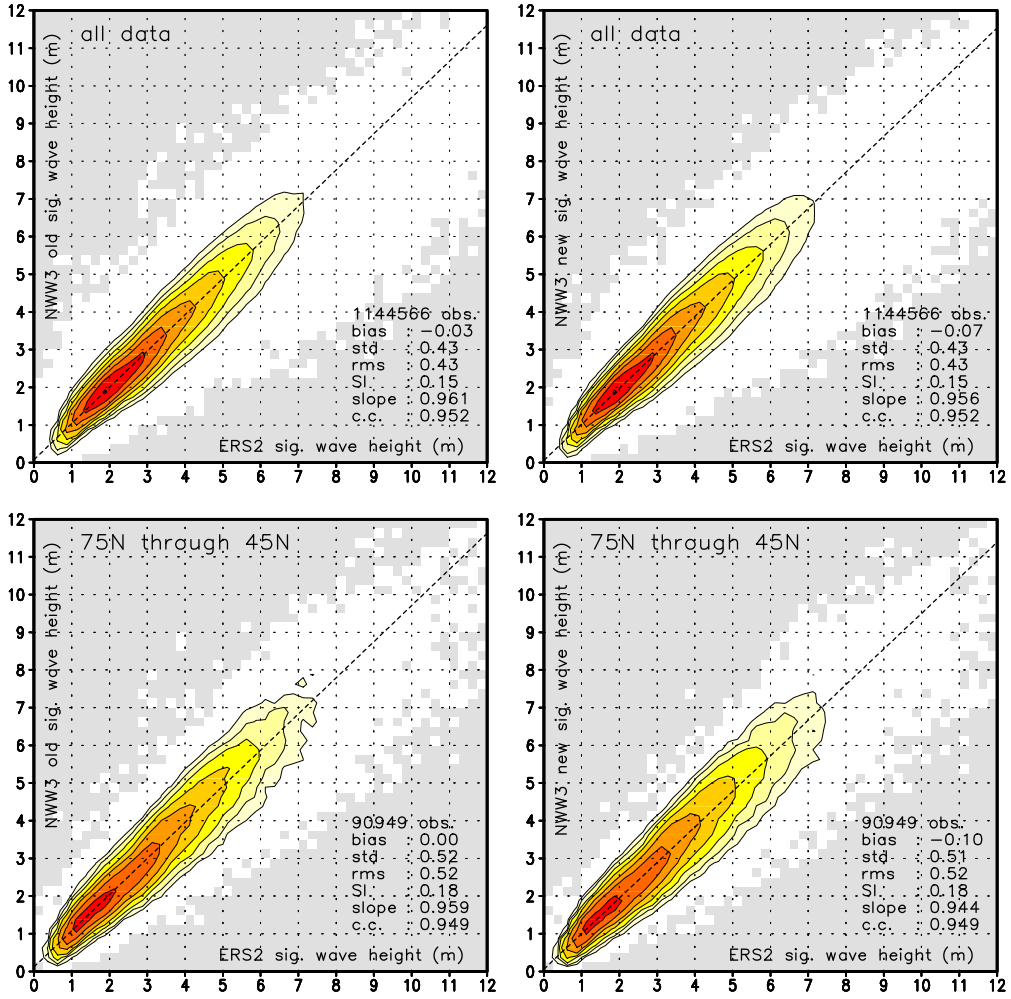

Fig. 7.3 : Probability density function (pdf) of model significant wave height H_s against ERS-2 altimeter data and mean statistics. pdf resolution $\Delta H_s = 0.25$ m. Lowest contour at 0.005 m^{-2}. Contours increase by factor 2. Shaded area identifies no data. Left panels old NWW3 model, right panels new NWW3 model. Data as identified in panels.

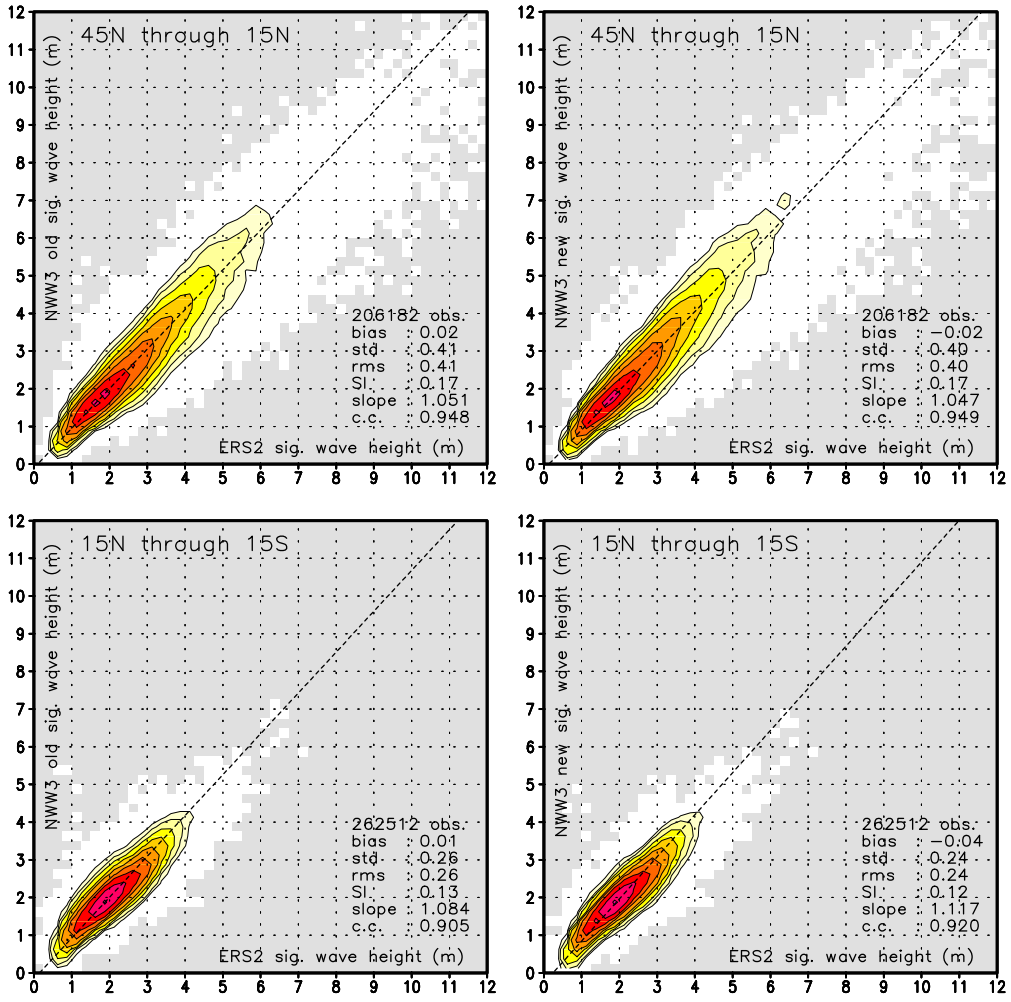

Fig. 7.3 continued.

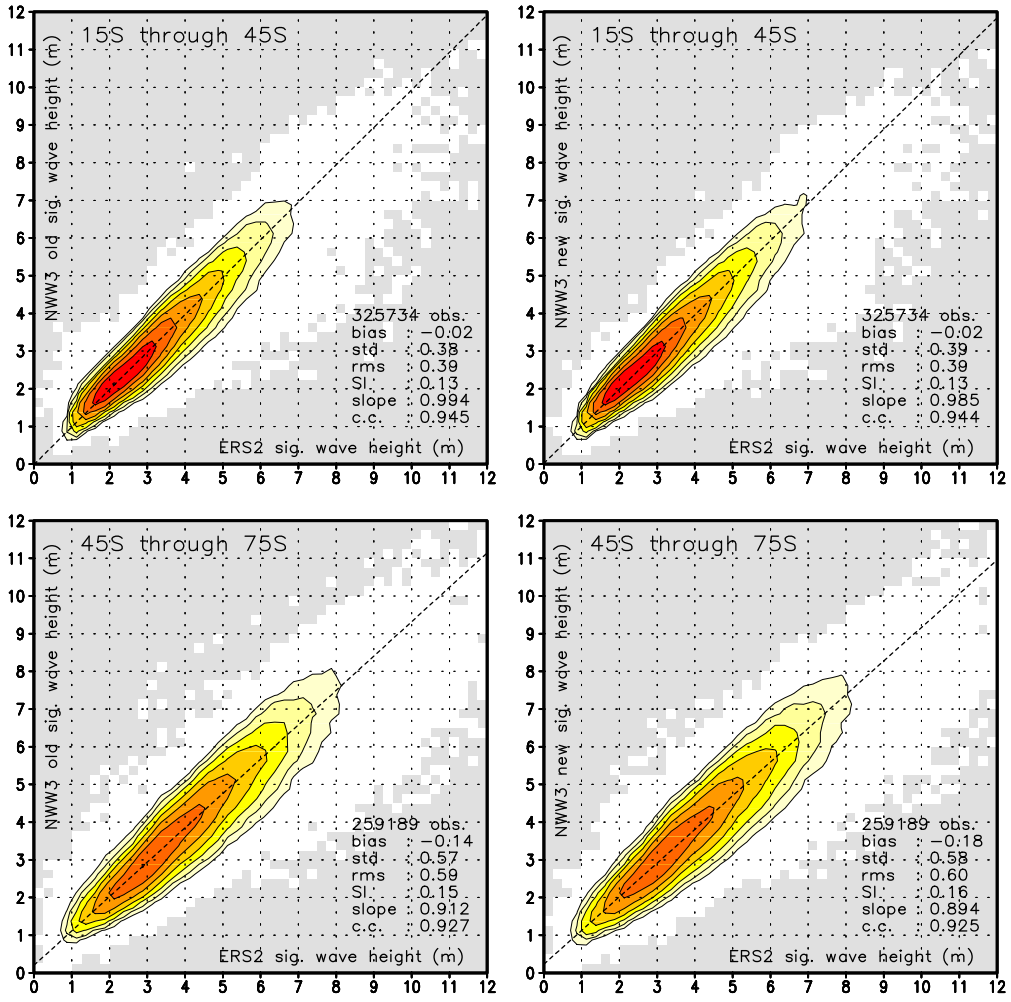

Fig. 7.3 continued.

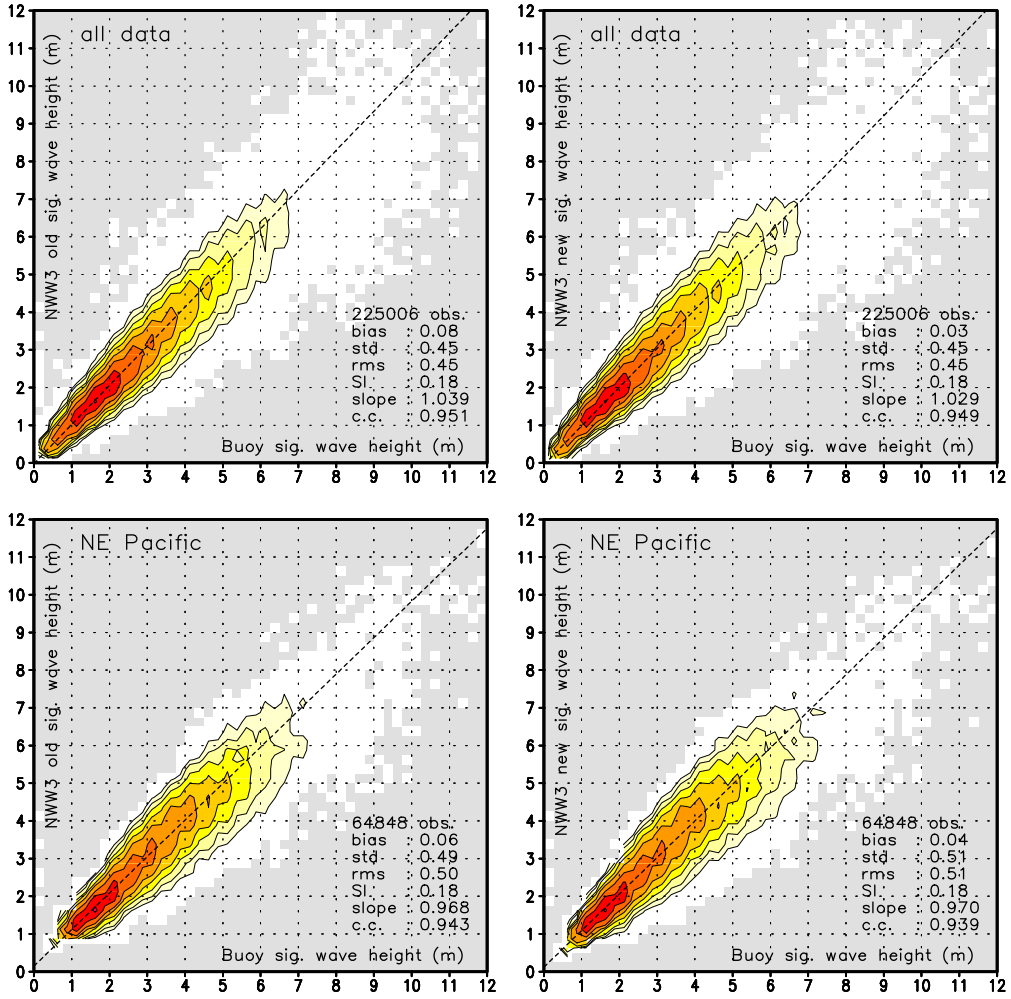

Fig. 7.4 : Probability density function (pdf) of model significant wave height H_s against buoy data and mean statistics. pdf resolution $\Delta H_s = 0.25$ m. Lowest contour at 0.005 m^{-2}. Contours increase by factor 2. Shaded area identifies no data. Left panels old NWW3 model, right panels new NWW3 model. Data as identified in panels.

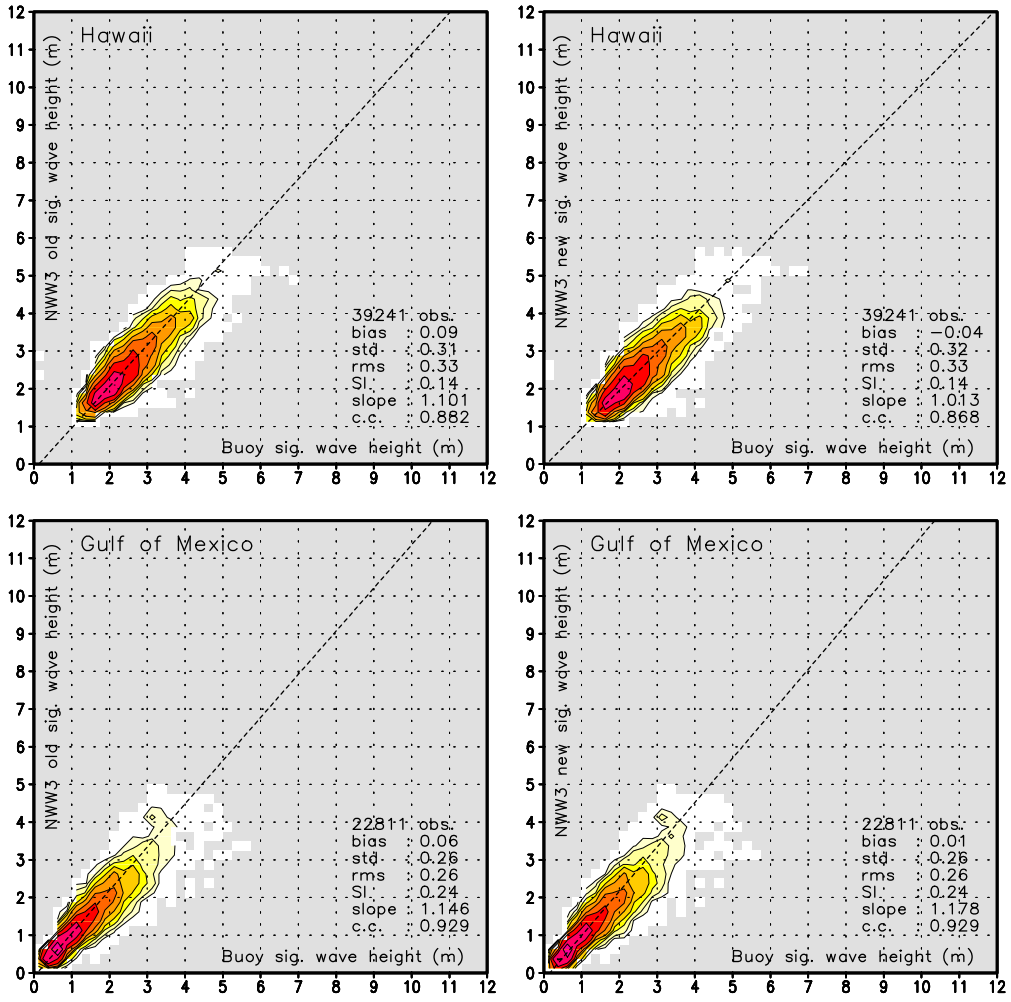

Fig. 7.4 continued.

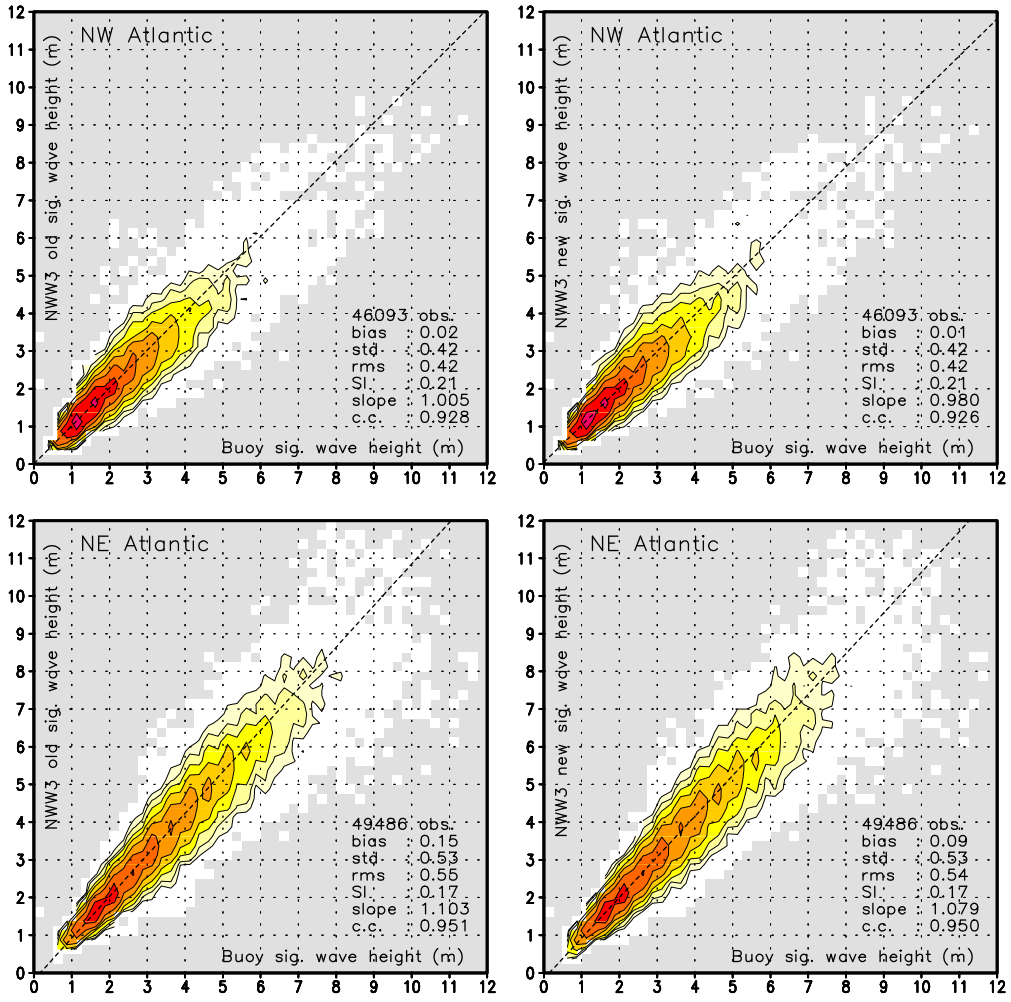

Fig. 7.4 continued.

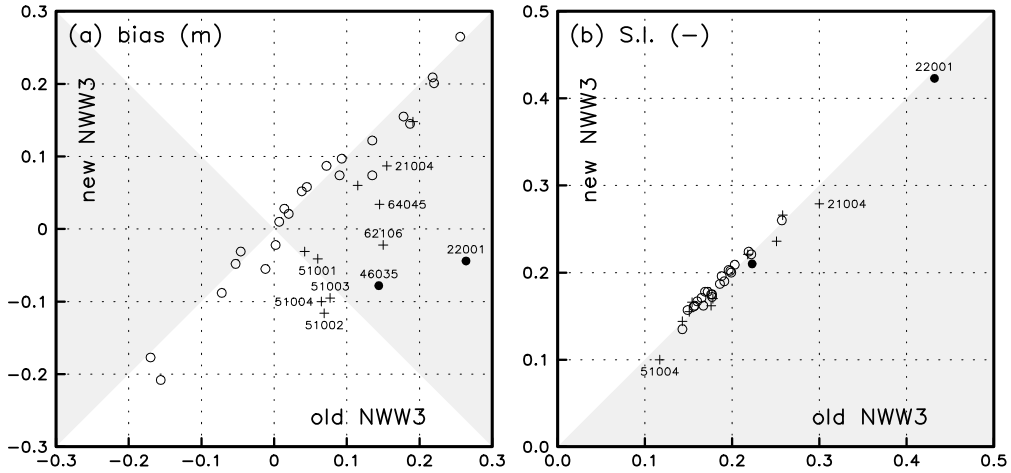

Fig. 7.5 : Wave height biases (panel a, in meters) and Scatter Indices (panel b, in m) for the new NWW3 model versus the old NWW3 model for the entire 1 year period for individual buoys. ∘ : model-to-model SI MMSI $< 5\%$. • : MMSI $> 10\%$. + : Otherwise. Selected buoys identified in plot. Grey shaded area indicates model improvement.

some impact can be observed. For the NE Pacific, errors are marginally increased. For Hawaii and the Gulf of Mexico, biases are improved, and for Hawaii, the regression slope shows significant improvement. For the NW Atlantic, the impact is generally negligible, and for the NE Atlantic, errors are marginally reduced.

A more detailed level of model comparison can be obtained by looking at statistics and time series of individual buoys. Figure 7.5 shows a comparison of biases and Scatter Indices of the old and new global NWW3 models for individual buoys as identified in Fig.1.1. These data are stratified by the model-to-model SI (MMSI), defined as the rms difference between model results, normalized with the mean model wave height.

Figure 7.5a shows a distinct impact of the model changes on model biases. The impact is mostly positive, with the majority of the data points residing in the grey shaded areas. The positive impact is biggest for output locations with the largest MMSI (• and +), and also generally most positive. The impact of the model changes on the SI in Fig. 7.5b is generally much smaller, with alternate small positive or negative impacts.

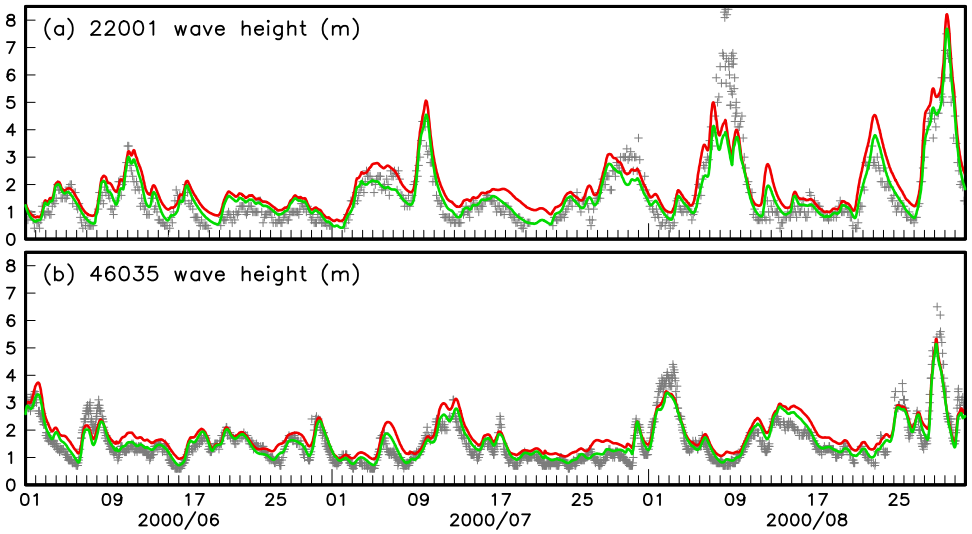

Fig. 7.6 : Time series of wave heights (H_s) observed at buoys (+), from the old NWW3 model (dashed or red lines) or the new NWW3 model (solid or green lines) for June through August 2000 for buoys 22001 and 46035.

The largest impact of the model changes is found at buoys 22001 and 46035, with MMSI's of 20 and 11%, respectively (data not presented here). To illustrate the impact of the model changes for these two buoy locations, time series of wave heights for the months of June through August are presented in Fig. 7.6. This time frame was chosen for being fairly representative for both buoy locations.

For buoy 22001 (Fig. 7.6a), the changes in the model result in a systemically lower wave condition. This is due to the fact that wave conditions at this location almost always have a significant contribution of wave fields generated East of the Ryukyu islands. Even for extreme typhoon conditions in August, some impact of the model changes can be observed. For buoy 46035, similar periods of clear impact are seen, together with periods of limited impact. This indicates that wave conditions at 46035 are alternately dominated by wave events inside or outside of the Bering Sea.

Note that the SI for both models at location 22001 is more than 40% (Fig. 7.5b), suggesting a moderate skill of the model. The SI for this location, however, are systematically large because rms errors are dominated by single typhoon events with large wind speed errors (see section 5 and Fig. 5.18),

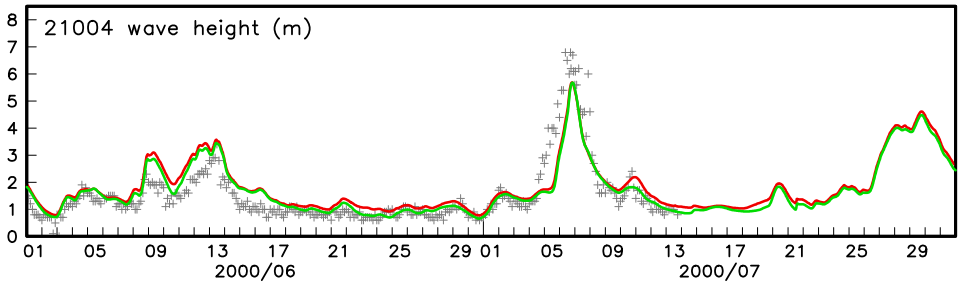

Fig. 7.7 : Like Fig. 7.6 for July and August 2000 for buoy 21004.

whereas the normalization is dominated by generally low wave conditions. In fact, for the low wave conditions in March through July (before the severely missed typhoon conditions), the model changes reduced the model SI from 35 to 27%, which, considering the low wave conditions of 1.3 m average, indicates more than acceptable forecast skill. Hence the high SI for 22001 is misleading with respect to the model forecast skill as well as the model improvement, as is also obvious from Fig. 7.6a.

For ten other output locations, MMSI's are between 5 and 10%. These are 21004 (7.1%), 51001 through 51004 (5.7, 7.7, 8.5 and 9.4%) 42001 (7.7%), 42003 (9.3%) 44138 (7.6%) 62106 (8.7%) and 64045 (6.1%).

Buoy 21004 is located on the East of the Ryukyu Islands in the Pacific ocean. The impact of the model changes is occasional, with large periods without impact of model changes. This is illustrated in Fig. 7.7 with wave heights for both models for July and August. This behavior indicates that the wave conditions at this location are generally not dominated by the wave conditions west of the Ryukyu Islands. Note that both the bias and the SI at this location are markedly improved by the model changes (Fig. 7.5). Unlike for buoy 22001, no severely missed typhoon conditions are present at this buoy location due to failure of the instrument just before the main typhoon events.

For the Hawaiian buoys 51001 through 51004 the impact of the model changes has a distinct seasonal cycle, as already discussed in section 5 with Figs. 5.20 and 5.21. For the old and new models, similar figures are presented here as Fig. 7.8 and 7.9. In the Hawaiian summer, wave conditions are dominated by tradewinds and southern swells. For such conditions, buoy 51004 is generally not sheltered by the Hawaiian Islands, and shows a generally

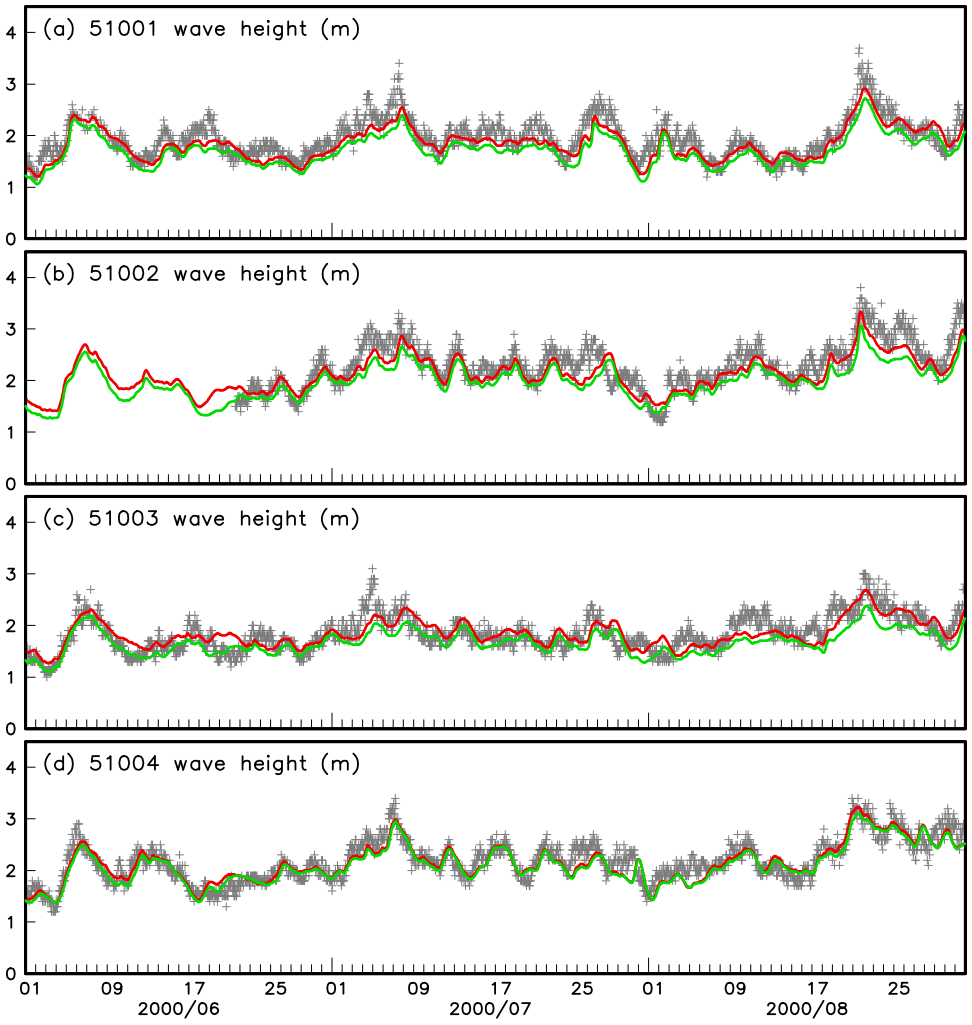

Fig. 7.8 : Like Fig. 7.6 for June through August 2000 for Hawaiian buoys.

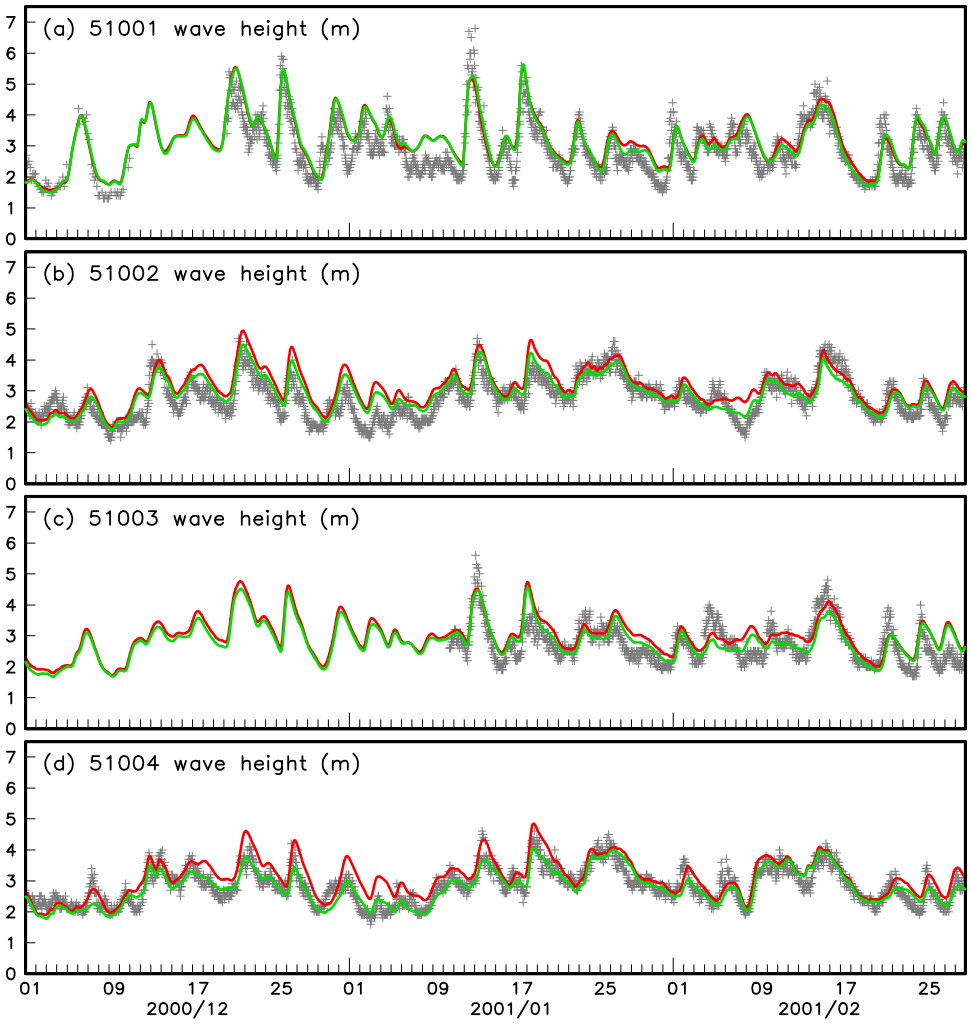

Fig. 7.9 : Like Fig. 7.6 for December 2000 through February 2001 for Hawaiian buoys.

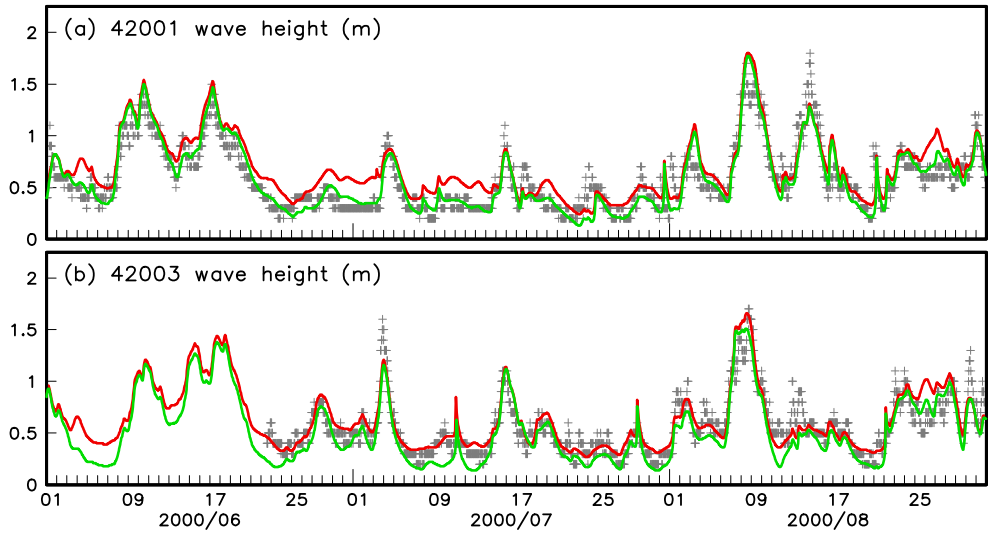

Fig. 7.10 : Like Fig. 7.6 for June through August 2000 for selected Gulf of Mexico buoys.

negligible impact of the model changes (Fig. 7.8d). The other three buoys show a small systematic reduction in wave height. In the Hawaiian winter, wave conditions are dominated by storm events north of Hawaii. In such conditions, buoy 51001 is least sheltered, and shows the smallest impact of model changes. Particularly buoy 51004 shows large changes. In particular for late December, the improvements at 51004 are impressive. The mean biases at all four buoys have changed from slightly positive to slightly negative (Fig. 7.5a). Only at buoy 51004, the SI shows a distinct impact, reducing from 11.7 to 10.0% (Fig. 7.5b). Note that such a small SI indeed indicates excellent model behavior, particularly since it approaches the sampling variability of the wave height as observed by buoys (approximately 8%, Donelan and Pierson, 1983).

For buoys 42001 and 42003, the impact of the model changes is mostly due to the removal of spurious swell transmission through the Straits of Florida, as discussed in section 5, Fig. 5.22. For the summer months, this is illustrated in Fig. 7.10. For both buoy locations, the removal of the spurious swell has a clear positive impact. For both buoy locations, the bias is slightly improved. For 42003, the SI is marginally increased by 0.8%, for 42001 it is reduced by 1.5% (individual buoys not marked in Fig. 7.5).

For buoy 44138, the differences in model results are most likely due to

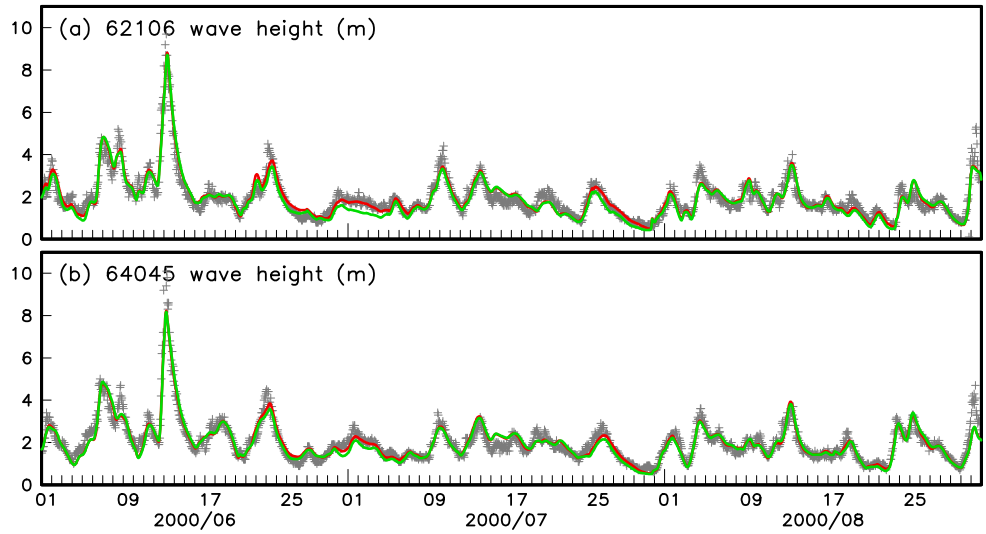

Fig. 7.11 : Like Fig. 7.6 for June through August 2000 for selected north-east Atlantic buoys.

the differences in the representation of Nova Scotia in the grid. This results in occasional model differences, mostly for lower wave conditions, with no significant impact on the bias and the SI (Figure not presented here, buoys not individually marked in Fig. 7.5

Buoys 62106 and 64045 are potentially sheltered behind the Shetland, Faroe and other islands around Scotland (see Fig. 5.1). For the summer months, this proved to have no discernible impact on model results (Fig. 7.11), with an occasional exception (e.g., first week of July at 62106). For the winter months, the differences are generally small, but more systematic, as is illustrated in Fig. 7.12, and mostly occur at the peak of individual wave events. For both locations the biases improve (Fig. 7.5a), whereas the SI's improve by 0.8 and 1.4%, respectively (buoys not individually marked in Fig. 7.5b).

In the above discussion seasonal effects have only been identified in the context of model changes. Also of interest with repect to forecasting is the seasonal behavior of the (new) model. Considering that buoys are not generally representative for the entire model, seasonal behavior is best assessed with satellite data. Figure 7.13 presents the model biases against ERS-2 wave height data per three month season, starting with the northern hemisphere spring in panel (a).

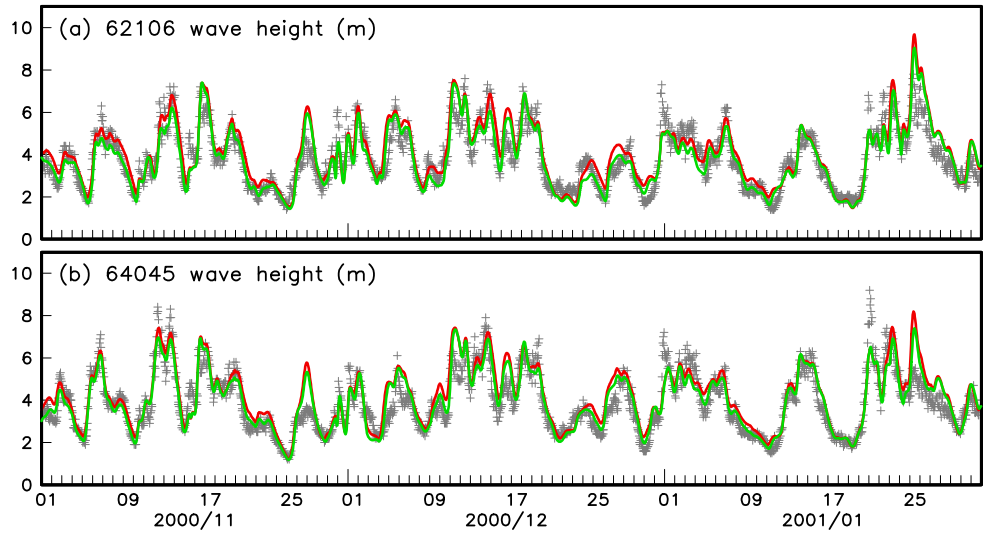

Fig. 7.12 : Like Fig. 7.6 for November 2000 through January 2001 for selected northeast Atlantic buoys.

The lowest biases are found in the spring and fall seasons (Fig.7.13a and c), In the northern hemisphere summer and southern hemisphere winter (Fig.7.13b), significant positive biases occur in the Indian Ocean. This area coincides with the area of maximum wave heights (figure not shown), and hence with the dominant storm tracks. In the northern hemisphere winter and southern hemisphere summer (Fig.7.13d), similarly large positive biases occur in the dominant northern hemisphere storm tracks. Anomalous behavior near the equator in the last panel will be discussed in some more detail below. Note that similar or even more pronounced seasonal bias patterns were found in the storm tracks in the old model (figure not presented here). Hence, the seasonal patterns are not on consequence of the model changes.

The combination of positive biases in storm tracks, and negative biases in the tropics suggests that wave growth is overestimated, whereas swell dissipation is also overestimated. Because this behavior could not be removed with simple tuning, it may well be a sign of shortcomings in the model physics.

Of course, model biases may also be a sign of shortcoming in the wind fields. Because wind fields have been produced using virtually all available data, no independent data is available to validate these wind fields. An exception is the altimeter wind, which has not been used in the GDAS.

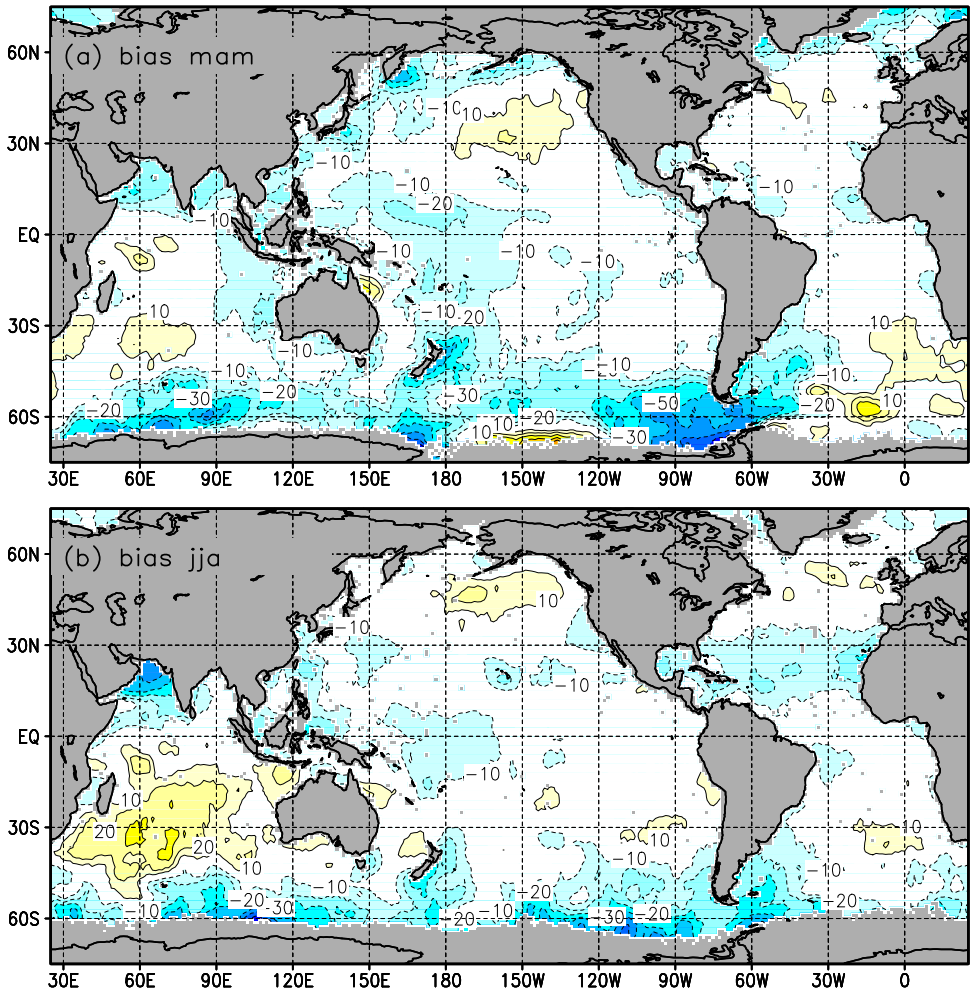

Fig. 7.13 : Bias ΔH_s in cm of the new NWW3 model against ERS-2 wave height data. Dark gray identifies lack of data. Contours at 10 cm intervals. Dotted contours correspond to negative values, $\Delta H_s = 0$ contour not shown. Negative ΔH_s shaded light gray in black and white version. (a) March – May, (b) June – August, (c) September – November, (d) December – February.

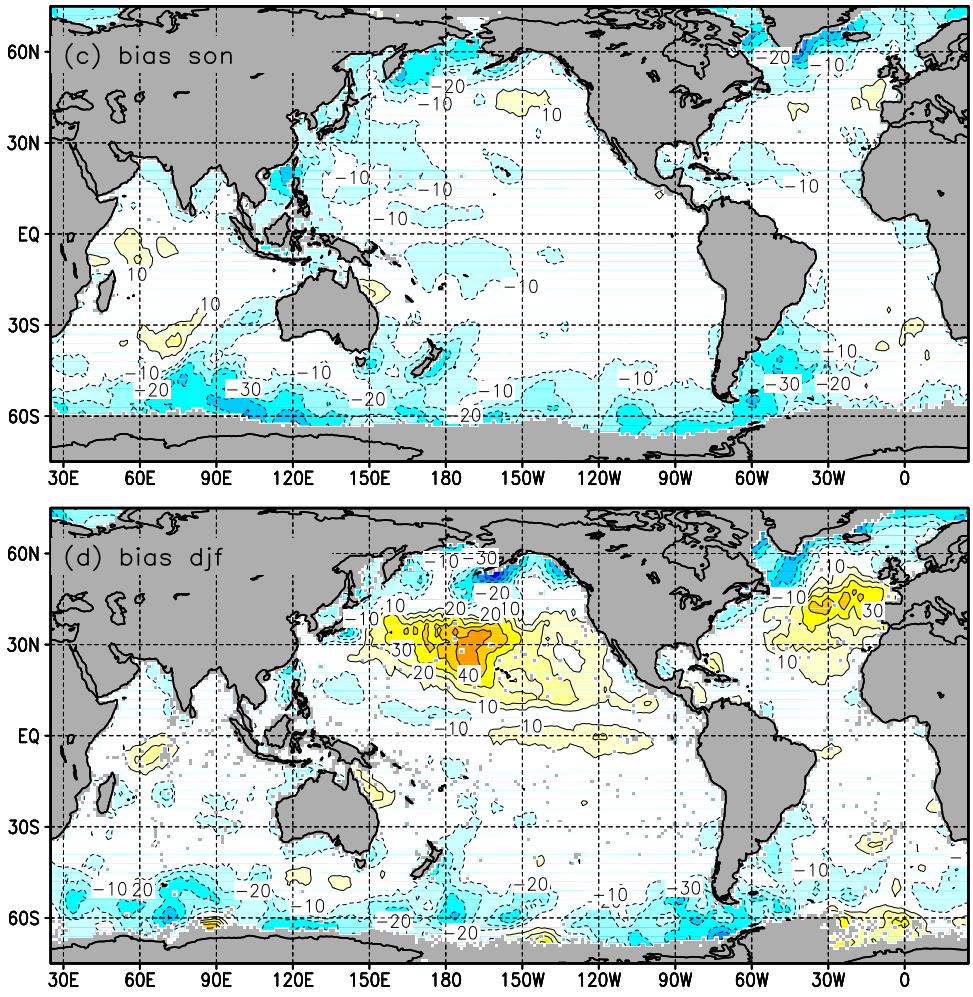

Fig. 7.13 continued

Unfortunately, altimeter winds are systematically contaminated by the underlying wave field, with little hope for independently removing this impact (Tolman, 1998b). If, however, the shortcomings of the altimeter winds are known, some qualitative statements may still be made regarding the GDAS wind fields.

First, the altimeter wind fields need to be corrected for biases. Similar to the ERS-1 bias correction used in Tolman (1998b), the ERS-2 wind bias correction based on collocation with buoy data is given as

$$U_{10,c} = 0.34\,\mathrm{ms}^{-1} + 1.01 U_{10,a} \quad , \tag{7.1}$$

where $U_{10,c}$ ($U_{10,a}$) is the corrected (original) altimeter wind speed. This altimeter correction was derived, mostly based on buoy data close to northern hemisphere storm tracks. The main problem with altimeter wind speeds is that in absence of winds, swell is mistaken for wind speed. This, combined with the generally unknown wave conditions for which the algorithm has been tuned, make objective use of such data difficult if not impossible.

Figure 7.14a shows some wind speed biases derived from ERS-2 data for the entire year considered. It appears that the negative wind biases at high latitudes in the southern hemisphere are somewhat correlated with the negative wave height biases in the same region (compare with Fig. 7.1). It is therefore tempting to attribute such wave model biases to the driving winds. However, many of these areas also feature massive swells, which might well result in at least a partially spurious bias against the altimeter data. No buoy data is available is this area to guarantee that the altimeter wind retrieval algorithm in this area at least is free of bias. Moreover, large negative wind biases suggested by the altimeter data in the southern Atlantic, do not at all correlate with wave field errors. This illustrates the danger of using wind validations with altimeter data.

Nevertheless some objective observations may be made based on altimeter data. For the period of December through February, the altimeter data suggests a distinct positive wind speed bias at the equator in the eastern Pacific. In this area, swell dominated condition will in essence guarantee that the altimeter overestimates wind conditions. If the GDAS produces a positive bias against positively biased wind data, it is virtually guaranteed that this GDAS bias is real. This equatorial wind speed bias only occurs in this season, and also occurred in the previous and following years[3]. This bias

[3] see http://polar.wwb.noaa.gov/waves/validation

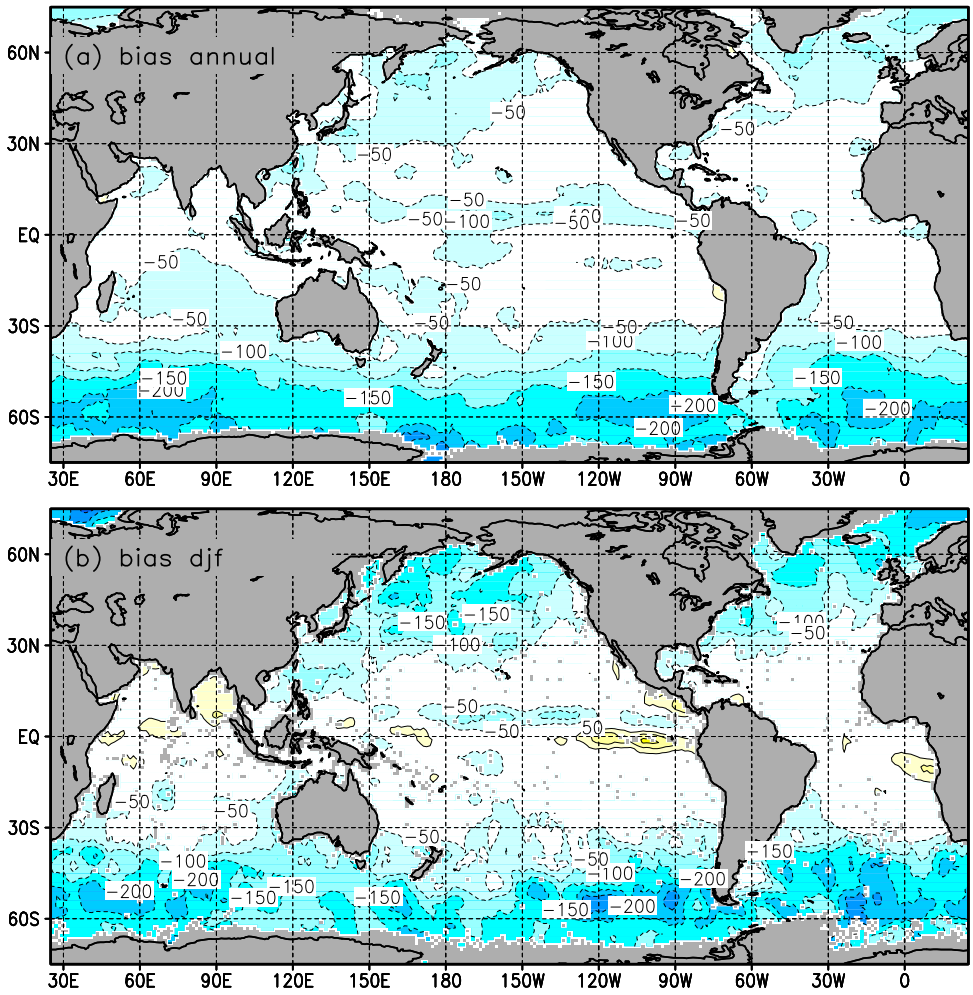

Fig. 7.14 : Bias ΔU_{10} in cm/s of the GDAS wind speeds against ERS-2 data. Dark gray identifies lack of data. Contours at 50 cm/s intervals. Dotted contours correspond to negative values, $\Delta H_s = 0$ contour not shown. Negative ΔU_{10} shaded light gray in black and white version. (a) Entire year, (b) December – February.

appears closely corelated with a wind wave height bias at the equator in this season (fig: 7.13d). The latter bias is therefore most likely at least partially caused by a wind speed bias in the GDAS winds.

After this fairly extensive discussion of the global NWW3 model, a similar analysis of the regional AKW and WNA models will be presented. Figures 7.15 and 7.16 show the bias and SI of the new and old AKW model against ERS-2 wave height data, similar to Figs. 7.1 and 7.2 for the global NWW3 model.

Positive bias patterns near the Aleutians in the old model (Fig. 7.15b) have been replaced by negative biases, similar to the biases further north in the Bering Sea. Note that the resulting bias pattern also is fairly similar to the bias pattern in the global model (Fig. 7.1). This bias removal is associated with a significant reduction of the SI (Fig. 7.16b), also with a fairly similar final SI pattern as in the global model (Fig. 7.2). Note that on the North Slope of Alaska, a significant negative impact of the change in the integration scheme, and a positive impact of the continuous ice modeling in essence cancel, leaving only small differences in the SI of the old and new models.

Figures 7.17 and 7.18 show pdf's and bulk statistics of both models against altimeter and buoy data, respectively. For both data sets, the impact of the model changes are essentially negligible, with minor positive changes for against the altimeter data, and even smaller negative impacts against buoy data. This is not surprising, considering the localized impact of model changes.

Figure 7.19 shows a comparison of biases and Scatter Indices of both models for individual buoys as identified in Fig.1.2. These data are again stratified by the MMSI. Generally, the impact of the model changes is smaller than for the global model, with only two buoys with MMSI's of more than 5% (46035 at 7.3% and 46041 at 5.2%).

Figure 7.19a shows systematically more positive biases of 2 to 4 cm for all buoys with small impact of model changes ($\circ$), accompanied by an increase of the SI of on average 0.5%. This is mostly likely due to the retuning. This retuning was based on global model behavior, and apparently has a minor small negative impact on the buoys in the AKW model. Compared to the impact against the altimeter in Fig. 7.16, this is another case where buoys apparently do not present a representative validation of the entire model.

Buoy 46035 is present in both the global NWW3 and the regional AKW

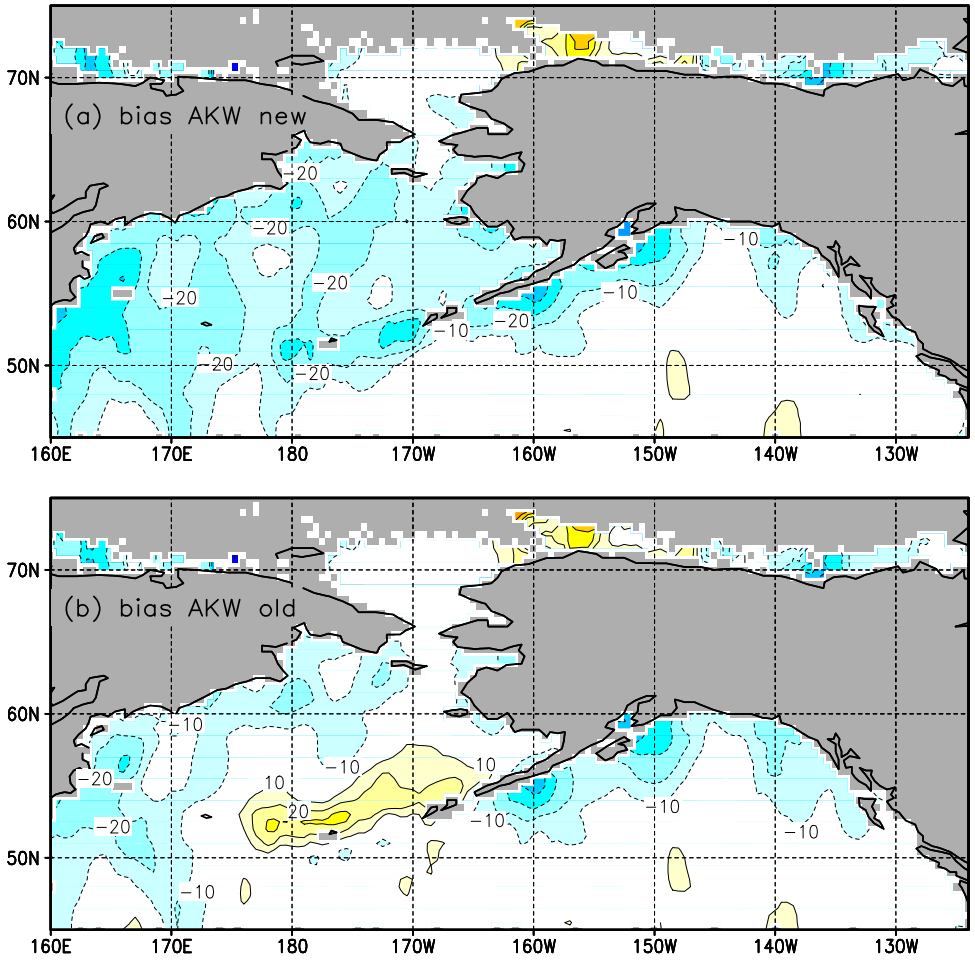

Fig. 7.15 : Bias ΔH_s in cm of models against ERS-2 wave height data. Dark gray identifies lack of data. Contours at 10 cm intervals. Dotted contours correspond to negative values, $\Delta H_s = 0$ contour not shown. Negative ΔH_s shaded light gray in black and white version. (a) New AKW (E), (b) Old AKW (0).

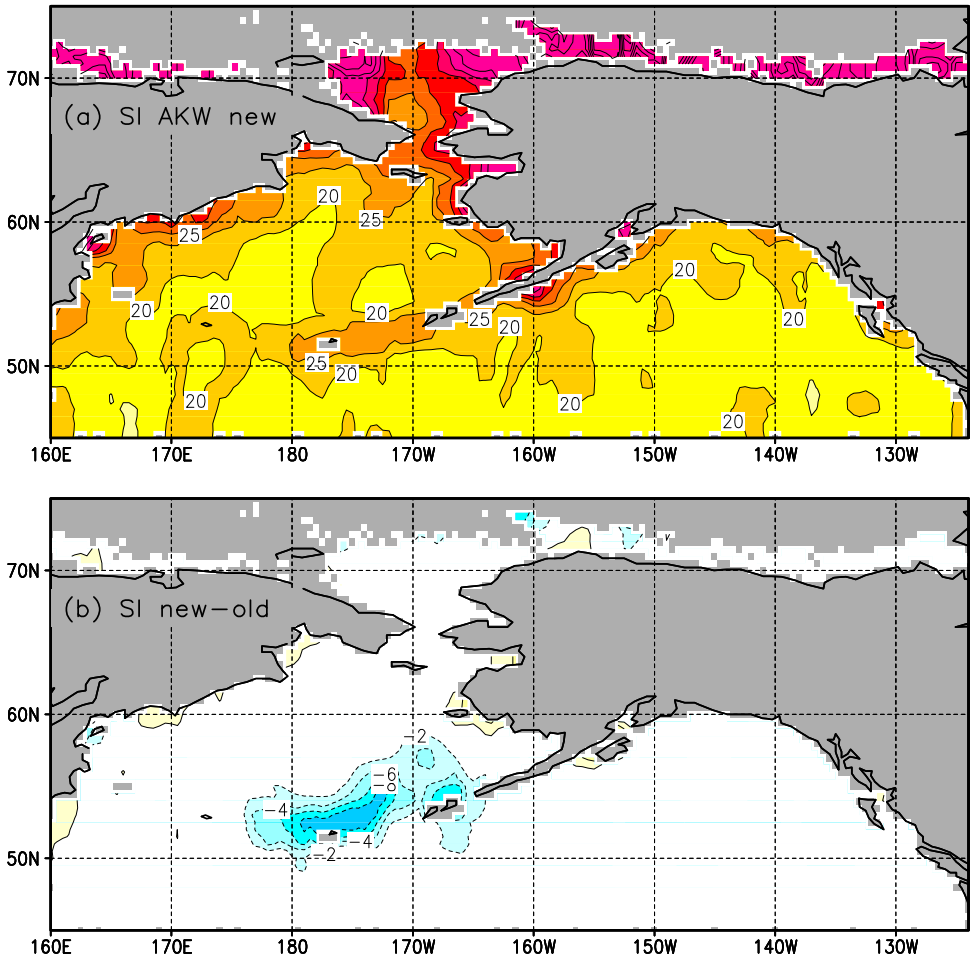

Fig. 7.16 : Scatter index (SI) in % of models against ERS-2 wave height data. Dark gray identifies lack of data. (a) New AKW model, contours at 5% intervals. (b) ΔSI = AKW new - old, contours at 2% intervals. Dotted contours correspond to negative values, ΔSI = 0 contour not shown. Negative ΔSI shaded light gray in black and white version.

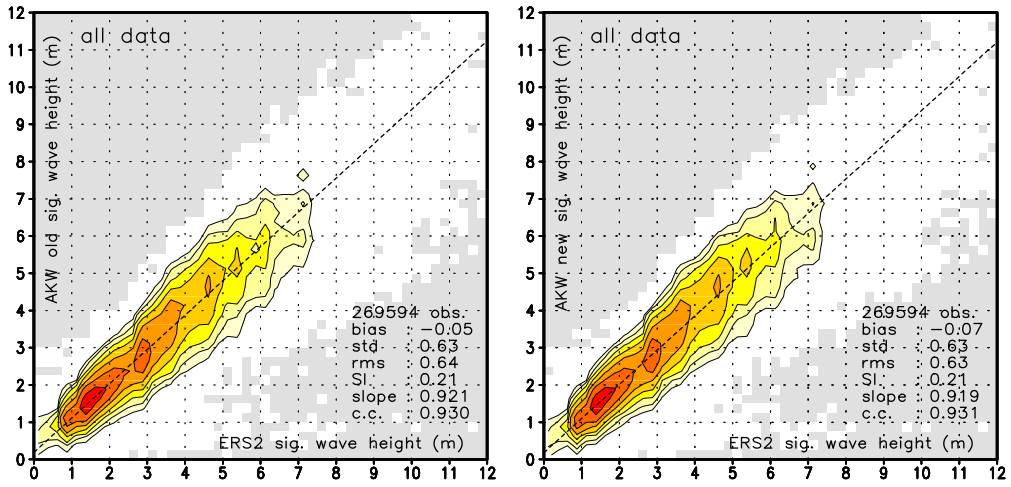

Fig. 7.17 : Probability density function (pdf) of model significant wave height H_s against ERS-2 altimeter data and mean statistics. pdf resolution $\Delta H_s = 0.25$ m. Lowest contour at 0.005 m^{-2}. Contours increase by factor 2. Shaded area identifies no data. Left panel old AKW model, right panel new AKW model.

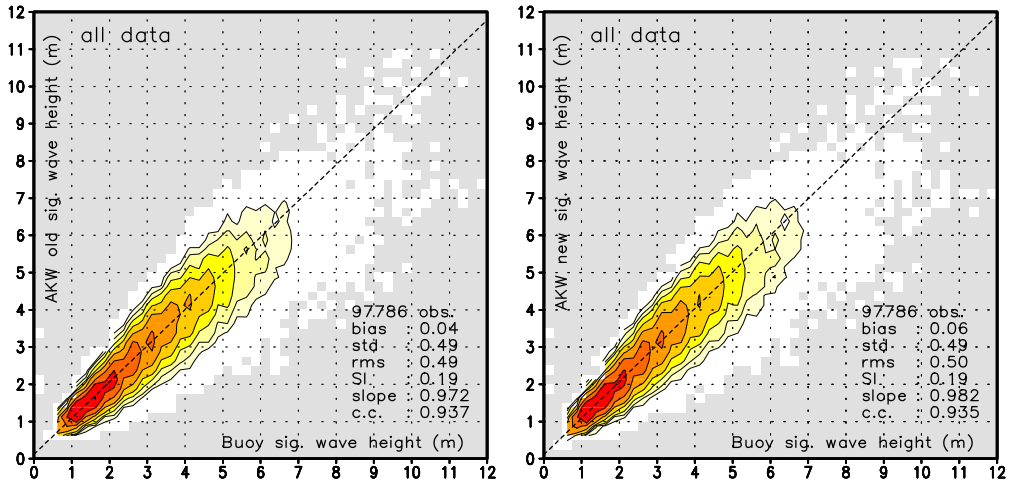

Fig. 7.18 : Like Fig. 7.17 for buoy data.

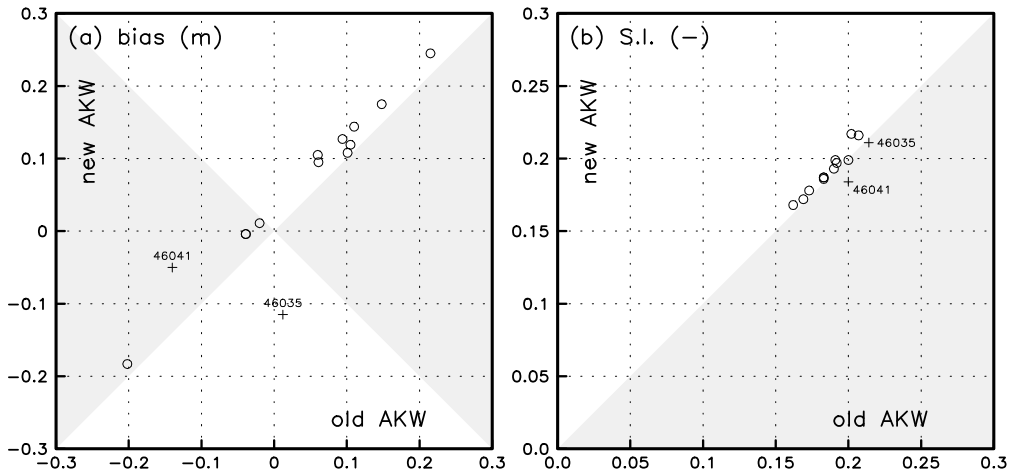

Fig. 7.19 : Like Fig. 7.5 for the new AKW model versus the old AKW model.

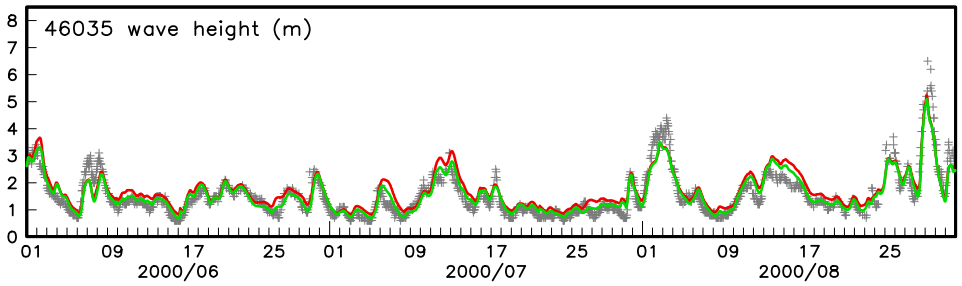

Fig. 7.20 : Time series of wave heights (H_s) observed at buoys (+), from the old NWW3 model (dashed or red lines) or the new NWW3 model (solid or green lines) for June through August 2000 for buoy 46035.

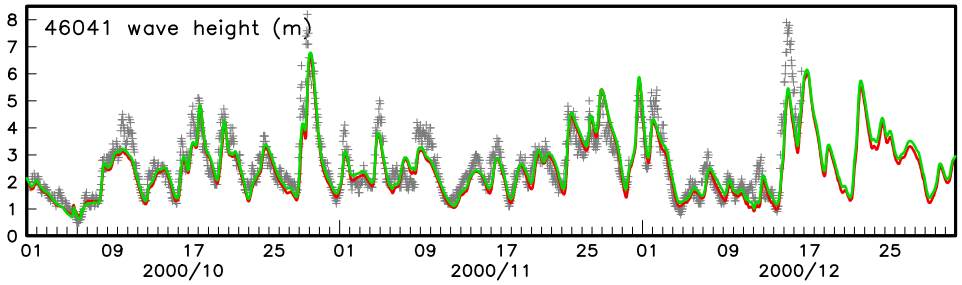

Fig. 7.21 : Like Fig. 7.20 for October through December 2000 for buoy 46041.

model. Figure 7.20 shows model results for buoy 46035 from the AKW model, for the same time period as is presented for the global model in Fig. 7.6. These figures show a similar but smaller impact for the AKW model, which could be expected because the old AKW model resolves more of the Aleutian Islands than the old NWW3 model. Hence, including these islands on a subgrid level is expected to have a smaller impact in the AKW model than in the NWW3 model. The bias for 46035 in the AKW model goes from nearly non-existent to moderately negative. The SI shows a negligible improvement (Fig. 7.19).

Figure 7.21 shows time series of wave heights at buoy 46041 for October through December 2000. The major change for this output point has been its relocation to get a better local depth description in the model. This has increased the water depth at the output location (Table 6.2). The larger water depth results in increased wave heights, as is illustrated in Fig. 7.21. This has removed about half of the negative bias from the old model (Fig. 7.19a), and in the process reduced the SI by 1.6% (Fig. 7.19b). The differences between the old and new models at the buoy location occur mostly at more moderate wave conditions, as is illustrated in Fig. 7.21.

Seasonal variations in the AKW model behavior generally follow those of the global model, and therefore will not be discussed here in any detail.

Finally, results for the regional WNA model need to be presented and discussed. Figures 7.15 and 7.16 show the bias and SI of the new and old WNA model against ERS-2 wave height data, similar to Figs. 7.1 and 7.2 for the global NWW3 model.

Distinct positive bias patterns near the Bahamas and the Lesser Antilles in the old model have been completely removed in the new model (Fig. 7.22),

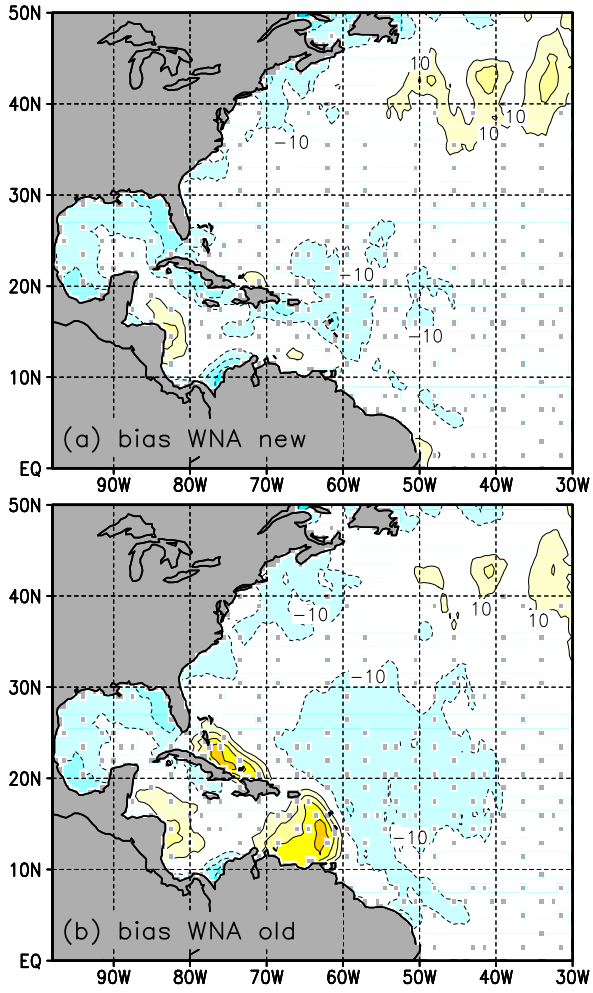

Fig. 7.22 : Bias ΔH_s in cm of models against ERS-2 wave height data. Dark gray identifies lack of data. Contours at 10 cm intervals. Dotted contours correspond to negative values, $\Delta H_s = 0$ contour not shown. Negative ΔH_s shaded light gray in black and white version. (a) New WNA model (E), (b) Old WNA model (0).

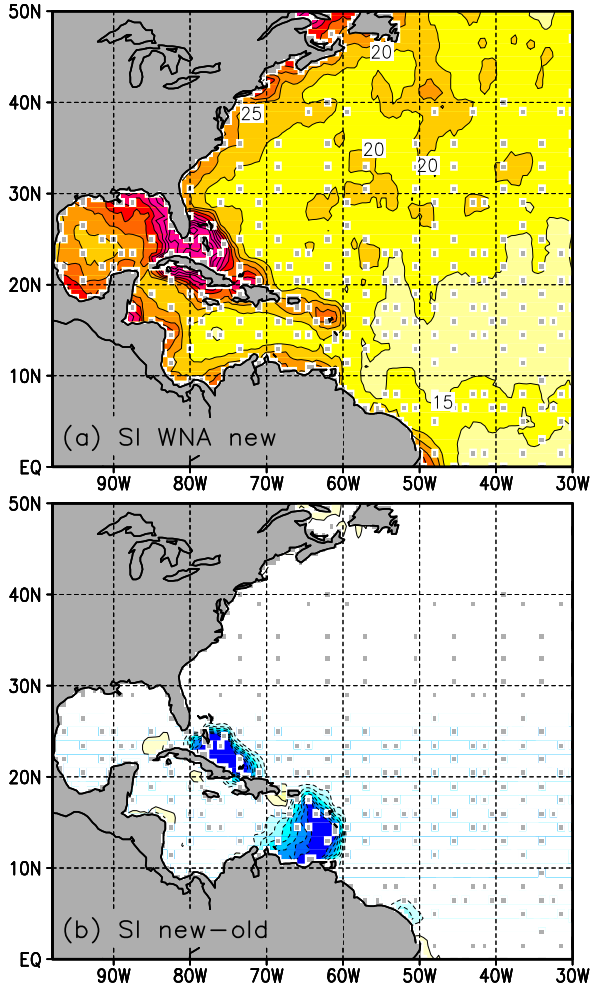

Fig. 7.23 : Scatter index (SI) in % of models against ERS-2 wave height data. Dark gray identifies lack of data. (a) New WNA model, contours at 5% intervals. (b) ΔSI = WNA new - old, contours at 2% intervals. Dotted contours correspond to negative values, ΔSI = 0 contour not shown. Negative ΔSI shaded light gray in black and white version.

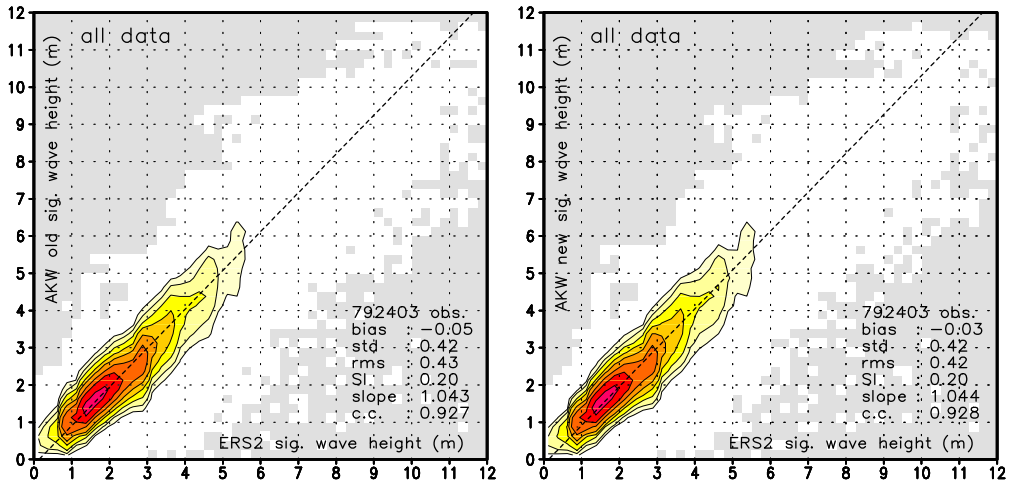

Fig. 7.24 : Probability density function (pdf) of model significant wave height H_s against ERS-2 altimeter data and mean statistics. pdf resolution $\Delta H_s = 0.25$ m. Lowest contour at 0.005 m^{-2}. Contours increase by factor 2. Shaded area identifies no data. Left panel old WNA model, right panel new WNA model.

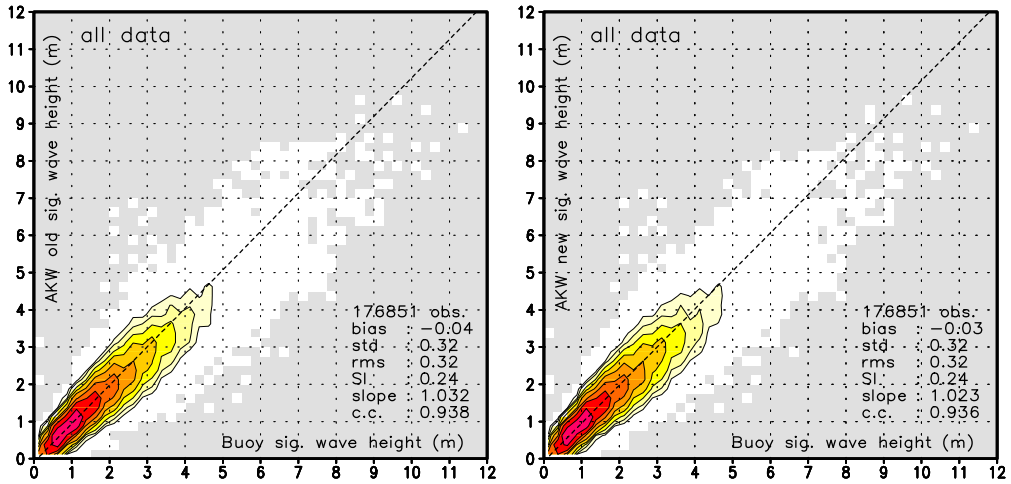

Fig. 7.25 : Like Fig. 7.24 for buoy data.

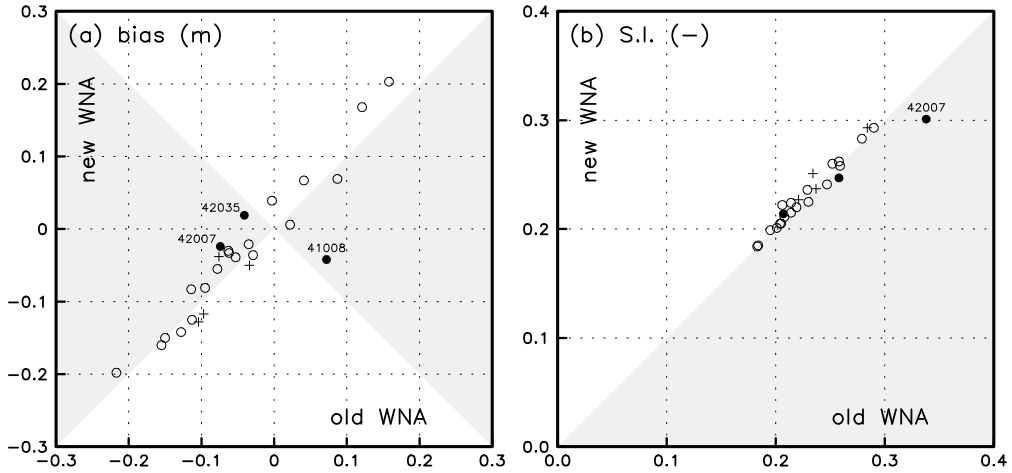

Fig. 7.26 : Like Fig. 7.5 for the new WNA model versus the old WNA model.

due to the sub-grid representation of the corresponding islands. The model changes furthermore appear to have reduced moderate negative biases in the Atlantic south of 30°N slightly, and has similarly resulted in a modest increase in positive biases more to the north. The bias removal near the unresolved islands has resulted in a major reduction of SI's near the Bahamas and the Lesser Antilles (Fig. 7.23), with much more moderate impact elsewhere.

In spite of the large local impact of the model changes, the impact on the entire volume of altimeter data again is virtually non-existent. This is illustrated in Fig. 7.24 with the pdf's and bulk statistics from the old and new model against the ERS-2 altimeter data. This is also true for the total volume of buoy data, as is shown in Fig. 7.25.

Figure 7.26 shows a comparison of biases and Scatter Indices of both models for individual buoys as identified in Fig. 1.3, stratified as before. Generally, the impact of the model changes is similar to those for the global model, with only three buoys with MMSI's of more than 10% (42007 at 18.4%, 41008 at 16.4%, and 42035 at 10.1%). Larger changes in the bias are generally positive, whereas negative changes are generally small. The impact on the SI is alternately positive and negative, with generally small changes due to the model changes.

For the three buoys with the largest impact of the model changes, output locations in the model have been changed to get a better representation of

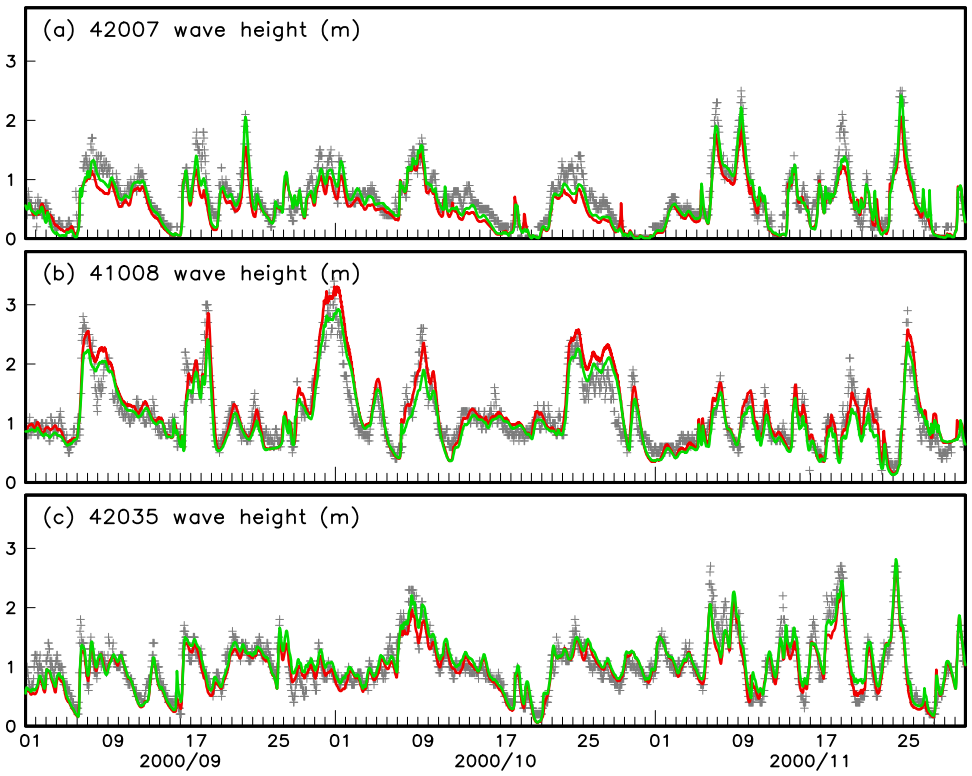

Fig. 7.27 : Time series of wave heights (H_s) observed at buoys (+), from the old WNA model (dashed or red lines) or the new WNA model (solid or green lines) for September through November 2000 for the selected buoys as identified in the panels.

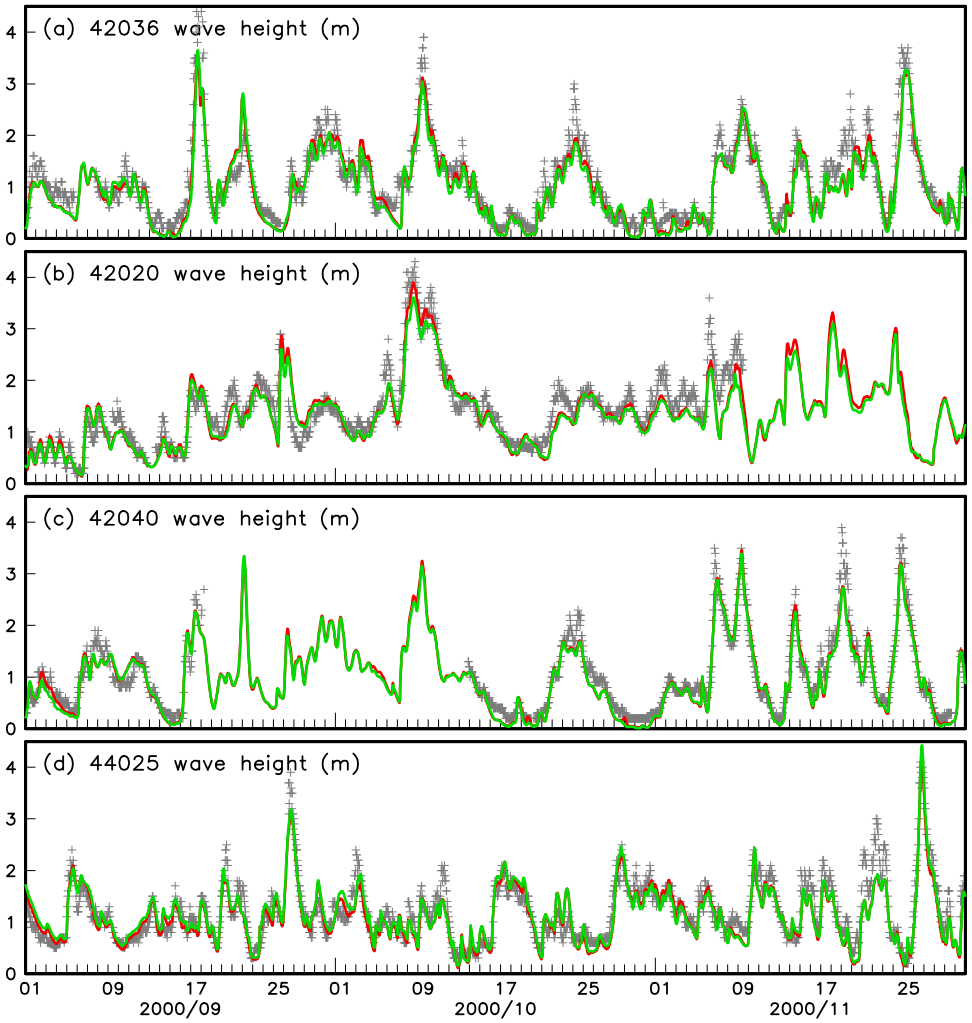

Fig. 7.28 : Like Fig. 7.27 for additional buoys.

the local water depth. All three buoys are furthermore in fairly shallow water with depths of less than 20 m (see Table 6.3). For buoys 42007 and 42035 the water depth in the model is increased by the change of model output location. This results in a systematic increase of model wave heights in the new model. For location 41008 the depth is decreased, resulting in a systematic decrease of wave heights. This is illustrated with time series of wave heights for September through November in Fig. 7.27. For these three buoys, the model changes have improved the biases (see Fig. 7.26a). For buoy 42007, the SI against data has improved by a significant 3.7%, making this the only buoy at which a sizeable change in SI occurs (see Fig. 7.26b). For buoys 41008 and 42035 the changes in SI are moderate at an improvement of 1.1% and a deterioration of 0.7%, respectively.

MMSI's of more than 5% were found at four additional buoys, 42036 (6.9%), 42020 (6.2%), 42040 (5.7%) and 44025 (5.5%). the first two of these buoys are moved to reduce the local water depth, but water depth are fairly large (see Table 6.3). As is illustrated in Fig. 7.28, this leads to a systematic decrease of wave heights, albeit more moderate than for the previously discussed buoys (see Fig. 7.27). For the remaining two buoys, no output point relocation has been performed. Most likely, the differences in model results for these buoys are related to their proximity to the coast, combined with differences in the old and new wave model grids.

8 Summary and conclusions

In this final section, a summary of the results presented will be given. Furthermore, some comments on the impact of the model changes on model run times will be given. In an operational environment, model run times are of the utmost importance.

The conversion of the model source code to FORTRAN-90 was a low impact change with respect to model results. In principle, no change is expected to occur at all. Some change in results was acceptable, as the orders in which calculations are performed was slightly changed to improve model transparency. With respect to model maintenance, this change has major impact. The use of allocatable arrays virtually eliminates the need for generating new executables for new implementations, or when the number of output points is increased. Also from a development point of view, maintenance of the code has become easier due to the strict use of the concept of modules in the new code.

The changes in the integration scheme also have a virtually negligible impact on the model results. This change is mostly made with an eye to the future. The smoother spectral integration will make it easier to derive additional parameters from the spectrum, and is expected to positively influence development of new physics (source terms) parameterizations.

The new GSE alleviation method adopted also represents a low impact model change with respect to model results. In fact, only for latitudes higher than 65°N or S relevant model differences are found, because the new method does not require artificial filtering at high latitudes (unlike the old model). This change is mainly made for reasons of economy (Tolman, 2001, 2002a). For most present operational models the reduction in run time is only 4%. For the North Atlantic Hurricane (NAH) version of the WNA model, however, the reduction can be as much as 37% (for the hardware used here). For even higher resolution models, as might be deemed necessary in the future, the impact on run time may be even more dramatic. In fact, this model change might well mean the difference between such models being economically feasible or not.

The introduction of a sub-grid representation of islands in the model, together with the subsequent retuning, has a massive (local) impact on model results. In some cases it reduces the local model errors by more than a factor of 2. For the NWS, this change is critical for regional wave forecasting around the Bahamas. With the old model, the wave model results in practice can

only be used to the North of the Bahamas. With the proper representation of the Bahamas as closed barriers in the new model, the wave model also becomes a useful forecast tool behind these barriers. To a lesser extend, the same holds true for many island groups around the world.

With respect to a bulk validation of the new model with altimeter or buoy data, the impact of the model changes might look minimal. In case of the buoy data for the AKW model, even a slight negative impact is shown. This is in stark contrast with the maps of validation results based on altimeter data. This is a good indication of the well established facts that (i) bulk validations are not suitable to properly show the impact of model changes with a local character, and (ii) that due to their sparse and selective spatial distributions, (bulk) validations with buoys data are in many cases not properly representative for an entire model.

Finally, some remarks need to be made regarding the model economy. This is particularly important, because operational models have been considered here. In such models, timely model completion is of the utmost importance. For the global NWW3 model, the impact on the model run times of the model changes has been moderate. On the hardware on which the model has been tested, the final model version E takes 6.6% more run time than the original version 0, of which 2.5% is due to the fact that the continuous ice treatment increases the number of active grid points in the calculations. The increase in model run time is considered acceptable considering the major model improvements associated with it. For the NAH model, an additional 37% speed up is associated with the new GSE alleviation method. This makes the NAH model an estimated 33% faster. This is obviously a desirable aspect of the model changes. Finally, the new GSE alleviation method removes additional computational burdens from model with even higher resolution than the present regional models. Therefore, it makes future models with higher spatial resolution more feasible, and opens avenues for additional applications to be considered.

References

Booij, N. and L. H. Holthuijsen, 1987: Propagation of ocean waves in discrete spectral wave models. *J. Comput. Physics*, **68**, 307–326.

Caplan, P., J. Derber, W. Gemmill, S.-Y. Hong, H.-L. Pan and D. Parish, 1997: Changes to the 1995 NCEP operational medium-range forecast model analysis/forecast system. *Wea. Forecasting*, **4**, 335–243.

Chao, Y. Y., L. D. Burroughs and H. L. Tolman, 1999a: Wave forecasting for Alaskan Waters. Technical Procedures Bulletin 456, NOAA/NWS, online[1].

Chao, Y. Y., L. D. Burroughs and H. L. Tolman, 1999b: Wave forecasting for Western North Atlantic and adjacent waters. Technical Procedures Bulletin 459, NOAA/NWS, online[2].

Chao, Y. Y., L. D. Burroughs and H. L. Tolman, 2001: The North Atlantic Hurricane wind wave forecasting systems. Technical Procedures Bulletin 478, NOAA/NWS, online[3].

Chen, H. S., L. D. Burroughs and H. L. Tolman, 1999: Ocean surface waves. Technical Procedures Bulletin 453, NOAA/NWS, online[4].

Derber, J. C., D. F. Parish and S. Lord, 1991: The new global operational analysis system at the National Meteorological Center. *Wea. Forecasting*, **6**, 538–547.

Donelan, M. and W. J. Pierson, 1983: The sampling variability of estimates of spectra of wind-generated gravity waves. *J. Geophys. Res.*, **88**, 4381–4392.

Grumbine, R. W., 1996: Automated passive microwave sea ice concentration analysis at NCEP. Tech. Note 120, NOAA/NWS/NCEP/OMB, 13 pp.

Hargreaves, J. C. and J. D. Annan, 1998: Integration of source terms in WAM. in *Proceedings of the 5th International Workshop on Wave Forecasting and Hindcasting*, pp. 128–133.

Hargreaves, J. C. and J. D. Annan, 2001: Comments on improvement of the short fetch behavior in the WAM model. *J. Atmos. Oceanic Techn.*, **18**, 711–715.

Holthuijsen, L. H., N. Booij, R. C. Ris, I. G. Haagsma, A. T. M. M. Kieftenburg and E. E. Kriezi, 2001: *SWAN Cycle III version 40.11 user manual.*

[1] http://polar.wwb.noaa.gov/omb/tpbs/akwtpb/akwtpb.html

[2] http://polar.wwb.noaa.gov/omb/tpbs/wnatpb/wnatpb.html

[3] http://polar.wwb.noaa.gov/omb/tpbs/nah.tpb/tpb_nah_txt.htm

[4] http://polar.wwb.noaa.gov/omb/tpbs/nww3tpb/nww3tpb.html

Delft University of Technology, Department of Civil Engineering, P.O. Box 5048, 2600 GA Delft, The Netherlands, see http://swan.ct.tudelft.nl.

Kanamitsu, M., 1989: Description of the NMC global data assimilation and forecast system. *Wea. Forecasting*, **4**, 335–243.

Kanamitsu, M., J. C. Alpert, K. A. Campana, M. P. Caplan, D. G. Deaven, M. Iredell, B. Katz, H.-L. Pan, J. Sela and G. H. White, 1991: Recent changes implemented into the global forecast system at NMC. *Wea. Forecasting*, **6**, 425–435.

Leonard, B. P., 1979: A stable and accurate convective modelling procedure based on quadratic upstream interpolation. *Comput. Methods Appl. Mech. Engng.*, **18**, 59–98.

Leonard, B. P., 1991: The ULTIMATE conservative difference scheme applied to unsteady one-dimensional advection. *Comput. Methods Appl. Mech. Engng.*, **88**, 17–74.

Tolman, H. L., 1992: Effects of numerics on the physics in a third-generation wind-wave model. *J. Phys. Oceanogr.*, **22**, 1095–1111.

Tolman, H. L., 1995: On the selection of propagation schemes for a spectral wind wave model. Office Note 411, NWS/NCEP, 30 pp + figures.

Tolman, H. L., 1998a: Effects of observation errors in linear regression and bin-average analyses. *Quart. J. Roy. Meteor. Soc.*, **124**, 897–917.

Tolman, H. L., 1998b: Validation of NCEP's ocean winds for the use in wind wave models. *The Global Atmosphere and Ocean System*, **6**, 243–268.

Tolman, H. L., 1999: User manual and system documentation of WAVEWATCH III version 1.18. Tech. Note 166, NOAA/NWS/NCEP/OMB, 110 pp.

Tolman, H. L., 2001: Improving propagation in ocean wave models. in B. L. Edge and J. M. Hemsley, editors, *Ocean Wave Measurement and Analysis*, pp. 507–516. ASCE.

Tolman, H. L., 2002a: Alleviating the garden sprinkler effect in wind wave models. *Ocean Mod.*, **4**, 269–289.

Tolman, H. L., 2002b: Treatment of unresolved islands and ice in wind wave models. *Ocean Mod.*, Submitted.

Tolman, H. L., 2002c: User manual and system documentation of WAVEWATCH III version 2.22. Tech. Note 222, NOAA/NWS/NCEP/OMB, 133 pp. (DRAFT).

Tolman, H. L., 2002d: Validation of WAVEWATCH III version 1.15 for a global domain. Tech. Note 213, NOAA/NWS/NCEP/OMB, 33 pp.

Tolman, H. L., B. Balasubramaniyan, L. D. Burroughs, D. V. Chalikov,

Y. Y. Chao, H. S. Chen and V. M. Gerald, 2002: Development and implementation of wind generated ocean surface wave models at NCEP. *Wea. Forecasting*, **17**, 311–333.

WAMDIG, 1988: The WAM model – a third generation ocean wave prediction model. *J. Phys. Oceanogr.*, **18**, 1775–1809.

Wingeart, K. M., W. C. O'Reilly, T. H. C. Herbers, P. A. Wittmann, R. E. Jenssen and H. L. Tolman, 2001: Validation of operational global wave prediction models with spectral buoy data. in B. L. Edge and J. M. Hemsley, editors, *Ocean Wave Measurement and Analysis*, pp. 590–599. ASCE.